

Laser Desorption Solid Phase Microextraction

by

Yan Wang

A thesis

presented to the University of Waterloo

in fulfilment of the

thesis requirement for the degree of

Doctor of Philosophy

in

Chemistry

Waterloo, Ontario, Canada, 2006

© Yan Wang 2006

Declaration

I hereby declare that I am the sole author of this thesis. This is a true copy of the thesis, including any required final revisions, as accepted by my examiners.

I understand that my thesis may be made electronically available to the public.

Abstract

The use of laser desorption as a sample introduction method for solid-phase microextraction (SPME) has been investigated in this research project. Three different types of analytical instruments, mass spectrometry (MS), ion mobility spectrometry (IMS) and gas chromatography (GC) were employed as detectors. The coupling of laser desorption SPME to these three instruments was constructed and described in here.

Solid-phase microextraction/surface enhanced laser desorption ionization fibers (SPME/SELDI) were developed and have been coupled to two IMS devices. SPME/SELDI combines sampling, sample preparation and sample introduction with the ionization and desorption of the analytes. Other than being the extraction phase for the SPME fiber, the electroconductive polymer coatings can facilitate the ionization process without the involvement of a matrix assisted laser desorption/ionization (MALDI) matrix. The performance of the SPME coatings and the experimental parameters for laser desorption SPME were investigated with the SPME/SELDI-IMS devices. The new SPME/SELDI-IMS 400B device has a faster data acquisition system and a more powerful data analysis program. The optimum laser operation parameters were $250 \mu J$ laser energy and $20 Hz$ repetition rate. Three new SPME coatings, polypyrrole (PPY), polythiophene (PTH) and polyaniline (PAN) were developed and evaluated by an IMS and a GC. The PPY coating was found to have the best performance and was used in most of the experiments. The characteristics of the PPY and the PTH SPME/SELDI fiber were then assessed with both IMS

and MS. Good linearity could be observed between the fiber surface area and the signal intensity, and between the concentration and the signal intensities.

The ionization mechanism of poly(ethylene glycol) 400 (PEG) was studied with the SPME/SELDI-IMS 400B device. It was found that the potassiated ions and sodiated ions were both present in the ion mobility spectra. The results obtained with quadrupole time-of-flight (QTOF) MS confirmed the presence of both potassiated and sodiated ions. This result suggested that cationization is the main ionization process when polymers are directly ionized from the PPY coated silica surface. Four PEGs with different average molecular weights and poly(propylene glycol) 400 were also tested with this SPME/SELDI device. The differences between the ion mobility spectra of these polymers could be used for the fast identification of synthetic polymers.

The SPME/SELDI fibers were then coupled to QTOF MS and hybrid quadrupole linear ion trap (QqLIT) MS, respectively. Improved sensitivity could be achieved with QqLIT MS, as the modified AP MALDI source facilitated the ion transmission. The application of method for analysis of urine sample and the bovine serum albumin (BSA) digest were demonstrated with both PPY and PTH fibers. The LOD for leucine enkephalin in urine was determined to be $40 \text{ fmol } \mu\text{L}^{-1}$ with PTH coated fiber; and the LOD for the BSA digest was $2 \text{ fmol } \mu\text{L}^{-1}$ obtained with both PTH and PPY fibers.

A new multiplexed SPME/AP MALDI plate was designed and evaluated on the same QqLIT MS to improve the throughput, and the performance of this technique.

The experimental parameters were optimized to obtain a significant improvement in performance. The incorporation of diluted matrix to the extraction solution improved the absolute signal and S/N ratio by $104\times$ and $32\times$, respectively. The incorporation of reflection geometry for the laser illumination improved the S/N ratio by more than two orders of magnitude. The fully optimized high throughput SPME/AP MALDI configuration generated detection limit improvements on the order of $1000\text{-}7500\times$ those achieved prior to these modifications. This system presents a possible alternative for qualitative proteomics and drug screening.

Laser desorption SPME as a sample introduction method for the fast analysis of non-volatile synthetic polymers was also demonstrated here. The coupling of laser desorption SPME to GC/FID and GC/MS was performed, and the advantage of laser desorption over traditional thermal desorption was demonstrated in this research. Laser desorption PEG 400 was observed more efficient than thermal desorption. Good separation was obtained even with a 1-m or 2-m column. These results demonstrate the potential of laser desorption SPME as a sample introduction method for the fast GC analysis of non-volatile compounds such as synthetic polymers.

Acknowledgments

I would like to thank my supervisor Dr. Janusz Pawliszyn for his guidance and support, which helped me to work on this exciting and challenging project. I also thank the members of my committee, Dr. Susan Mikkelsen, Dr. Jacek Lipkowski, and Dr. Terry McMahon for their guidance and advice in the past four years. I would also like to thank my internal examiner Dr. Carol Ptacek from department of earth sciences, and external examiner Dr. Herbert Hill from Washington State University, for their valuable suggestions on my manuscript.

I am very grateful to Dr. Bradley Schneider and Dr. Bruce Thomson from MDS SCIEX for offering me the great opportunity to conduct part of my experiments at SCIEX, and their enlighten discussions. Working with them is a rewarding and enjoyable experience to me.

I am very grateful to Dr. Sabatino Nacson from Smiths Detection for generously lending an IONSCAN 400B ion mobility spectrometer for my project. His valuable advice and consistent technical support are highly appreciated.

I would like to thank the excellent technicians from University of Waterloo Scishop for their wonderful technical support. They are: Mr. Jacek Szubra, Mr. Zhenwen Wang and Mr. Harman Vender Heide.

I would like to thank Mr. Colin Campbell from Information System & Technology, University of Waterloo for his kind help on programming.

I would like to thank Dr. Richard Smith for his technical support and valuable

discussion.

I would like to thank the members of Dr. Pawliszyn's research group, whom I've met during my study in here, for being great company both as colleagues and friends. I thank them for creating and maintaining a nice academic atmosphere. In more or less chronological order, these include: Dr. Tiemin Huang, Dr. Markus Walles, Maria Liu, Dr. John O'Reilly, Dr. Yong Chen, Dr. Zhen Liu, Dr. Heather Lord, Dr. Don Parkinson, Allen Wang, Dr. Tao Bo, Dr. Zhaoguo Tong and Dr. Xinyu Liu. I also thank all the current group members, even though I can't list all the names here.

Many thanks to my friends Nan Chen, Howie Siu, and Dr. Jun Gu for their encouragement and friendship.

Finally I would like to thank my family for their love, support, understanding and encouragement.

To

the memory of my beloved mother

Contents

1	Introduction	1
1.1	Introduction to Solid-Phase Microextraction (SPME)	1
1.1.1	Principles of SPME	2
1.1.2	Extraction Modes	5
1.1.3	Desorption Methods	5
1.1.4	SPME Fiber Coatings and Fiber Preparation	6
1.2	Interfacing SPME to Analytical Instruments	9
1.2.1	SPME-GC Interface	9
1.2.2	SPME-HPLC Interface	10
1.2.3	Other Interfaces	10
1.3	Laser Ablation, Laser Desorption, MALDI and SELDI	11
1.3.1	Laser Ablation	12
1.3.2	Laser Desorption	14

1.3.3	Matrix Assisted Laser Desorption/Ionization	16
1.3.4	Surface Enhanced Laser Desorption/Ionization	21
1.4	Analytical Instruments for Laser Desorption SPME	22
1.4.1	Principles of IMS	22
1.5	Laser Desorption and SPME	27
1.6	Objectives of this Work	29
2	Development of a SPME/SELDI-IMS Device	31
2.1	Introduction	31
2.2	Experimental	34
2.2.1	Preparation of SPME/SELDI Fibers	34
2.2.2	Coupling SPME/SELDI to IMS Model 350	36
2.2.3	Data Acquisition	37
2.2.4	Data Analysis	40
2.3	Results and Discussion	41
2.3.1	Optimization of PPY Coating Procedure	41
2.3.2	Characterization of PPY Coated SPME/SELDI Fiber	44
2.3.3	Extraction Time Profile	47
2.3.4	Calibration Curve	48
2.3.5	Extraction Area vs. Peak Intensity	49

2.4	Conclusion	50
3	Construction of SPME/SELDI-IMS400B	52
3.1	Introduction	52
3.2	Experimental	53
3.2.1	Chemicals	53
3.2.2	Preparation of PPY Coated Fibers	53
3.2.3	Sampling Process	54
3.2.4	Instrumentation	54
3.3	Results and Discussion	57
3.3.1	Comparison of Data Acquisition Methods	57
3.3.2	IMS Gate Width	59
3.3.3	Optimization Laser Related Parameters	59
3.3.4	Mass-Reduced Mobility Calibration Curve	62
3.3.5	Extraction Related Parameters	63
3.3.6	Determination of Verapamil in Urine Sample	65
3.4	Conclusion	68
4	Evaluation of SPME/SELDI Coatings	69
4.1	Experimental	69

4.1.1	Chemicals	69
4.1.2	Preparation of SPME Fibers	70
4.1.3	Preparation of PPY Coated Fibers	71
4.1.4	Preparation of PTH Coated Fibers	71
4.1.5	Preparation of PAN Coated Fibers	72
4.1.6	Sampling Process	72
4.1.7	Instrumentation	73
4.2	Results and Discussion	74
4.2.1	Characteristic of Coatings	74
4.2.2	Laser Energy Profiles	76
4.2.3	Comparison of Coating Capacities with GC	78
4.3	Conclusion	79
5	Study of Ionization Mechanism for PEG	81
5.1	Introduction	81
5.2	Experimental	82
5.2.1	Chemicals	82
5.2.2	Preparation of PPY Coated Fibers	82
5.2.3	Sampling Process	83
5.2.4	Instrumentation	83

5.3	Results and Discussion	85
5.3.1	Comparison of Laser Desorption/Ionization and ^{63}Ni Ionization	85
5.3.2	Addition of of Alkali Metal Ions	88
5.3.3	Confirmation with SPME/SELDI Coupled to QTOF MS . .	89
5.3.4	Application	91
5.4	Conclusion	94
6	The Coupling of SPME/SELDI with Mass Spectrometry	95
6.1	Introduction	95
6.2	Experimental	98
6.2.1	Materials	98
6.2.2	Preparation of PPY SPME/SELDI Fiber	99
6.2.3	Instrumentation	99
6.2.4	SPME/SELDI-QTOF MS	100
6.2.5	SPME/SELDI-QqLIT MS	101
6.3	Results and Discussion	103
6.3.1	Results from Q-TOF MS	104
6.3.2	Results from QqLIT MS	107
6.4	Conclusion	110

7	Development of SPME/AP MALDI Plate	112
7.1	Introduction	112
7.2	Experimental	115
7.2.1	Chemicals	115
7.2.2	Preparation of PPY and PTH Coated Fibers	116
7.2.3	Preparation of Multiplexed SPME/MALDI Plate	116
7.2.4	Extraction Process	117
7.2.5	SPME/AP MALDI Coupled to a QqLIT MS	118
7.3	Results and Discussion	120
7.3.1	Optimization of Performance	120
7.3.2	Evaluation of Analytical Performance	128
7.4	Conclusion	137
8	Laser Desorption SPME as Fast Sample Introduction Method for Fast GC Analysis	138
8.1	Introduction	138
8.2	Experimental	142
8.2.1	Chemicals	142
8.2.2	Preparation of PPY Coated SPME Fibers	143
8.2.3	Sampling Process	143

8.2.4	Instrumentation	143
8.2.5	Laser Desorption to GC/FID	144
8.2.6	Laser Desorption to GC/MS	145
8.3	Results and Discussion	147
8.3.1	Laser Desorption PEG to GC/FID	147
8.3.2	Laser Desorption PEG to GC/MS	151
8.4	Conclusion	155
9	Conclusions and Recommendations	157
9.1	SPME/SELDI-IMS	158
9.2	SPME/SELDI-MS	160
9.3	Laser Desorption SPME to GC	162
9.4	Recommendations	162
A	MATHCAD Program for IMS 350 Data Analysis	177
B	MATLAB Program for Data Analysis	180
C	Schematic of Control Box and Divider for IMS 400B	196
D	List of Abbreviations	199

List of Figures

1.1	Schematic of laser desorption	13
1.2	Schematic of MALDI mechanism	18
1.3	Schematic of ion mobility spectrometer	25
2.1	Schematic of SPME/SELDI-IMS device	37
2.2	Picture of SPME/SELDI-IMS 350 device	38
2.3	Interface of data acquisition program	39
2.4	Data analysis with Matlab	41
2.5	Comparison of PPY preparation methods	43
2.6	SEM image of a PPY-coated tip surface	44
2.7	Laser energy profile obtained by single laser pulses	45
2.8	Laser desorption profile obtained by single laser pulses	46
2.9	3D laser desorption profile plotted by Matlab	47
2.10	TOAB extraction time profile	48

2.11	TOAB calibration curve	49
2.12	Extraction area profile	50
3.1	SPME/SELDI coupled to modified IMS 400B	56
3.2	Comparison of data acquisition methods	58
3.3	Laser repetition rate profile	59
3.4	Laser energy profile obtained with PPY coated fiber	61
3.5	IMS mass calibration curve	62
3.6	Verapamil extraction temperature profile	64
3.7	Verapamil extraction time profile	65
3.8	Verapamil calibration curve	66
3.9	Ion mobility spectra of verapamil spiked urine sample	68
4.1	SEM images of SPME/SELDI coatings	75
4.2	Laser energy profile obtained with PPY fibers	76
4.3	Laser energy profile obtained with PTH fibers	77
4.4	Laser energy profile obtained with PAN fibers	77
4.5	Calibration curve of TOAB obtained with GC	78
4.6	Comparison of coating capacities	79
5.1	Schematic of SPME/SELDI-Micromass QTOF MS	85

5.2	Comparison of the peak intensities with the addition of alkali metal ions	89
5.3	Ion mobility spectra of synthetic polymers	93
6.1	Schematic of SPME/SELDI-SCIEX prototype QTOF MS device	100
6.2	Schematic of the coupling of SPME fiber with Qtrap MS	102
6.3	Mass spectrum of TOAB obtained with SPME/SELDI fiber	103
6.4	Mass spectra of PPY fiber blank and after extraction from 9 pmol μL^{-1} leucine enkephalin	105
6.5	Detection limit of leucine enkephalin in urine	108
6.6	MS spectra of BSA digest obtained with PPY and PTH fibers	109
7.1	Schematic of the SPME/AP MALDI configuration	118
7.2	Comparison of performance for a 10 fmol μL^{-1} sample of BSA digest with transmission and reflection geometry	121
7.3	Comparison of performance for 100 fmol μL^{-1} angiotensin II using direct ionization from the surface of the PPY fiber (no matrix addition) and incorporating various amounts of matrix to the extraction solvent	123
7.4	Scanning electron microscope images of the PPY coating and the PPY coating after extraction from a mixture containing 10 fmol μL^{-1} BSA digest and matrix	125

7.5	Scanning electron microscope images of the PTH coating and the PTH coating after extraction from a mixture containing 10 fmol μL^{-1} BSA digest and matrix	126
7.6	Mass spectra of four peptide mixture extracted by PPY fibers	129
7.7	Analytical performance for samples of 5 fmol μL^{-1} BSA digest, 500 amol μL^{-1} BSA digest, and a blank	134
8.1	Schematic of laser desorption SPME to GC	145
8.2	Laser desorption of PEG 400 using different temperature parameters	146
8.3	Laser desorption PEG to GC/FID	148
8.4	Thermal desorption and laser desorption PEG to GC/FID	151
8.5	Comaprison of laser desorption and thermal desorption with GC/MS	153
8.6	GC/MS chromatograms of laser desorption and thermal desorption	154
A.1	Plotting IMS spectrum with Mathcad	178
A.2	Integrating peak area with Mathcad	179
C.1	Schematic of laser control box for coupling with IMS	197
C.2	Schematic of the divider in laser control box for IMS	198

List of Tables

1.1	Commonly used UV-MALDI matrices.	19
5.1	PEG 400 peaks produced by Ni radioactive ionization.	86
5.2	PEG 400 peaks produced by laser desorption/ionization.	87
5.3	Mass table of laser produced ions.	90
7.1	Quantitative comparison of fiber-fiber reproducibility for extractions from four different sample wells.	132
7.2	List of the BSA digest peptide peaks.	135
7.3	List of the BSA digest peptide peaks (continued).	136

Chapter 1

Introduction

1.1 Introduction to Solid-Phase Microextraction (SPME)

Solid-phase microextraction (SPME) is a sample preparation and sample introduction technique invented by Pawliszyn and co-workers in 1989.^{[1][2]} It integrates sampling, extraction, concentration, and sample introduction into a single solvent-free step. It has been successfully applied to a wide variety of volatile and semi-volatile compounds from environmental, food, clinical, and pharmaceutical samples. More recently, it has also been directly coupled to high-performance liquid chromatography (HPLC) and HPLC/MS to analyze non-volatile or thermally labile compounds not suitable for GC or GC/MS.

1.1.1 Principles of SPME

SPME was developed to address the need to facilitate rapid sample preparation both in the laboratory and on-site (in the field). In SPME, a small amount of extraction phase associated with a solid support is exposed to the sample for a pre-determined amount of time. If the extraction time is long enough, a partition equilibrium between the sample matrix and extraction phase is reached. In this case, the amount extracted is independent of the extraction time and the convection conditions. If the extraction is conducted in a short time, i.e. pre-equilibrium extraction, then the amount of analyte extracted is related to the extraction time if the convection/agitation are kept constant.

There are two different implementations of the SPME technique that have been extensively studied. The first, in-tube SPME, involves a polymeric extraction phase that is coated on the internal surface of a capillary tube; the second implementation, which is considered more traditional, is associated with the fiber design, and the polymer is coated on the outer surface of fiber. As SPME used in the research presented herein is closer to the fiber design, in-tube SPME will not be discussed.

Fiber-designed SPME involves the transport of analytes from the sample matrix to the coating (extraction phase), which starts when the coated fiber is placed in contact with the sample. The amount of analyte extracted by the SPME fiber increases with the extraction time until an equilibrium is reached between the sample solution and the extraction phase. In practice, the extracted amount is independent of a further increase in the extraction time. In a two-phase system

(sample-coating), the equilibrium conditions can be expressed as:

$$n = \frac{K_{fs} \cdot V_f \cdot V_s \cdot C_0}{K_{fs} \cdot V_f + V_s} \quad (1.1)$$

Where n is the number of moles extracted by the coating at equilibrium, V_s and V_f are the volumes of the sample and fiber coating, respectively, C_0 is the initial concentration of a given analyte in the sample, and K_{fs} is a fiber coating/sample matrix distribution coefficient. This equation is limited by the partition equilibrium between the sample and liquid polymeric coating such as poly(dimethylsiloxane). In most cases, V_s is much larger than the coating capacity ($V_s \gg K_{fs} \cdot V_f$), therefore the amount of analyte that is extracted by this type of coating is directly proportional to the initial analyte concentration in the sample.

$$n = K_{fs} \cdot V_f \cdot C_0 \quad (1.2)$$

This feature, combined with the other advantages of SPME (flexibility and portability), makes SPME fiber suitable for field sampling and analysis.

Solid sorbent coatings, including poly(dimethylsiloxane)/divinylbenzene (PDMS/DVB), CarbowaxTM/divinylbenzene (CW/DVB) and CarbowaxTM/template resin coatings, extract analytes by adsorption. This extraction process is limited to the surface of the coating. Because the number of active sites on the surface of the coating is limited, saturation of the surface can occur with high analyte concentrations. Therefore, a linear response for these coatings can be expected only when

the concentration of the analyte is low. Similarly, the competitive interference from the sample matrix can displace the target analyte from the surface of the coating. A theory based on Langmuir's adsorption theory could be used for this type of coating:

$$n = K_{fs} \cdot V_f \cdot V_s \cdot C_0 \cdot \frac{(C_{f_{\max}} - C_f^\infty)}{[V_S + (K_{fs} \cdot V_f \cdot (C_{f_{\max}} - C_f^\infty))]} \quad (1.3)$$

where $C_{f_{\max}}$ is the maximum concentration of active sites on the coating, and C_f^∞ is the equilibrium concentration on the coating. The other terms in the equation have the same meaning as in Equation 1.1, with the exception of the distribution coefficient, K_{fs} . In Equation 1.3, K_{fs} is defined as the adsorption equilibrium constant, but it is the partition coefficient in Equations 1.1 and 1.2.

The main difference between Equation 1.1 and Equation 1.3 is the presence of the coating concentration term $(C_{f_{\max}} - C_f^\infty)$ in the numerator and denominator of Equation 1.3. For very low analyte concentrations on the coating, it can be assumed that $C_{f_{\max}} \gg C_f^\infty$. For this condition to be fulfilled, the analyte concentration in the sample and/or its affinity towards the coating must be low. Under these circumstances, a linear dependence should be observed. Otherwise, non-linear adsorption relationship will be obtained.

1.1.2 Extraction Modes

Three typical SPME extraction modes are commonly used: direct extraction, headspace SPME, and a membrane-protected SPME extraction.

In the direct extraction mode, the coated fiber is directly immersed in the sample solution and the analytes are transported directly from the sample matrix to the extraction phase. This mode is mostly used for non-volatile and polar compounds. In the headspace mode, the analytes are transported through the air barrier before they can reach the coating. The fiber is exposed to the vapor phase above a gaseous, liquid or solid sample. This mode can protect the fiber coating from damage by high molecular weight compounds and other non-volatile interferences present in the sample matrix. The headspace mode allows for the alteration of the sample matrix to facilitate the extraction without damaging the fiber. When using a SPME fiber to extract through a membrane, the membrane serves as a barrier to protect the fiber when the sample is considered dirty.

1.1.3 Desorption Methods

After extraction from the sample solution, the analytes extracted by the SPME fiber are desorbed and introduced to the appropriate analytical instruments for further analysis. The choice of desorption method for SPME depends on the instrument that is used to analyze the sample and the chemical and physical properties of the analytes. Thermal desorption is applicable for volatile and semi-volatile compounds that are thermally stable. Therefore it is widely used to introduce an analyte into a

GC and an IMS. It has also been reported that for volatile analyte, such as toluene, direct desorption from the SPME fiber by electrons can occur inside an ion trap MS.^[3] For polar and/or non-volatile analytes, a solvent is used to desorb the analyte to a HPLC and a HPLC/MS. Recently, efforts have been made to directly couple SPME with MS for polar and non-volatile compounds. SPME with biocompatible particle coatings were coupled to nanospray MS by directly desorbing analytes in a nanospray tip with a solvent.^[4] Pulsed laser was also used to desorb analytes extracted by a SPME/MALDI fiber to IMS and MS.^[5] This solvent-free desorption method will be extensively discussed in this work.

1.1.4 SPME Fiber Coatings and Fiber Preparation

SPME Fiber Coatings

The efficiency of the extraction process is dependent on the distribution coefficient K_{fs} . This parameter characterizes the fiber coating properties, as well as its selectivity toward a certain analyte versus other compounds present in the sample matrix. The coating volume determines the method sensitivity according to Equation 1.1. A better sensitivity can be obtained if a thicker coating is used, but a longer extraction time is needed for a thicker coating. Therefore, it is important to choose the appropriate coating for a specific application.

To date, most analytes that are of low polarity can be successfully analyzed by commercially available fibers. Therefore, the development of new SPME coatings

that exhibit high extraction ability for the polar analytes is one way to expand the application of SPME for the analysis of polar analytes. Conductive polymers have found wide application in many fields, including separation science, chemical sensors and electrochemical analysis, due to their inherent multifunctional properties, such as their hydrophobicity, acid-base properties, π - π interactions, hydrogen bonding, anion exchange capacity, etc. The widely used electroconductive polymers are based on polypyrrole, polythiophene and polyaniline. Of these three classes of materials, polypyrrole and its derivatives have been extensively studied in recent years. Recently, PPY coated SPME has been developed to analyze polar and ionic analytes.

Other than conductive polymers, extraction materials with high selectivity are also considered for use as SPME coatings. For example, molecularly imprinted polymers and immobilized antibodies facilitate high-selectivity extraction with minimum nonspecific adsorption. HPLC stationary phase particles are also good candidates for better sensitivity due to the choices of their affinity towards analytes with different polarity. The development and evaluation of the above new SPME fiber coatings is intensively under investigation in Prof. Pawliszyn's research group.

SPME Fiber Preparation

There are different methods for preparing coatings for a SPME fiber. The dipping method involves placing a fiber in a concentrated solution of coating material for a short time. Once the fiber is removed from the solution, the organic solvent is

evaporated and the deposited coating material can be crosslinked.^[1] The preparation of commercial fiber coatings is identical to the preparation of optical fibers.^[6] The coating process is carried out simultaneously during the drawing of the fused-silica rod. The reproducibility of the coating thickness is typically excellent. Good reproducibility can also be obtained by using a piece of hollow fiber membrane. The membrane is treated with an appropriate volatile organic solvent, and then the swelling membrane is placed onto the tip of the fiber, and the solvent is left to evaporate. The thickness of the coating is determined by the membrane thickness.

The aforementioned fiber preparation methods involve the depositing of a polymer material onto the fibers. The development of new extraction materials also introduces new fiber preparation methods. To prepare a PPY coated fiber, for example, the electrodeposition method can be used when stainless steel is used as the SPME fiber support ^[7]. When silica is used as the support, the fiber tip is dipped in the reactant solution so that PPY can grow on the fiber tip by chemical polymerization.^[8] Molecularly imprinted polymers, C18 particles, and ion-exchange particles are deposited by dipping the fiber in a glue diluted with an organic solvent, and then the fiber is rolled in the particles. The particle coatings can also be prepared by dipping the fiber in a slurry of particle and glue mixture. In both methods, organic solvent is evaporated and the glue can be cured at a specific temperature.

1.2 Interfacing SPME to Analytical Instruments

As a widely used simple and efficient, solvent-free sample preparation method, SPME has been successfully interfaced to various analytical instruments. GC and HPLC (HPLC/MS) are most commonly coupled with SPME. Recently, SPME has also been coupled to capillary electrophoresis (CE), ion mobility spectrometry (IMS) and mass spectrometry (MS).

1.2.1 SPME-GC Interface

The analytical instruments that most frequently have been used with SPME are GC or GC/MS. An autosampler for SPME-GC analysis is also available to improve the throughput and make the method less labor intensive. Due to its solvent-free nature, SPME can be easily interfaced to GC without the use of complex injectors to deal with the large amount of solvent vapor. The narrow inserts are required to increase the linear flow around the fiber, resulting in the efficient removal of the desorbed analytes. Although the desorption of analytes is very fast, rapid injection devices have been constructed to create a sharper injection zone and induce faster separation times.^[9] In this design, the close match between the inner diameter of the capillary and the outer diameter of the fiber assures a high linear flow rate of the carrier gas along the fiber, and effective heat transfer from the heater to the fiber. Heating rates up to 1000 °C/s have been achieved by using capacitive discharge. The fiber can also be heated rapidly by passing a current through the fiber.

In addition to the aforementioned injector and fiber devices, the use of a pulsed laser is an alternative solution for rapid desorption. The coupling of laser desorption SPME to GC and GC/MS will be discussed further in this work.

1.2.2 SPME-HPLC Interface

Design of a SPME-HPLC interface was described by Chen and Pawliszyn for manually injection.^[10] This interface included a desorption chamber that was connected to a six-port injection valve. To improve the throughput of this method, samples were desorbed in a 96-well plate and then injected into the LC/LC-MS with an autosampler. Currently an integrated autosampler for LC/LC-MS is being constructed in Prof. Pawliszyn's research group.

1.2.3 Other Interfaces

The coupling of SPME and capillary isoelectric focusing (CIEF) with laser induced fluorescence detector (WCID) was reported recently for the analysis of proteins.^[11] The coupling of a SPME probe with CE was achieved on with a SPME probe adapter housed in a cartridge prepared in the laboratory. The outer diameter of the SPME probe (approximately 340 μm) was very close to the inner diameter of the hollow fiber (approximately 380 μm), and this set-up ensured a uniform distribution of the electrical field.

1.3 Laser Ablation, Laser Desorption, MALDI and SELDI

Since the 1960s, analytical chemists have been aware of the possibilities of using the interaction of laser radiation with a sample as a method of sub-sampling for the introduction of solid materials into spectrometers. Subsequently, laser sub-sampling appeared in the literature for use in atomic spectrometry. In the meantime, extensive investigations of the interaction of laser radiation with solids have been made, and there are considerable publications in the physics literature related to this topic. Many of the fundamental processes have been studied and the basic understanding of laser desorption sampling is useful to an analytical chemist for the evaluation of the possibilities of using this technique for analytical purposes. However, it has been reported in the literature that “the mechanism of vaporization of a solid by a laser beam is a complex process which, at present, is not fully understood”.^[12] Despite this fact, there are a few reviews by Moenke-Blankenburg^[13] and Radziemski and Cremers^[14] that are useful for general background information about laser ablation.

In addition to its use in analytical chemistry, the laser has been widely used in industrial and medical fields. The use of the laser as an industrial machining tool started several years after the invention of the laser. The early laser machining applications were drilling and welding. More recently, the laser has been applied widely in drilling, cutting, welding, heat treatment, and thin-film deposition pro-

cedures. In the medical field, lasers were introduced as a promising way of providing less invasive, non-traumatic, quick-healing, cost-effective treatment.^{[15][16]} The most publicized medical applications of laser ablation are ocular keratotomy (eye surgery) ^[17] and dentistry ^[18]. It has also been used to destroy the tissue blocks arteries, ^{[19][20]} and as the treatment of tumors and malignancies ^[21].

In this chapter, only the use of the laser as a sample introduction method for analytical instruments will be discussed, i.e., the use of laser ablation to introduce atoms into atomic absorption spectrometry and inductively coupled plasma atomic emission spectrometry, and laser desorption molecules to mass spectrometry.

1.3.1 Laser Ablation

Strictly speaking, laser ablation refers to a laser-induced material ejection. Usually, “the term is associated with a ‘macroscopic’ material removal and pronounced morphological changes that are affected on condensed phases upon irradiation with intense laser pulses”.^[22] When laser light is absorbed by a solid, a variety of heating phenomena occur. The effects include surface heating, vaporization, dissociation and excitation of materials and a change of phase inside the sample. Laser ablation is widely used as a sample introduction method for atomic absorption spectrometry, and inductively coupled plasma atomic emission spectrometry, because the focused beam of a pulsed laser is capable of vaporizing or ablating all materials.

At moderate laser irradiances, the interaction between the laser beam and the sample causes rapid heating and ejection of a plume of material from the surface of

the sample. The plume contains vaporized atomic and molecular species as well as liquid and solid particles and it is usually associated with visible emission, particularly at higher laser fluences, because the optically induced breakdown generates a microplasma. In this case, atomic emission spectroscopy and atomic absorption spectroscopy were used to analyze the atoms or ions in the plasma. Thus the elemental composition of the solid samples could be obtained. This method is used to analyze inorganic samples or the inorganic components in both biological and organic samples. In general, laser radiation with a 0.5 - 1 Joule laser output energy generates a plasma with a high concentration of ions. Therefore, mass spectrometry was considered to be coupled with laser desorption.

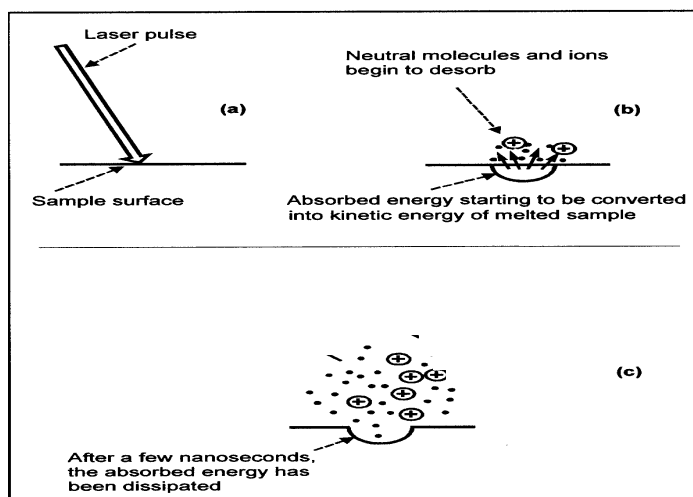


Figure 1.1: Schematic of laser desorption.

1.3.2 Laser Desorption

Ablation relates to several other applications in the broad sense of “material removal”. The most relevant one, desorption, refers to the various schemes that employ laser irradiation for ejecting molecules in the gas phase for their characteristic and/or spectroscopic study.

Laser mass spectrometry is performed by direct desorption/ ionization in one step (laser desorption mass spectrometry, LDMS),^{[23][24]} or a two-step combination of desorption and photoionization (two-step laser mass spectrometry, L2MS).^{[25]–[27]} MALDI is a variation of LDMS, where an appropriate matrix is added to the sample to enhance both the sample volatilization and the formation of ions.^{[28][29]} The details of MALDI will be discussed later in this chapter. One of the main differences between these methods is the location where the ions are formed. It is commonly believed that the ions are formed directly on the surface in LDMS (Figure 1.1), in the desorption plume in MALDI, and in the ionization volume defined by the post-ionization beam in L2MS.

Laser desorption (LD) combined with mass spectrometry was first reported by Vastola et. al. at 1966.^[30] In 1978, Posthumus and co-workers described LD of intact parent ions and fragments from nonvolatile compounds, such as oligosaccharides, peptides and nucleosides.^[31] At that time, most of the non-volatile compounds were ionized by field desorption to be subsequently analyzed by mass spectrometry. The biggest challenge with the mass spectrometry of these molecules has been the difficulty of volatilizing the analytes without thermal degradation. How-

ever, progress in LD and other approaches, such as fast atom bombardment, and secondary ion mass spectrometry, have made it possible to analyze compounds with higher mass and/or polarity by mass spectrometry. Time-of-flight (TOF) analyzers were chosen for the mass separation of ions being produced by laser pulses due to several advantages over magnetic sector and quadrupole mass analyzers available at that time, including:

- high ion throughput resulting in high sensitivity;
- ease of construction and operation;
- theoretically unlimited mass range; and
- ideal for mass separation of ions being produced by pulsed methods.

It was later recognized that the LDMS approach possesses three disadvantages. First, the ion yield is low, with the ion-to-neutral ratio of $10^{-3} - 10^{-5}$.^{[32][33]} Second, the laser fluences needed to produce an adequate ion current are high enough to induce significant fragmentation. Third, a serious ionization matrix effect can occur.^[34] L2MS was developed to overcome these method weaknesses. In L2MS, a desorption laser with laser power less than the ion formation threshold, typically an IR laser, is used for the laser-induced thermal desorption of molecules from a substrate. A second pulsed laser is then fired after an appropriate time delay with respect to the desorption laser pulse, for post-ionization of the desorbed neutral particles. The ionization laser beam is focused only 1-2 mm above the sample

surface.^[35] The L2MS approach is based on the spatial and temporal separation of the desorption and ionization step. This allows for the optimization of the laser parameters separately, therefore the matrix effects can be dramatically decreased. The quantitative analysis can be carried out with a wide linear dynamic range. Moreover, fragmentation is negligible, making it easier to interpret mass spectra.

1.3.3 Matrix Assisted Laser Desorption/Ionization

As an alternative matrix approach for LDMS, MALDI was reported by Tanaka ^[28] and Karas^[29] in 1988. Since then, it has been one of the most successful ionization techniques for the analysis of non-volatile, large molecular weight compounds. MALDI is widely used for the mass spectrometric analysis of larger non-volatile biomolecules, such as peptides, proteins, oligonucleotides, and oligosaccharides. Synthetic polymers with high molecular weight are also studied by MALDI-MS; information on the mass of the oligomer spacing, end-groups, the presence of rings, and molar mass distributions can be obtained.

The fundamentals of this phenomenon, including mechanistic study of this ionization mechanism, and the exact role of the matrix are still not fully understood. Several research groups have proposed their point of view: the correlation of the ejection process of the biomolecules with the laser and matrix parameters has been examined by Dreisewerd to reveal the relative merits and limitations of different models.^[36] Dreisewerd concluded that the biomolecule ejection is similar to the suggested volume ejection of material, though several additional features are involved.

A hypothesis for the MALDI ion formation has been proposed both by Karas and Zenobi.^{[37][38]} Karas and Krüger proposed an explosive-like separation of the ejected ionized clusters pattern during MALDI ion formation.^[37] A detailed analysis of the plausible processes responsible for the primary ionization of matrix and analytes in the condensed phase is presented to support their theory. In contrast, Knochenmuss and Zenobi emphasized the importance of the secondary charge-transfer processes in the plume.^[38] In this case, thermodynamic factors account for the final ion patterns. The correlation of the observed ion patterns with the thermochemical data is presented by the authors to support their hypothesis.

In short, a common and simple explanation for the MALDI mechanism (shown in Figure 1.2) is described here.

1. The matrix absorbs UV or IR laser energy;
2. The matrix ionizes and dissociates; it undergoes a phase change to a super-compressed gas; charge is passed to some of the analyte molecules;
3. The matrix expands at a supersonic velocity, additional analyte ions are formed in the gas phase, and ions are entrained in the expanding plume;
4. Ions may be pre-formed and released by the expanding plume, and the matrix supplies proton donors for gas-phase chemical ionization.

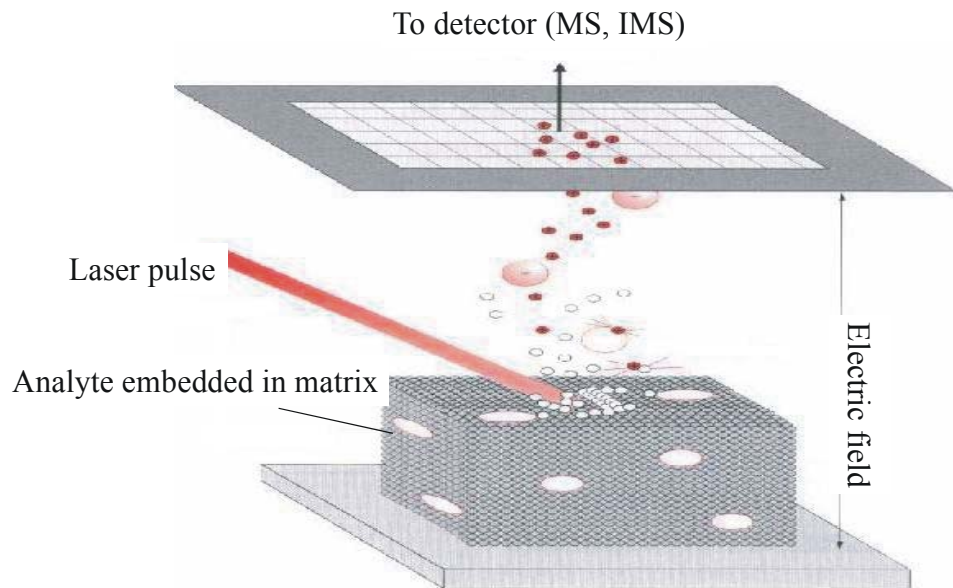


Figure 1.2: Schematic of MALDI mechanism.

The matrix effect was described to be three fold:^[37] First a controllable energy transfer to the condensed phase matrix-analyte mixture produces a “uniform and soft desorption”; second, chemical reactions promote ionization; and third, “favorable prerequisites” are generated by isolating the analyte molecules in the excess matrix. The commonly used matrices for UV-MALDI are listed in Table 1.1.

Physical Matrix

In addition to the study of large non-volatile biomolecules, MALDI-MS is also widely used for the analysis of small molecules such as drugs, peptides, and synthetic polymers. For the analysis of small molecules, the chemical background from the matrix has been an issue. To accomplish laser desorption ionization with good

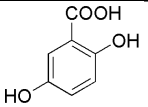
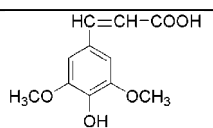
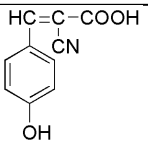
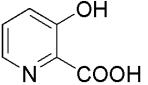
Matrix	Structure	Wavelength	Major Applications
2,5-dihydroxy benzoic acid		337 nm, 353 nm	proteins, peptides, carbohydrates, synthetic polymers
Sinapinic acid		337 nm, 353 nm	proteins, peptides
o-cyano-4-hydroxy cinnamic acid		337 nm, 353 nm	peptides
3-hydroxy picolinic acid		337 nm	nucleic acid

Table 1.1: Commonly used UV-MALDI matrices.

sensitivity and free of chemical background, new materials have been explored to facilitate laser desorption and ionization without the involvement of a MALDI matrix. In comparison with a chemical matrix, herein the term “physical” matrix is used to describe these surfaces and substrates.

Among all of the reported physical matrices, desorption ionization on silicon surface (known as DIOS) is the most successful and has been commercialized.^{[39]–[44]} By silylation of an oxidized porous silicon surface, an unprecedented detection limit of 800 ymol for des-Arg9-bradykinin could be achieved on a silylated DIOS chip.^[43] Au coated alumina has also been reported to facilitate ionization.^[45]

Carbon, metal and metalloid nanoparticles suspended in vacuum stable liquids (such as glycerol and lactic acid) have also been investigated for use as a physical matrix. In addition, the use of carbon,^{[46][47]} Au,^{[48][49]} TiN,^[50] and TiO₂^[51] nanoparticles have been reported. Carbon nanotubes were also reported to be used as a physical matrix.^{[52]–[54]} Other than the inorganic substrates mentioned above, some organic compounds have also been applied on a silica surface and functioned as matrices; DHB derived sol-gel ^{[55][56]} and PPY are two examples.^[8]

The mechanisms of desorption and ionization from these physical matrices are still under investigation. Thermal surface desorption might be one mechanism. Meso- and nanostructures are believed to enhance the sensitivity due to large accessible surface areas, higher heating rates and peak temperatures due to the reduced heat conduction. A chemically modified surface can strongly enhance adsorption, and subsequently desorption of certain analytes.

1.3.4 Surface Enhanced Laser Desorption/Ionization

Surface enhanced laser desorption/ionization (SELDI) was first used by Hutchens and Yip to describe their approach on sample preparation chips for MALDI-TOF MS.^[57] The principle of SELDI is very simple. Proteins are captured on a solid-phase protein chip surface by adsorption, partition, electrostatic interaction, or affinity. SELDI is similar to MALDI MS in which a laser ionizes samples that have been co-crystallized with a matrix on a target surface. Unlike MALDI target surfaces, the protein chip surfaces on SELDI are designed to retain proteins from complex mixtures according to their specific properties. After adding a matrix solution, proteins can be ionized with a nitrogen laser and are then analyzed by TOF MS.

SELDI-TOF MS can directly analyze complex samples in an array format, which allows for high-throughput measurements. Biofluids such as serum, urine, and plasma can be directly spotted on the protein chip surface with little or no sample cleanup. After the sample application, a series of washes with an appropriate solvent or buffer is required to elute unbound proteins and interfering substances. Once the chip surface is dry, a matrix solution is added, and the array is inserted into the MS to be analyzed.

SELDI-TOF MS is a high-throughput technique that allows for the fast screening for disease biomarker identification. However the cost of the protein chip is high, and the need for a special SELDI interface adds to the expense of this method.

The term “SPME/SELDI fiber” will be discussed extensively in this thesis, and refers to a SPME fiber with a coated tip to facilitate sample preparation for MALDI MS analysis. If certain coatings are applied, such as an electroconductive PPY coating, the coated surface can also be used as a physical matrix to facilitate the ionization process.

1.4 Analytical Instruments for Laser Desorption

SPME

In this thesis, a pulsed laser was employed to desorb the analytes extracted by a SPME fiber. This laser desorption SPME device was coupled with three kinds of analytical instruments, MS, IMS and GC. Because GC and MS are considered routine analytical methods, only the basic aspects of IMS will be introduced here.

1.4.1 Principles of IMS

Traditionally IMS has been widely used for the detection of illegal drugs, explosives and chemical warfare agents. IMS is also an important technique for mobile, on-site investigations in process and environmental analyses. Most IMS devices employ a ^{63}Ni ion source. Limitations of this conventional IMS system are that only volatile compounds in the gas phase are accessible, and the resolution or selectivity achieved is often not sufficient for complex analytical tasks. Only certain compounds such as polycyclic aromatic compounds, synthetic polymers and mostly recently, proteins

and peptides, could be analyzed with IMS due to the above limitations. To extend the applicability of this technique, electrospray and MALDI have been used as an ion source for IMS. The direct use of the emission of a pulsed laser for both desorption and ionization has also been reported for the analysis of PAHs and ion-molecular collisions.

Theory

In the presence of a neutral drift gas, IMS separates gas-phase ions on the basis of their differential migration through a weak homogeneous electric field. Ions drifting through a buffer gas under the influence of a weak uniform electric field ($E, V\text{ cm}^{-1}$) quickly reach an equilibrium between forward acceleration due to the electric field and retarding effect due to collisions with the buffer gas resulting in a constant drift velocity ($v_d, \text{cm}^2\text{ s}^{-1}$). The drift field is weak when the steady flow of ions along the electric field is much slower than the random motion leading to diffusion. The mobility ($K, \text{cm}^2\text{ s}^{-1}\text{ V}^{-1}$) is the proportionality constant between v_d and E . An ion's mobility is proportional to its collision cross section and charge if the analyte ions are much greater than the drift gas molecule. The mobility of an ion ($K, \text{cm}^2\text{ s}^{-1}\text{ V}^{-1}$) is determined by the velocity ($v_d, \text{cm}^2\text{ s}^{-1}$) attained under the influence of a weak electric field gradient in the present of a buffer gas given by:

$$v_d = K \cdot E \tag{1.4}$$

If the time taken to traverse a drift cell of length d (cm) is t_d (s), then:

$$K = \frac{d}{t_d \cdot E} \quad (1.5)$$

Ion mobilities are usually expressed as reduced mobility (K_0) corrected to standard conditions of temperature (T in *Kelvin*) and pressure (P in *Torr*):

$$K_0 = K \cdot \frac{273}{T} \frac{P}{760} \quad (1.6)$$

Ion mobility is related to the experimental conditions and analyte characteristics by the simplified equation:

$$K = \left(\frac{3q}{16N} \right) \left(\frac{2\pi}{\mu \cdot k \cdot T} \right)^{\frac{1}{2}} \frac{1}{\Omega_D} \quad (1.7)$$

where q is the ion charge, N is the number density of the drift gas, μ is the reduced mass of the ion, k is the Boltzmann constant, T is the temperature of the drift gas and Ω_D is the collision cross section (i.e. size and shape) of the ion. Therefore the mobility of an ion at a given drift gas pressure and temperature is determined by the reduced mass, charge and collision cross section of the ion. For large ions, Ω is approximated by a simple hard sphere collision cross section in a neutral buffer gas. For smaller ions, attractive components of the ion/neutral interaction potential must be considered. These hard sphere and generalized potential equations may be used, in conjunction with molecular modelling, to provide accurate approximations of ion mobility that allow predicted structure/mobility correlations to be established.

The relationship between K and Ω is only valid at the low field limit, where the electric field strength (E) to buffer gas density number (N) ratio is small ($\leq 2 Td$, where $1 Td(Townsend) = 10^{-17} C cm^2$) and the measured mobility is independent of the drift field. At higher values of E/N , the mobility is no longer constant but field dependent. This feature of gas phase mobility is the principle of ion separation in differential mobility spectrometry or high-field asymmetric waveform ion mobility spectrometry. This type of IMS was not used in this research and therefore will not be discussed further.

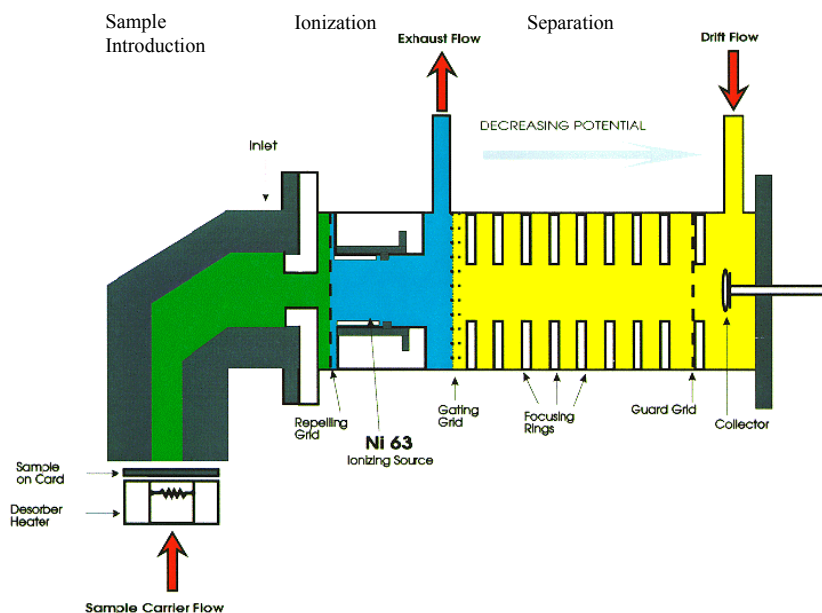
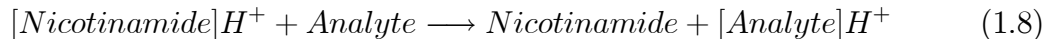


Figure 1.3: Schematic of ion mobility spectrometer.

Instrumentation

A typical IMS drift tube configuration is shown in Figure 1.3. Ions are generated in an ionization region by ^{63}Ni source. β rays emit from the ^{63}Ni foils initiate a charge transfer cascade in the reaction region that produces both positive and negative ions. In the positive ion mode, the gating grid and counter-current drift gas inhibits anions and neutral molecules from entering the drift region of the spectrometer. The electronic field and the gas flow are used to move the ions towards the drift region, where they encounter a gating grid that pulses the ions into the drift tube. Upon entering the drift tube, the ions are subjected to a uniform weak electric field, which accelerates them towards a detector situated at the end the drift tube. A drift gas is present in the drift region at a constant pressure, which may be between 1 Torr and atmospheric pressure, depending on the IMS configuration. An ion passing through the buffer gas encounters a number of collisions, which impede its progress towards the detector. Larger ions with greater collision cross sections encounter more collisions than smaller ions and therefore take longer to traverse the drift tube. The separation of ions of differing shape and size therefore becomes possible.[58] Ionization selectivity is obtained for compounds whose proton affinities are greater than that of the reactant ion, through an equilibrium shift that is determined by the relative proton affinities of the reactant and the analyte. Nicotinamide is present in the IMS used in this research as the reactant agent. In the reaction region, the protonated nicotinamide transfers a proton to the sample molecule according to



This reaction only proceeds if the proton affinity of the sample molecule is greater than that of nicotinamide. Most illegal drugs are hence readily ionized using this technique. Instead of drift time, reduced mobilities are often used for analyte identification. The reduced mobilities of unknown peaks can also be calculated using the following equation:

$$K_0 = \frac{K_{0C} \cdot t_C}{t} \quad (1.9)$$

where K_0 is the reduced mobility of unknown peak, K_{0C} is the reduced mobility of nicotinamide ($1.8810 \text{ cm}^2 \text{ s}^{-1} \text{ V}^{-1}$), t_C and t are the drift time of nicotinamide and the unknown, respectively.

1.5 Laser Desorption and SPME

SPME fibers used for laser desorption in this study are different from the commercial SPME fibers. Commercial SPME fibers utilize a small fused-silica fiber coated with a polymeric stationary phase of a certain thickness. The SPME fibers used in this work are optical fibers with SPME coatings on one tip, to extract the analytes, followed by laser desorption from the back or the front of the fiber tip.

SPME/SELDI fiber was first developed in this research project for sampling and sample introduction to IMS and MS. The fiber itself could be used as the interface to IMS for three reasons. With the SPME coating on the fiber tip, the fiber can extract analytes from the sample solution like other SPME fibers. In addition, the optical fiber also transmits the laser pulse from the back to the coated tip to desorb the analytes. Finally, the electroconductive polymer coating can also be used as the substrate to facilitate the ionization of analytes without the presence of the MALDI matrix.

Only one study was conducted on laser desorption SPME to IMS and MS prior to this study.^[5] Therefore, this technology was far from being well developed and evaluated. The focus of this thesis is on the investigation and development of this approach.^{[8][59]}

As mentioned in the previous section, laser desorption has been used to introduce non-volatile analytes from the tip of an optical fiber into GC for fast analysis in 1987, even before the development of the SPME technique.^[60] In that study, laser desorption was demonstrated to be an effective sample introduction method for fast GC analysis. However, no more attention was focused on the method, due to the more common use of thermal desorption SPME. In this research, for the first time since its introduction, the coupling of laser desorption SPME to GC and GC/MS are presented.

1.6 Objectives of this Work

The main objective of this work involved the further development of the laser desorption SPME technique, including the development of laser desorption SPME devices, and the interfacing of the laser desorption SPME devices to various analytical instrumentations, such as MS, IMS and GC. The applications with these devices are also presented.

Chapter 2 describes the development of the SPME/MALDI-IMS 350 system. The construction of the device, along with two data acquisition and data analysis programs, are discussed. The characteristics of the PPY coated SPME/SELDI fiber with this device are presented in this chapter. To improve the throughput of this device, as well as the performance, SPME/SELDI was coupled to an IMS model 400B device and described in Chapter 3. The optimization of the laser parameters was pursued and the analysis of verapamil is also presented in this chapter.

Three different SPME/SELDI fiber coatings were developed and evaluated with IMS and GC, and presented in Chapter 4. PPY was found to have the best performance among these three coatings.

In Chapter 5 the mechanism of direct laser desorption polyethylene glycol from the PPY surface with IMS are discussed and confirmed by the results obtained with MS. These results are in good agreement with both the theoretical expectations and the experimental results obtained with some other methods. The analysis of several synthetic polymers are presented, and the potential use of the characteristic

ion mobility spectra could be used for the fast identification of different polymers is explored.

Chapter 6 describes the coupling of SPME/SELDI fiber with mass spectrometry.^[8] The SPME/SELDI fibers were coupled to a QTOF MS and a QLIT MS respectively. Application of the SPME/SELDI-MS device to analyze small peptides, and urine samples was examined and better sensitivity could be obtained with QLIT MS.

In chapter 7, the development of a multiplexed SPME/MALDI plate is first reported, and the performance of this automated SPME/MALDI plate is evaluated.^[59] This approach expands the application of SPME into the bioanalytical field, and the automation makes it possible to use SPME/MALDI plates for high throughput screening analyses.

Chapter 8 illustrates the use of laser desorption SPME to GC and GC/MS for the analysis of synthetic polymers. Laser desorption proved to be more efficient than traditional thermal desorption when non-volatile synthetic polymers were used. This phase of the research explored the potential of laser desorption SPME as a sample introduction method for the fast GC analysis of non-volatile and/or high molecular weight compounds.

Chapter 9 summarizes the conclusions from the experimental findings and provides some recommendations for further research.

Chapter 2

Development of a SPME/SELDI-IMS Device

2.1 Introduction

Ion mobility spectrometry (IMS) has been successfully used for the detection of explosives, drugs, chemical warfare agents and environmental pollutants.^{[61][62]} The separation of ions in the drift region in an IMS is based on the mobility of ions. The mobility of an ion is determined by the structure (size and shape), the mass and the charge of the analytes.^{[63][64]} The most commonly used ion source is ^{63}Ni .^[58] The sample is introduced to the source region and then the ^{63}Ni foil, which is located inside the source, emits β particles, which initiates the formation of positive and negative reactant ions by atmospheric pressure chemical ionization. The neutral analytes are ionized by a series of ion-molecule reactions with the reactant ions.

The ions are then pulsed into the drift tube by an ion shutter. Once the ions enter the drift tube, they are subjected to a weak electronic field, which accelerates them toward the detector for subsequent detection.

Currently, the most widely used sample introduction technique in IMS is direct thermal desorption. The sample solution is first deposited on a membrane, then vaporized by a heater and introduced to the source region by a purified gas flow. Other sample introduction methods include direct headspace injection,^[65] adsorption of sample vapor onto a nickel wire,^[66] permeation tubes,^[67] diffusion tubes,^[68] and laser desorption.^[69] GC, LC and CE have also been coupled to IMS.^{[70]–[74]} In recent years, new ion introduction methods for IMS, such as electrospray (ESI)^{[75]–[78]} and MALDI^{[79][80]} have been reported. These two methods make it possible to analyze compounds with large molecular weight, or thermal labile compounds, such as synthetic polymers, peptides and proteins by IMS. Most of the MALDI-IMS devices had been hyphenated with MS, and laser desorption and ionization occurs inside of the drift tube.^{[79][82]} The MALDI ion source has also been installed outside of the IMS/MS instrumentation.^[83] Finally, the coupling of AP MALDI and IMS has been reported by several research groups.^{[80]–[85]}

As a sample preparation technique, solid-phase microextraction (SPME) has been widely used since 1990.^{[2][86]} It integrates sampling, sample preparation, and sample preconcentration into one single step, with the convenient introduction of the extracted analytes to an analytical instrument for detection. SPME has been routinely used with gas chromatography (GC) and GC/MS.^[87] With the develop-

ment of new polar and biocompatible coatings, SPME has also been coupled to liquid chromatography [88] and, mostly recently, IMS and MS.[5][8] The combination of commercial SPME fibers with IMS was reported by Orzechowska et. al. for the detection of heroin and cocaine in 1997.[89] Recently SPME was also coupled with IMS to analyze parabens in pharmaceutical formulations,[90] chemical warfare agents in soil,[91] and explosives in open area.[92] All of these SPME-IMS combinations employed commercial SPME fibers, therefore the method was limited to the detection of non-polar and semi-polar compounds. In addition, the analytes were introduced into IMS by thermal desorption, so it was difficult to analyze non-volatile and thermally labile compounds with these methods.

The introduction of SPME/SELDI fibers has expanded the application of the SPME-IMS technique to the analysis of non-volatile and/or large molecules. The polar silylated silica [14] and polypyrrole (PPY) coating [15] more easily extract polar analytes. The use of laser desorption facilitates the desorption of non-volatile and large and/or thermally labile molecules, such as peptides. Moreover, the PPY coating can also be used as a surface to assist the ionization of the analytes without the use of a MALDI matrix.

In this chapter, the construction of a SPME/SELDI-IMS device is introduced, followed by a discussion of the optimization of laser related parameters that were used for this device. The preparation of SPME/SELDI fibers is described, as well as the characterization of the PPY coating fibers.

2.2 Experimental

2.2.1 Preparation of SPME/SELDI Fibers

Chemicals

Pyrrrole, anhydrous ferric chloride, tetraoctylammonium bromide (TOAB), and sodium dodecylbenzenesulfonate (NaDBS) were purchased from Sigma-Aldrich (St. Louis, MO). Ammonium persulfate (APS) was purchased from BDH Chemicals (Toronto, ON, Canada). All the chemicals were used as received. HPLC grade ethanol, methanol, isopropanol and deionized water were used for all of the experiments.

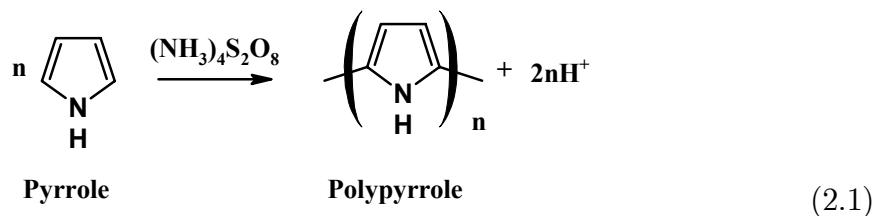
Preparation of SPME Fibers

High OH silica optical fibers with core diameters of 300, 400, 500, 600 μm were purchased from Polymicro Technologies Inc.(Phoenix, AZ) for the performance assessment of different optical configurations. The connector ferrule, F-112 epoxy glue, polishing disc and polishing films (5, 3, 1 and 0.3 μm) were purchased from Thorlabs Inc.(Newton, NJ). The silica optical fibers were cut into 1-meter sections with a capillary cutter from Restek (Bellefonte, PA). One end of the optical fibers was glued to a connector ferrule with F-112 epoxy glue from Thorlabs Inc.(Newton, NJ). After a 24 hour curing period, the fiber connector end (hereafter called the laser end) was polished with polishing films to ensure maximum light throughput. The other end of the optical fiber, hereafter called the sampling end, was coated

with a polymer coating and used for extraction. About 1 cm of the optical fiber was first cut from the sampling end to ensure a fresh clean surface for the subsequent coating process. Then the fiber tip was etched with 400-grit silicon carbide polishing paper. The etching step ensured that the polymer adhered to the fiber tip. The tip was then sonicated in methanol to remove the impurities on the fiber tip. After a water rinse, the fiber tip was ready for the coating process.

Preparation of Polypyrrole (PPY) Coated Fibers

Polypyrrole was prepared by chemical oxidation of pyrrole monomer with ammonium persulfate. (Equation 7.4) All of the solutions were freshly prepared prior to the coating procedure. Up to ten fibers were prepared simultaneously. First the fiber tips were immersed in 20 mL of 0.4 M ammonium persulfate aqueous solution. Then 20 mL of 0.4 M pyrrole solution in isopropanol:water (50:50) was added in a dropwise manner. The mixture was stirred for 3 hours. After the reaction was stopped, a layer of black polymer coating was observed on the tips and the sides of the fiber. The tips were then rinsed with deionized water and left to air dry.



Sampling Process

A TOAB stock solution was made at 10 mg mL^{-1} in ethanol and then diluted with ethanol to the desired concentration. The extraction process involved the immersion of the SPME fiber tip in the sample solutions at a 2-3 mm depth. Unless otherwise stated, the extraction time for TOAB was 1 minute. The tip was air dried after extraction.

2.2.2 Coupling SPME/SELDI to IMS Model 350

The schematic diagram of SPME/SELDI-IMS device is shown in Figure 2.1. A photodiode was placed near the laser source to detect the laser pulse and then trigger the oscilloscope to initiate data acquisition. Laser pulses with a width of 5 ns were fired manually, and the laser light was focused on the laser end of the SPME/SELDI fiber. The laser end was attached to an X, Y, Z adjustable stage. By adjusting the relative position between the lens and the laser end connector, laser light with different energies could be obtained. The laser pulse travelled through the SPME/SELDI fiber and desorbed and ionized the analytes from the SPME coating on the sampling end.

Because a laser was employed as the ionization source, the source region of the ion mobility spectrometer was modified. The original ^{63}Ni ion source was disassembled and the ion gate was disabled. A piece of stainless steel tubing with an outer thread was welded to the inlet flange plate of the drift tube. A GC liner

(I.D. 1 mm) was inserted into this stainless steel tubing. This modification acted as a guide for the SPME/SELDI fiber to reach the center of the drift tube, to ensure a maximum response.

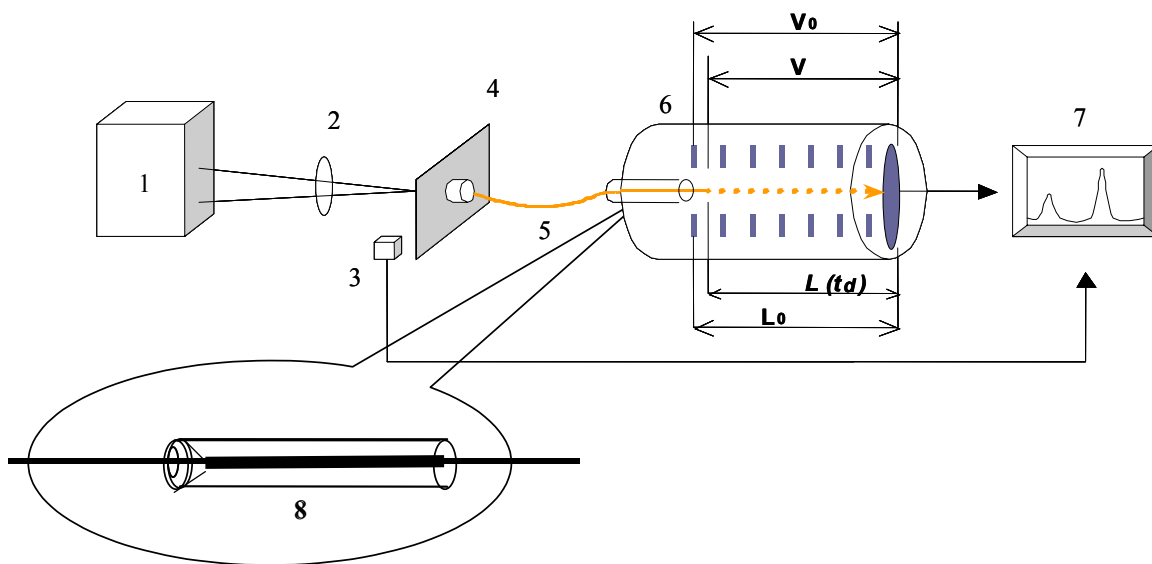


Figure 2.1: Schematic of SPME/SELDI-IMS device. 1– laser source, 2– focusing lens, 3– photodiode, 4– fiber holder, 5– SPME/SELDI fiber, 6– IMS, 7– oscilloscope, 8– GC liner.

2.2.3 Data Acquisition

Data Acquisition with Oscilloscope

A signal output was built on the IONSCAN model 350 IMS. A TDS3032 digital phosphor oscilloscope was used for ion mobility data acquisition and was purchased from Tektronix Inc.(Wilsonville, OR). After the SPME fiber was inserted into the

IMS, one single laser pulse was fired to desorb and ionize the analyte. The data acquisition was triggered by the signal from the photodiode, which was placed close to the laser source. The signal was then collected by the oscilloscope and saved on a floppy disc. A photo of this device is shown in Figure 2.2.

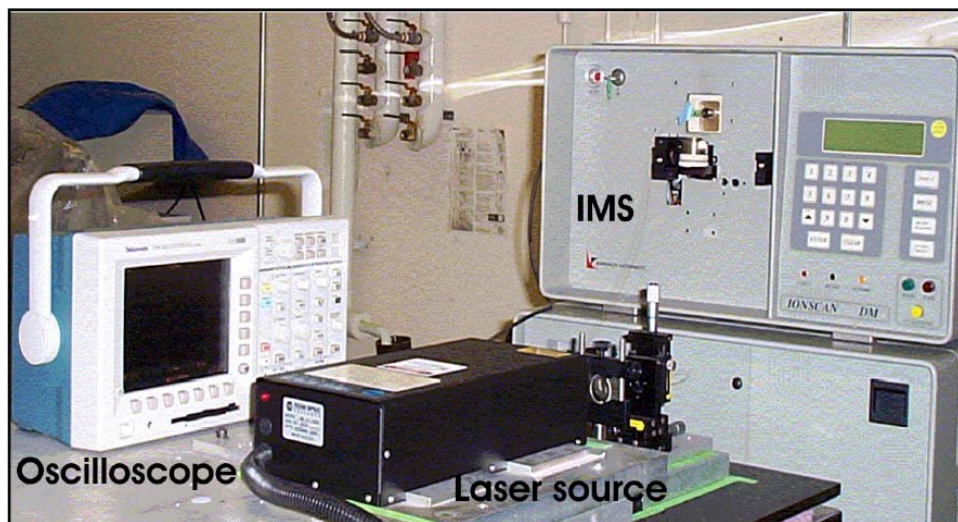


Figure 2.2: Picture of SPME/SELDI-IMS 350 device.

Data Acquisition with DAQ Board

Because the previous device could only collect data produced by single laser pulses, the S/N ratio and the reproducibility were poor. Moreover, the throughput of this device was limited by the recording speed on a floppy disc (> 1 min /spectrum). To improve the throughput and the spectrum quality, a new data acquisition device was constructed in house. This data acquisition included a PC equipped with a PCI-DAS6040 data acquisition board (Measurement Computing, Middleboro, MA), and an external laser modulation box built at the University of Waterloo SciShop.

The laser modulation box produced synchronized pulse signals to trigger the laser pulses and the DAQ board to collect the spectra (1 Hz was used for this part of the experiment). The DAQ board then recorded the data to the PC hard drive. The data acquisition was triggered by the laser modulation box, because sometimes the photodiode was unable to detect the laser pulses due to the saturation caused by external light. The interface of this data acquisition program is shown in Figure 2.3.

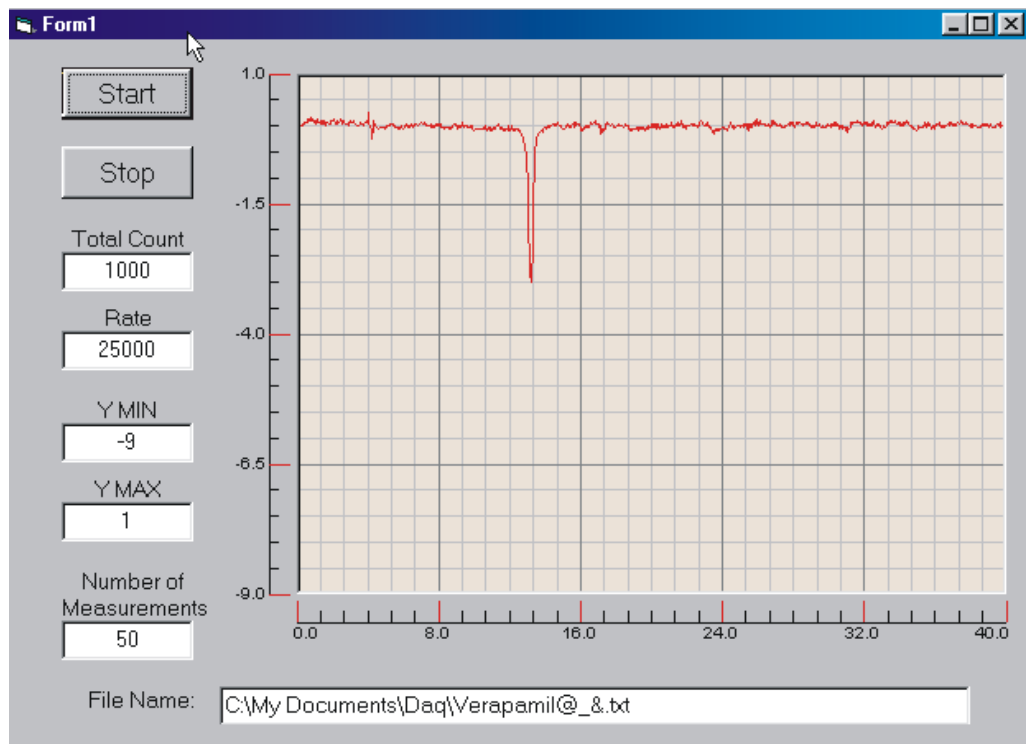


Figure 2.3: Interface of data acquisition program.

2.2.4 Data Analysis

Analysis of Oscilloscope Collected Data

Data collected by the oscilloscope were analyzed with a program written with Mathcad 2001*i* software produced by Mathsoft Engineering & Education Inc.(Cambridge, MA). The program is listed in Appendix A. Every ion mobility spectrum was first plotted and then the region where the analyte peak was located was further magnified. The analyte peak area was then integrated, as shown in Figure A.2. Because the oscilloscope could only collect a spectrum produced by a single laser pulse, this program was written for the analysis of single spectrum.

Analysis of DAQ Collected Data

Because the Mathcad program could not be directly used to average and accumulate data from multiple laser pulses, a more powerful and faster program was needed to process the data collected by the DAQ board. Matlab (The MathWorks Inc., Natick, MA) offers a number of data analysis functions, such as extracting sections of data, scaling and averaging, thresholding, peak finding, 3D plotting, and mathematical, statistical, and engineering functions to support all common engineering and science operations. Therefore Matlab was chosen for the analysis of the DAQ collected data. The program can be found in Appendix B.

With this Matlab program, the following tasks could be done: finding peaks; finding the threshold of peaks; averaging or accumulating a number of spectra;

calculating peak areas; and 3D plotting. The interface of this program is shown in Figure 2.4.

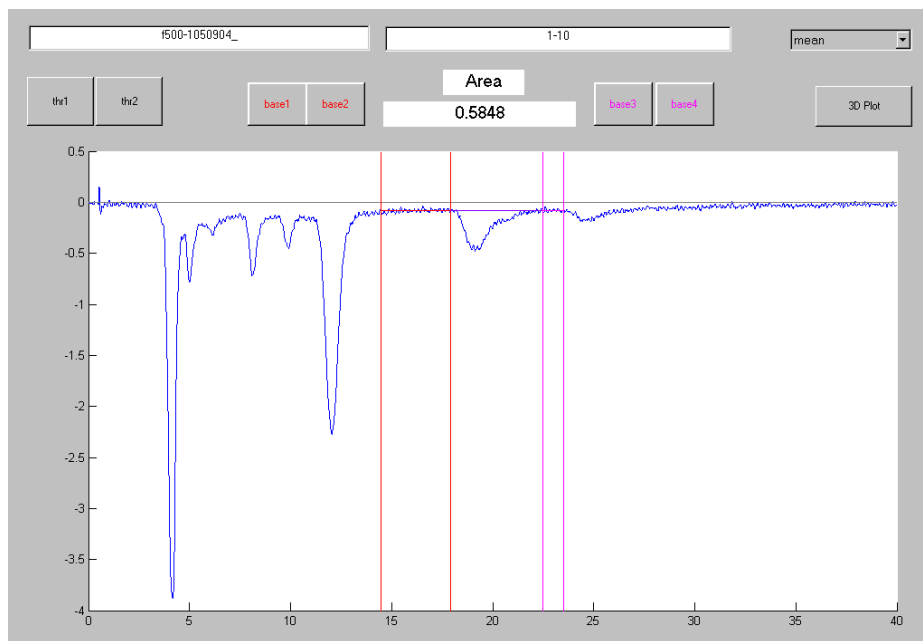


Figure 2.4: Data analysis with Matlab.

2.3 Results and Discussion

Both the optimization of PPY polymerization procedure and the characterization of PPY coated SPME/SELDI fiber are presented in this section.

2.3.1 Optimization of PPY Coating Procedure

Electrodeposition has been successfully used to prepare PPY coated stainless steel SPME fibers in Prof. Pawliszyn's group.^[7] Because the SPME fibers used in this

study were silica fibers, a chemical polymerization method was used instead. A number of oxidants, such as FeCl_3 , ammonium persulfate and perchlorate salts, could have been used for polymerization. Therefore the oxidant and the preparation procedure needed to be determined first. Different concentrations of the oxidant and pyrrole were tested (0.1, 0.2 and 0.4 M), and it was found that 0.4 M was the optimal concentration for both reactants. The PPY coating procedure was pursued with four different methods:

1. 0.4 M pyrrole monomer solution was added to 0.4 M FeCl_3 solution dropwise, then stirred for three hours;
2. 0.4 M pyrrole monomer solution was added to 0.4 M APS solution dropwise, stirred for three hours;
3. 0.4 M pyrrole monomer solution was mixed with 0.4 M APS, and the fiber tips allowed in the mixture for 30 minutes without stirring;
4. 0.4 M pyrrole solution with 0.05 M NaDBS was added to 0.4 M APS solution dropwise, stirred for three hours;

Three 600 μm fibers were used to compare the four methods. After each method was tested, fibers were sonicated in a mixture of H_2SO_4 and H_2O_2 for 10s, and MeOH for 2 min respectively. This cleaning process was repeated more than 3 times until the PPY coating was thoroughly removed from the fiber tip. Both an optical microscope and an IMS were used to assess the presence of PPY residue on

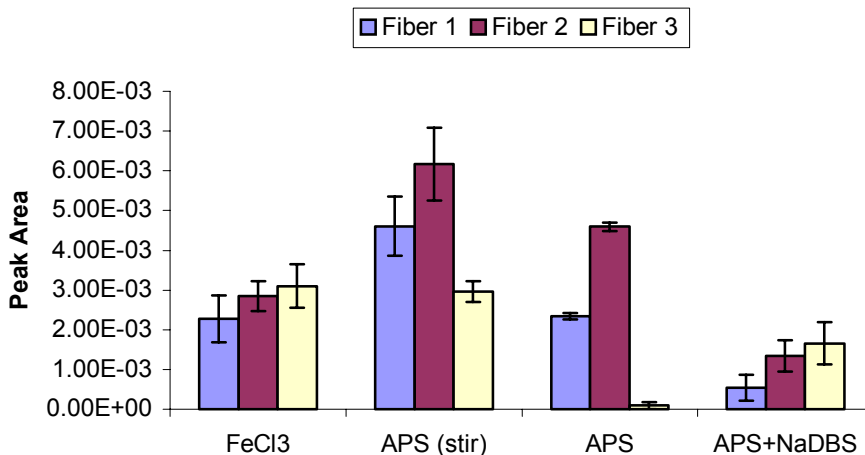


Figure 2.5: Comparison of PPY preparation methods (n=3).

the fiber tip. After the cleaning procedure, microscopic observation indicated no black coating remained on the fiber tips, and no peaks were observed when tested with IMS. The purpose of using the same fibers was to ensure the roughness of the fiber tips was the same when different coating methods were tested.

1 mg mL^{-1} TOAB solution was used as a test compound to evaluate the coating methods. The performance comparison plot is presented in Figure 2.5. The results indicate that when APS was used as the oxidant (method 2) with stirring, the highest signal intensity could be obtained. The third fiber used in the third method produced a very weak signal, in comparison with the other two fibers. The reason for this difference was that the tip of this fiber was broken before the coating process, so PPY was coated on an unetched silica surface, which was not favorable for the deposition of PPY. This also proved that the etching step was necessary to obtain a good coating. Based on the above results, method 2 was chosen for further

experiments.

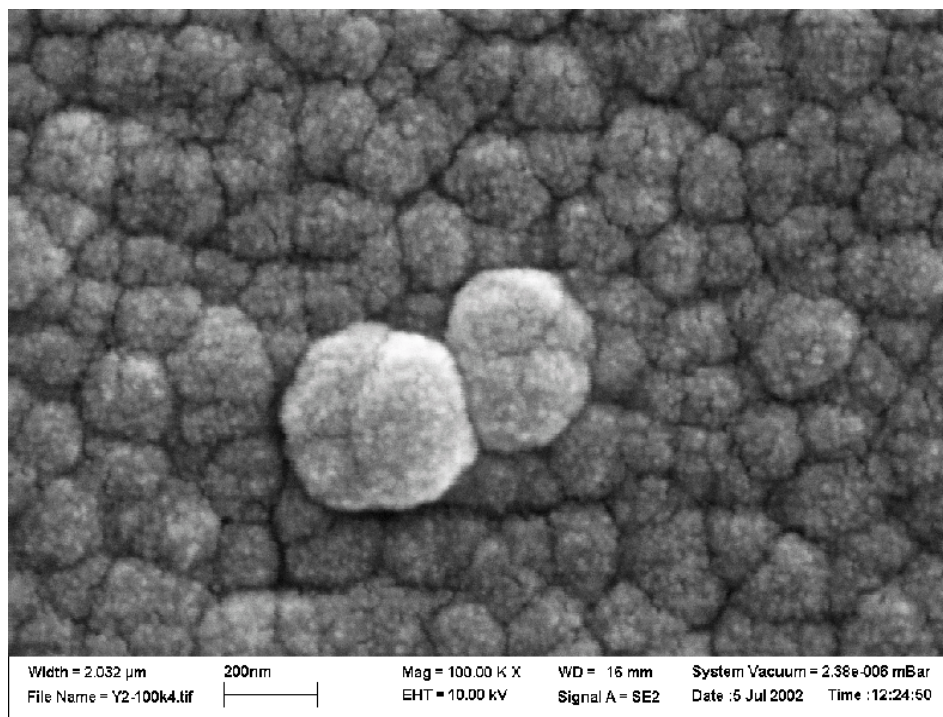


Figure 2.6: SEM image of a PPY-coated tip surface. Magnification: 100 KX; accelerator voltage: 10 kV.

2.3.2 Characterization of PPY Coated SPME/SELDI Fiber

Figure 2.6 illustrates the scanning electron microscope (SEM) images of the PPY coating on the etched fiber surface. The rough coating surface increased the extraction area, thereby increasing the sensitivity of the SPME/SELDI fiber, when compared with the silanized fiber.

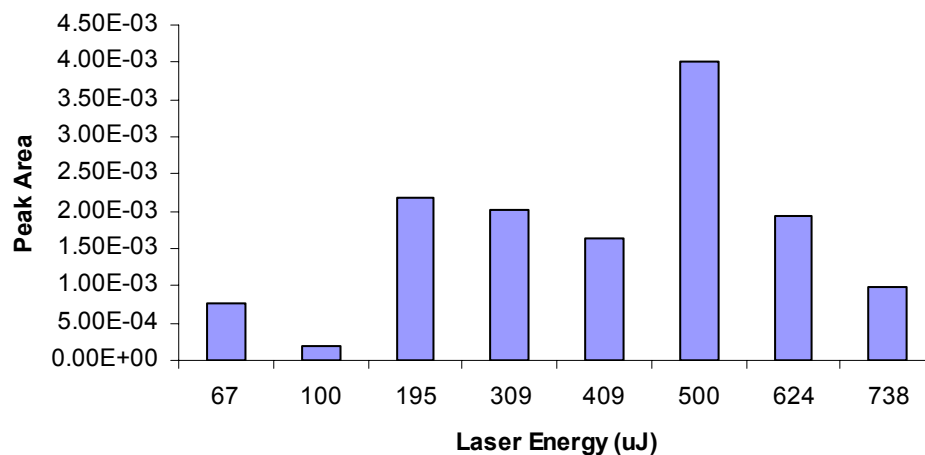


Figure 2.7: Laser energy profile obtained by single laser pulses.

Laser Energy

The optimum laser energy was investigated with data collected from the oscilloscope. The laser energy profile is shown in Figure 2.7. Technically it was difficult to set the laser energy at exactly the same level when each experiment was repeated, so the data presented here were obtained by single runs. It was difficult to determine the optimum laser energy based on the data shown in Figure 2.7. However, higher signal intensities could be observed at higher laser energy when the experiment was repeated. In most of the experiments at this stage, 500 μJ was used as the optimum laser energy. As will be described in chapter 3, the laser energy profile was investigated again with the SPME-IMS 400B device, and the optimum laser energy was determined to be much lower than the level used in these experiments. The difference could be attributed to the data sampling pattern. The

signal collected with the 400B device was produced by multiple laser pulses and the signal collected with the IMS 350 was produced by single laser pulses.

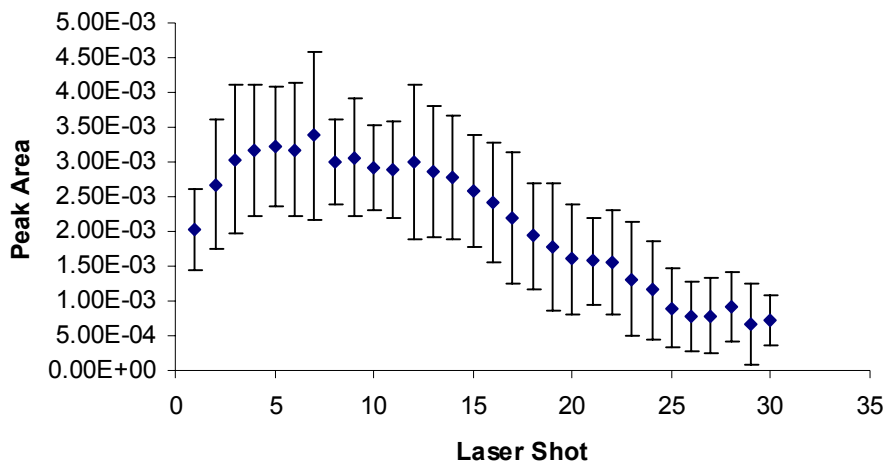


Figure 2.8: Laser desorption profile obtained by single laser pulses.

Laser Desorption Profiles

To investigate how the analyte was desorbed by a series of laser pulses, the laser desorption profile was plotted for a 1 mg mL^{-1} TOAB solution (Figure 2.8). The data were collected with an oscilloscope and processed with Mathcad. This experiment was repeated three times and the average peak intensity was plotted against the laser shots. From the laser desorption profile, it can be observed that the analyte was totally desorbed from the fiber tip with 30 laser shots. Generally, an increase in the signal intensities was observed within the first five shots. An improved intra-sample reproducibility is expected by integrating the signal accumulation and the

averaging functions in the data acquisition and processing steps.

The laser desorption profile obtained with multiple laser pulses was also collected by DAQ and plotted with Matlab for comparison. The same sample was used and 30 laser pulses were fired with 1 Hz repetition rate. The collected data were plotted as a 3D laser desorption profile in Figure 2.9, which illustrated a similar desorption profile to the one obtained with single laser pulses.

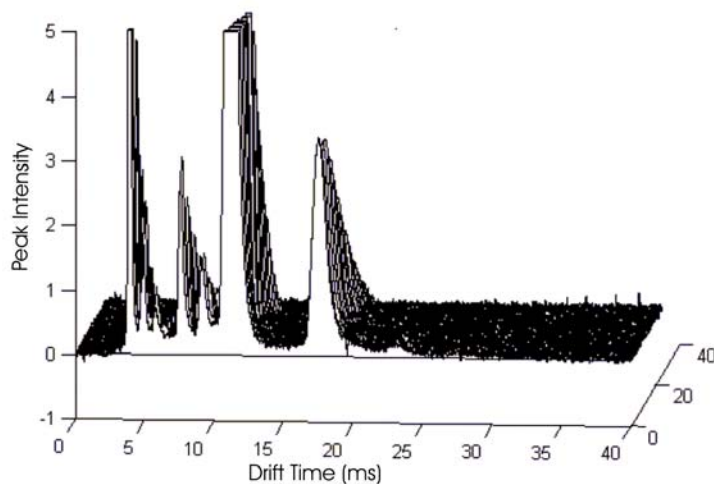


Figure 2.9: 3D laser desorption profile plotted by Matlab.

2.3.3 Extraction Time Profile

The extraction time profile of TOAB was investigated. The PPY coating is very thin, result in a very short extraction equilibrium time, as illustrated in Figure 2.10. Based on these results, a one minute extraction time was used in all subsequent experiments. The fiber could be used for approximately 300 extractions with careful handling of the laser fluence and other experimental conditions.

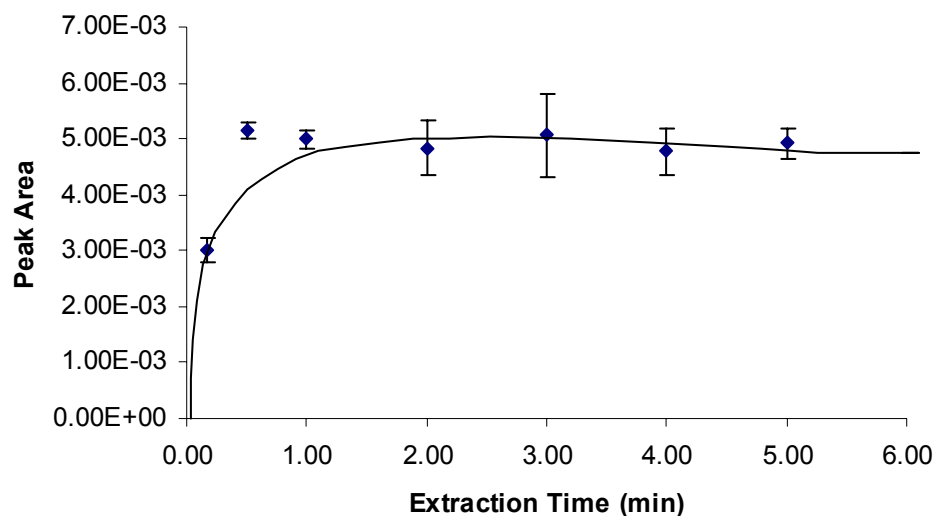


Figure 2.10: TOAB extraction time profile.

2.3.4 Calibration Curve

0.01, 0.02, 0.05, 0.1, 0.2, 0.5 and 1 mg mL^{-1} TOAB solutions were used to investigate the linear range of this SPME/SELDI method. Each concentration was tested three times and the average peak areas were plotted against the concentration (Figure 2.11). The plot shows a linear relationship between the concentration and the peak intensity in this range. This linear range is limited by the IMS [58]. The detection limit of this method was 0.01 mg mL^{-1} , calculated with a minimum S/N ratio of 3, which is typically used for MALDI analyses.

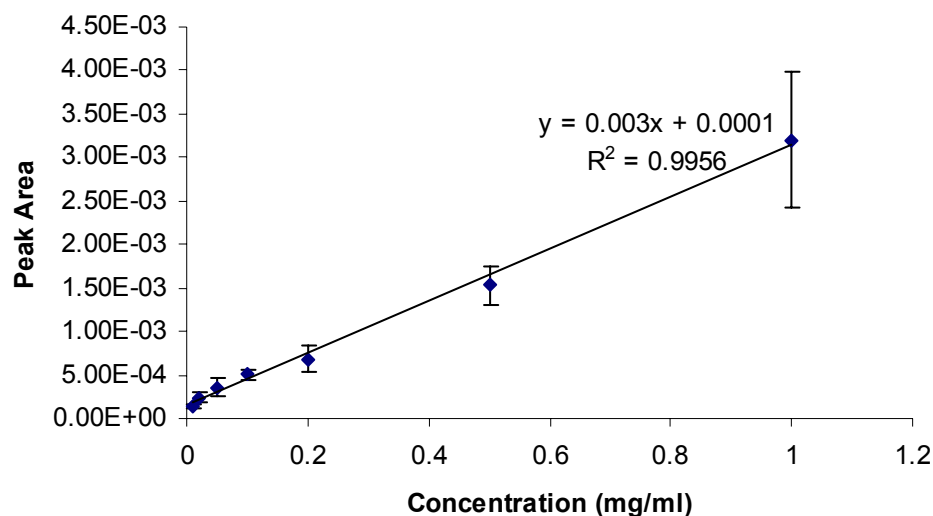


Figure 2.11: TOAB calibration curve.

2.3.5 Extraction Area vs. Peak Intensity

The extraction area of the fiber determines the capacity of the SPME/SELDI fiber. Because the laser light could only exit the fiber from the tip, only the analyte extracted by the PPY coating in this region can be desorbed and ionized by the laser. Therefore, the cross sectional area of the fiber can be used as the extraction area. Larger fibers should extract more analyte and thus increase the method sensitivity. Fibers with core diameters of 300, 400, 500 and 600 μm were prepared and tested using a 1 mg mL^{-1} TOAB solution. The surface area was plotted against the peak intensity (Figure 2.12). The plot indicates a linear relationship between the extraction area and the signal intensity for fiber sizes from 300 to 600 μm , or extraction areas from 0.071 to 0.283 mm^2 . Because the signal intensity is directly

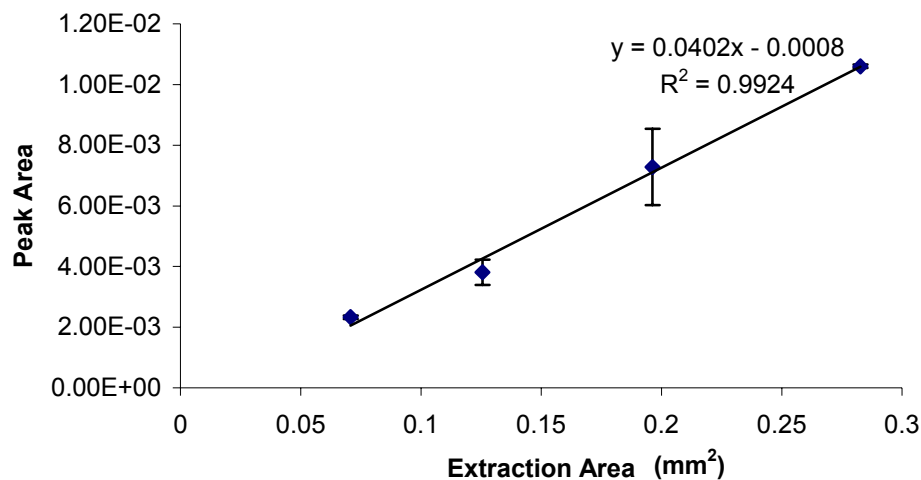


Figure 2.12: Extraction area profile.

related to the laser energy, the same laser fluence (energy density) was maintained throughout this experiment.

The use of fibers with a 800 μm diameter was unsuccessful, because the total laser energy was too high (~ 1.8 mJ). The laser end of the fiber and the PPY coating on the other end of the fiber could be burned. As a result, comparable data with the 800 μm fiber were not obtained.

2.4 Conclusion

The construction of a SPME/SELDI-IMS device was presented in this chapter. First, the setup of the SPME/SELDI-IMS device was described. During the early stage of this research, data acquisition was achieved with an oscilloscope, and only

the signals produced by single laser pulses could be collected and analyzed. It was found that the S/N ratio, the intra-sample reproducibility and the throughput of this device needed to be improved. Therefore, a faster data acquisition and a more powerful data analysis program were developed to improve the performance of this device. The time used for the data acquisition step could be shortened from 30-40 minutes to less than 1 minute for the collection of 30 spectra.

The optimization of the PPY coating was also investigated, and the optimum coating procedure was determined. The characteristics of the PPY SPME/SELDI fiber were then evaluated. It was observed that the PPY coated fiber could reach extraction equilibrium in one minute, and the analyte could be desorbed from the coating surface without the addition of a MALDI matrix. This suggested the possibility of fast analysis with this PPY SPME/SELDI fiber. Good linearity could be observed between the fiber surface area and the signal intensity, and between the concentration and the signal intensities. These results illustrate the possibility of using SPME/SELDI-IMS for quantitative analysis.

Chapter 3

Construction of SPME/SELDI-IMS400B

3.1 Introduction

To further investigate the potential of the SPME/SELDI-IMS technique, the performance of the SPME/SELDI-IMS device required improvement. The ion mobility spectra were produced by single laser pulses, which caused unsatisfactory performance, poorly affecting the S/N ratio, sensitivity, and reproducibility. Moreover, lack of a reference peak made the identification of unknown peaks difficult.

In this chapter, the construction of a new SPME/SELDI-IMS device is described. Higher throughput and better performance were obtained. The laser experimental parameters and SPME parameters were optimized with the new sys-

tem. The direct analysis of a urine sample was also performed and the results are discussed.

3.2 Experimental

3.2.1 Chemicals

Pyrrrole, verapamil hydrochloride, nicotinamide, reserpine, and TOAB were purchased from Sigma-Aldrich (St. Louis, MO). Ammonium persulfate was purchased from BDH Chemicals (Toronto, ON, Canada). Cocaine (1 mg mL^{-1} in methanol) was purchased from Cerilliant (Austin, TX). All of the chemicals were used as received. Nanopure water was obtained from a Milli-Q system (Millipore, Bedford, MA) and used exclusively in all of the experiments. HPLC grade ethanol, methanol and isopropanol were used in all of the experiments.

3.2.2 Preparation of PPY Coated Fibers

High OH silica optical fibers with core diameters of 600 μm were purchased from Polymicro Technologies Inc.(Phoenix, AZ). The preparation procedure for these fibers is described in Chapter 2.

3.2.3 Sampling Process

A TOAB stock solution was prepared to 10 mg mL^{-1} with ethanol, and then diluted with ethanol to the desired concentration. Verapamil was dissolved in water to a 2 mg mL^{-1} concentration. Urine samples were diluted 10 times and then spiked with verapamil at various concentrations. The extraction process involved the immersion of the SPME fiber tip in the sample solutions at a depth of 2-3 mm. Unless otherwise stated, the extraction times for TOAB and verapamil were 1 and 2 minutes respectively. The tip was air dried after extraction.

3.2.4 Instrumentation

Coupling SPME/SELDI to IMS Model 400B

The results obtained with the SPME/SELDI-IMS 350 device (Chapter 2) demonstrated the applicability of this technique. However, the performance still required further improvement. First, the throughput was still relatively low if compared with other commercial IMS or MALDI-MS devices, even with the help of a data acquisition (DAQ) board. Since the DAQ board recorded the signals produced by each laser pulse on the PC hard drive, the laser repetition rate had to be set to less than 1 Hz to ensure enough time for the data collection prior to the next firing of a laser pulse. In addition, most MALDI sources use a 10-20 Hz repetition rate, therefore signal from hundreds of laser pulses could be accumulated in tens of seconds. The accumulation of the signals ensures the S/N ratio, sensitivity and

reproducibility.

Due to the above limitations, it was deemed necessary to construct a new SPME/SELDI-IMS device. The new design of the SPME/ SELDI-IMS system was based on the design of the old system, which was constructed in our lab. In brief, the pulsed laser beam was focused on the laser end of the SPME/SELDI fiber, then traveled through the optical fiber, and came out from the sampling end of the SPME/SELDI fiber. The analytes extracted by the SPME coating on the fiber tip were desorbed and ionized by the laser beam and analyzed by IMS. The main changes made to this new device were the synchronization of the laser and data acquisition, and the synchronization of the data collection and analysis.

Synchronization of Laser and IMS Data Acquisition

An IONSCAN 400B IMS was modified for the new SPME/SELDI-IMS system. However the sample analysis could not be performed if the IMS failed the self-test due to the modification. To bypass this issue, the testing mode was chosen so that the data collection could be initiated without passing the self-test.

The synchronization of the triggering of the laser pulses and data acquisition were fundamental to the construction of the new SPME/SELDI-IMS device. The shutter pulses produced by the IMS power supply module were collected and modified to match the requirements of the trigger signals for the laser flash lamp and Q-switch, respectively. A control box was constructed to house this synchronization module. The trigger signals to the laser could be modified to trigger the laser

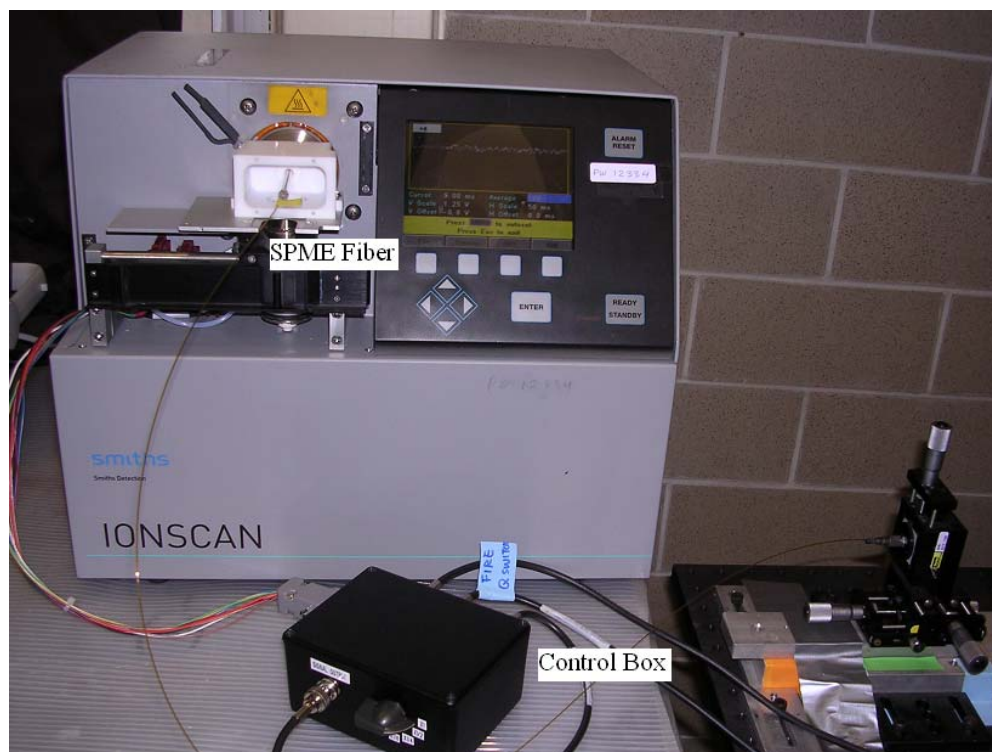


Figure 3.1: SPME/SELDI coupled to modified IMS 400B.

pulses at frequencies that ranged from 1.2, 2.5, 5, 10 to 20 Hz.

As a laser was employed as the ionization source for most part of the experiment, the original sample inlet was disassembled. Unless indicated, the ^{63}Ni ion source was removed from the IMS. A brass flange with a 1 mm diameter hole in the center was placed in contact with the source region. A 2000 V voltage was applied to the flange to force the ions into the drift tube region. The hole allowed for the insertion of the SPME/SELDI fiber, and ensured the fiber was pointed to the center of the drift tube for maximum ion transmission efficiency. A GC liner was placed in front of the source region to guide the SPME fiber. A diagram of this SPME-IMS device

is shown in Figure 3.1.

The laser end connector of the SPME/SELDI fiber was attached to an x, y, z adjustable stage. The laser beam was coupled to the fiber using an optic lens with a focal length of 15 cm. The energy exit from the sample end of the fiber per laser pulse was detected with a laser energy detector.

Following sample extraction, the SPME/SELDI fiber was inserted into the IMS and laser pulses were fired to introduce the analytes to IMS. The signal was then collected with IMS 32 (Smiths Detection, Mississauga, ON, Canada) software installed on a PC.

The IMS was programmed in the positive mode, using nicotinamide as the calibrant. The drift tube length was 7 cm and the drift field was 214 V cm^{-1} . The drift tube temperature was maintained at $234 \text{ }^\circ\text{C}$, and the heater for the desorber was disabled. The drift and exhaust flows rates were set to 300 ml min^{-1} . The sampling time was 30 sec, and the scan range was 50 ms. Unless otherwise indicated, the shutter width was set at $200 \text{ } \mu\text{s}$.

3.3 Results and Discussion

3.3.1 Comparison of Data Acquisition Methods

The DAQ data collection method was compared with the IMS32 software. When the DAQ was used for data collection, the speed was limited by the speed of data

recording onto the hard drive. Therefore, only three laser repetition rates were suitable for DAQ. Two data acquisition systems, DAQ and IMS 32 software, were used to collect data produced by the same laser pulses at the same time to compare the performance of these two methods.

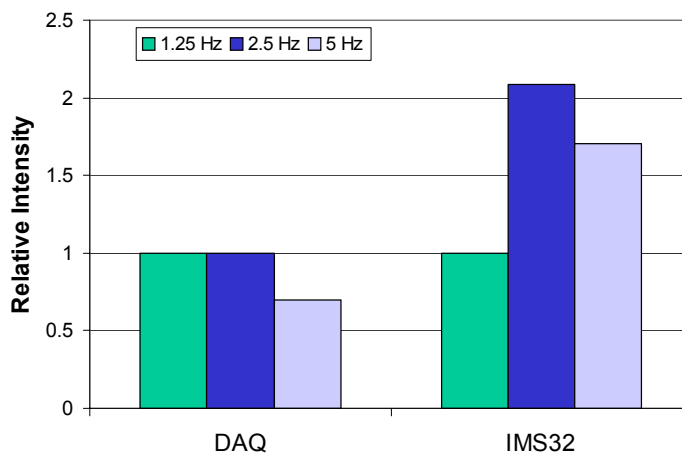


Figure 3.2: Comparison of data acquisition methods.

In Figure 3.2, the signal intensity collected by DAQ at 1.25 Hz was set at 1 and the relative intensities of the other signal intensities were used for comparison. Data collected by DAQ showed no difference on signal intensities that were collected with three different laser repetition rates. However, the data collected by the IMS32 software identified that the signal intensity doubled when the laser repetition rate increased from 1.25 to 2.5 Hz. Therefore, a higher signal was expected when the IMS 32 software was used for data collection.

3.3.2 IMS Gate Width

Different IMS shutter widths were tested with SPME/SELDI fibers. Four shutter gate widths (200, 400, 500, 800 μs) and an open shutter were tested with verapamil. It was observed that when the 200 μs shutter gate width was used, the best peak shape and separation between peaks could be obtained. Therefore, 200 μs was chosen for all subsequent experiments.

3.3.3 Optimization Laser Related Parameters

The optimization of the experimental parameters was conducted after the new SPME/ SELDI-IMS device was built. Laser related parameters such as the repetition rate and laser energy were optimized with TOAB as the test compound.

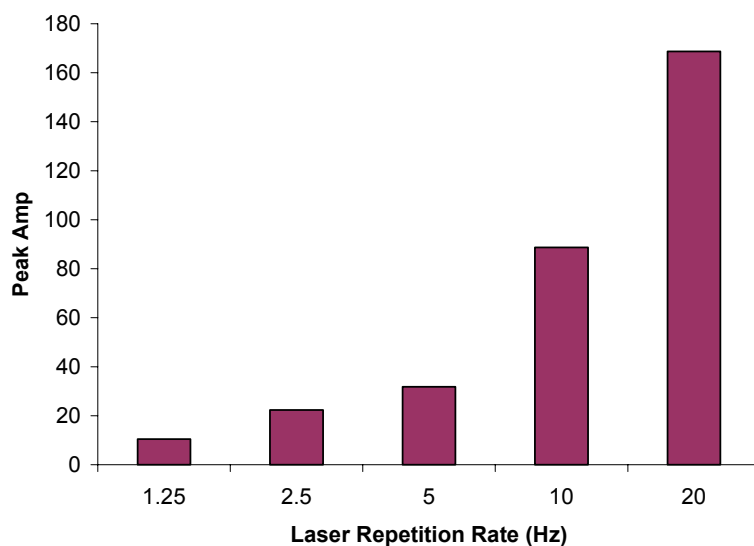


Figure 3.3: Laser repetition rate profile.

Laser Repetition Rate

As described above, the Q-switched laser could be fired at different repetition rates, from 1.2 to 20 Hz. The signal intensities for the different repetition rates are compared in Figure 3.3. It is evident that the signal intensity increases with an increase in the laser repetition rate. This is due to the difference between the IMS data acquisition rate and the laser repetition rate. The IMS data acquisition rate was set at 20 Hz and could not be modified. If the laser repetition rate was set lower than 20 Hz (IMS sampling rate), then the signal decreased. This can be observed in Figure 3.3, indicating that the signal intensity decreased to approximately 50% when the laser repetition rate decreased. Thus, 20 Hz was chosen as the optimal laser repetition rate for all subsequent experiments.

Laser Energy

Laser energy is also a very important parameter in SPME/SELDI-IMS. TOAB was used as a test compound to determine the optimal laser energy. Two peaks at drift times of 20.7 ms and 26.6 ms were observed in the ion mobility spectra. The first peak ($K_0 = 0.890\text{cm}^2\text{ V}^{-1}\text{ s}^{-1}$) can be interpreted as the protonated molecular ion as the reduced mobility ($K_0 = 0.800\text{cm}^2\text{ V}^{-1}\text{ s}^{-1}$) is very close to the reported value. The reduced mobility of the second peak could be calculated as $0.692\text{cm}^2\text{ V}^{-1}\text{ s}^{-1}$, and the mass could be calculated as 646. It could be tentatively explained as $[\text{MH} + \text{hydrated fragment}]^+$ cluster ion. The calculation of the reduced mobility and the mass of a peak will be introduced later in mass-reduced mobility section.

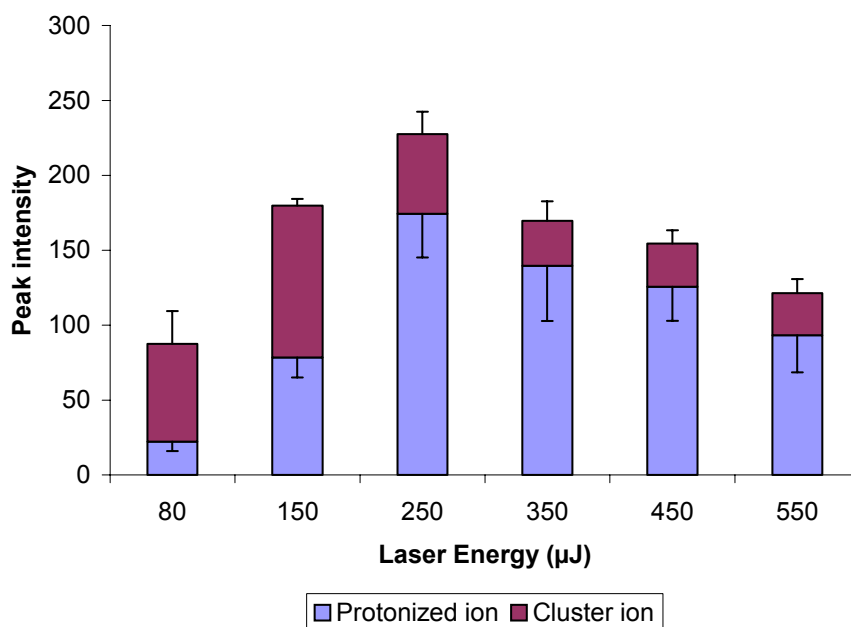


Figure 3.4: Laser energy profile obtained with PPY coated fiber.

Peak intensities of both peaks were plotted against the laser energy in Figure 3.4.

The maximum signal intensity of the protonated molecular ion could be obtained at laser energy $250 \mu\text{J}$. The peak intensity decreased at higher laser energy, as all the analytes might be ablated with a faster speed at higher laser energy. The peak intensity of cluster ions approached the maximum when the laser energy was set at $150 \mu\text{J}$. This might be explained because the cluster ions could be broken into protonated molecular ions and hydrated fragments at a high laser energy. The sum of the intensities of these two peaks was also plotted to reflect the effect of the laser energy on the total TOAB signal intensity. It exhibited the same trend, with the curve of the protonated molecular ion. Thus, $250 \mu\text{J}$ was chosen for all subsequent

experiments. The laser energy profiles of the two other SPME/SELDI coatings showed similar patterns and are presented in Chapter 4.

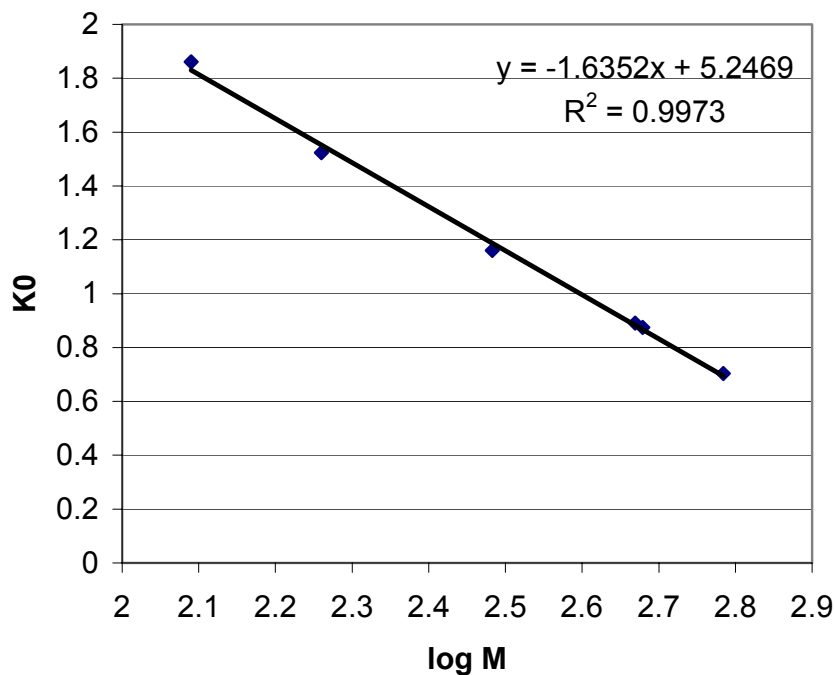


Figure 3.5: IMS mass calibration curve.

3.3.4 Mass-Reduced Mobility Calibration Curve

Compounds with a range of molecular weights (MW 123-609) were tested with the newly designed SPME/SELDI-IMS system to establish an experimental correlation between the molecular weight and the reduced mobility. Nicotinamide, cocaine, TOAB, verapamil and reserpine were tested. The reduced mobilities of these compounds can be calculated using the following equation:

$$K_0 = \frac{K_{0C} \cdot t_C}{t} \quad (3.1)$$

where K_0 is the reduced mobility of unknown peak, K_{0C} is the reduced mobility of nicotinamide ($1.8810 \text{ cm}^2 \text{ s}^{-1} \text{ V}^{-1}$), t_C and t are the drift time of nicotinamide and the compounds, respectively. A good linear relationship ($r^2 = 0.997$) could be observed between the mobility and the log of the mass (Figure 3.5). This mass-reduced mobility calibration curve can be used to estimate the molecular weight of unknown ions in a sample.

3.3.5 Extraction Related Parameters

Extraction Temperature

The extraction conditions for verapamil were investigated. The optimum extraction temperature was determined by performing extractions at 5 °C, 15 °C, 22 °C, 35 °C, and 45 °C. Room temperature (22 °C) appeared to be the best extraction temperature (Figure 3.6). The extraction time profile was also plotted to determine the optimum extraction time. The extraction equilibrium could be reached in 2 minutes.

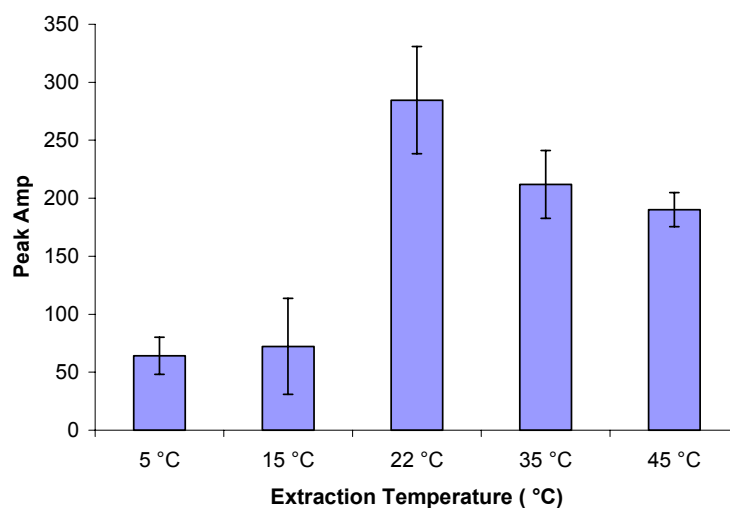


Figure 3.6: Verapamil extraction temperature profile.

Extraction Time

TOAB and verapamil was used as test compounds for most of the experiments. The extraction time for TOAB was determined to be one minute, according to previous studies. The extraction time profile for verapamil is shown in Figure 3.7, which indicates that the extraction equilibrium could be reached in 2 minutes. This equilibrium time is much shorter than that of commercial fibers used for other SPME-IMS applications (usually longer than 10 min). The short equilibrium time can be explained by the very thin PPY coating (less than 5 μm , measured with a scanning electronic microscope).

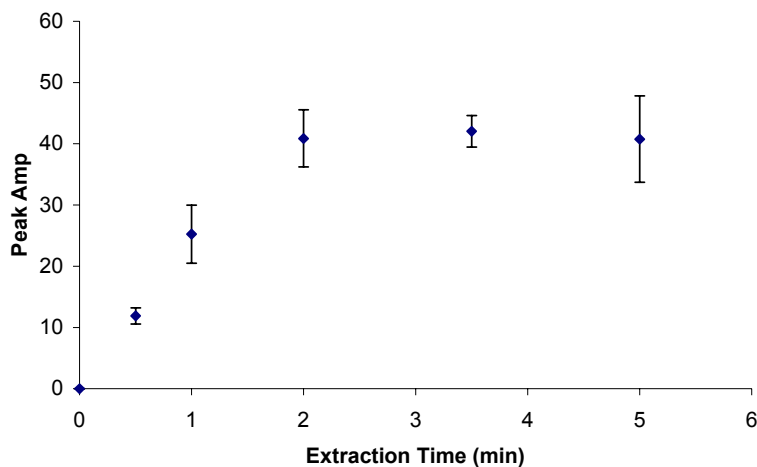


Figure 3.7: Verapamil extraction time profile.

3.3.6 Determination of Verapamil in Urine Sample

The calibration curve was obtained by extracting verapamil from standard solution. The calibration curve exhibited good linearity (Figure 3.8). A spiked urine sample with $10 \mu\text{g mL}^{-1}$ verapamil was prepared and extracted by the SPME/SELDI fiber. After extraction, the fiber was quickly rinsed with water. The ion mobility spectrum is shown in Figure 3.9C. For comparison, spectra produced from the extraction of a $10 \mu\text{g mL}^{-1}$ verapamil solution and blank urine sample are presented in Figure 3.9A and 3.9B, respectively. The peak at drift time 9.5 ms and 19.9 ms were from nicotinamide and verapamil, respectively. The peak at 12.4 ms in Figure 3.9C was from the urine matrix. The quantitation of verapamil in the sample was determined by the standard curve and the recovery was determined to be 80%. The RSD (n=3) was around 18%, which is reasonable if we consider that the run-run reproducibility

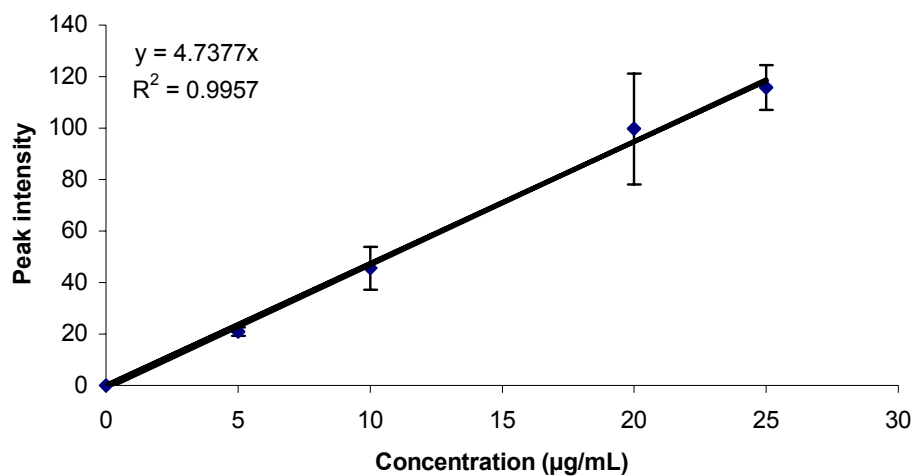
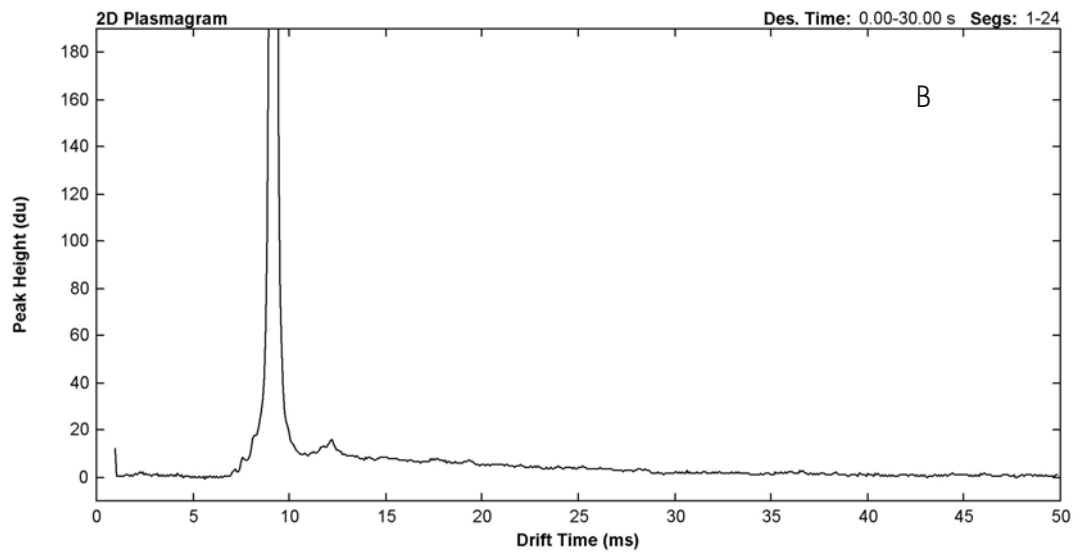
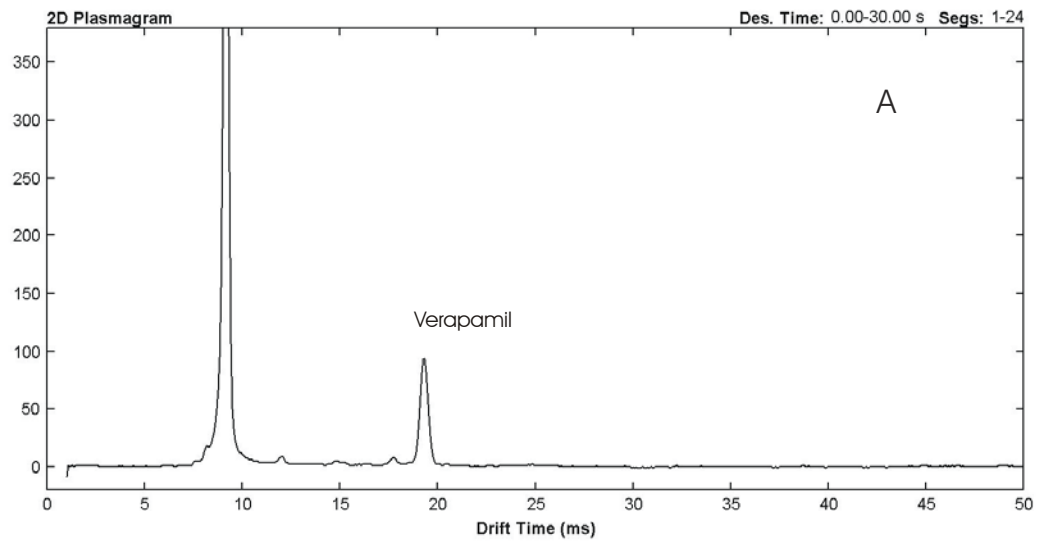


Figure 3.8: Verapamil calibration curve.

of this SPME/SELDI-IMS method ranged from 8-21%. The difference between the fiber coatings, and the fluctuation of the laser energy account for the high RSD values. These factors could be minimized by optimizing the coating procedure to improve the reproducibility between fibers, and employing an apparatus to stabilize the laser energy output. The detection limit was estimated to be $2 \mu\text{g mL}^{-1}$ in urine, based on a 3:1 signal to noise ratio.



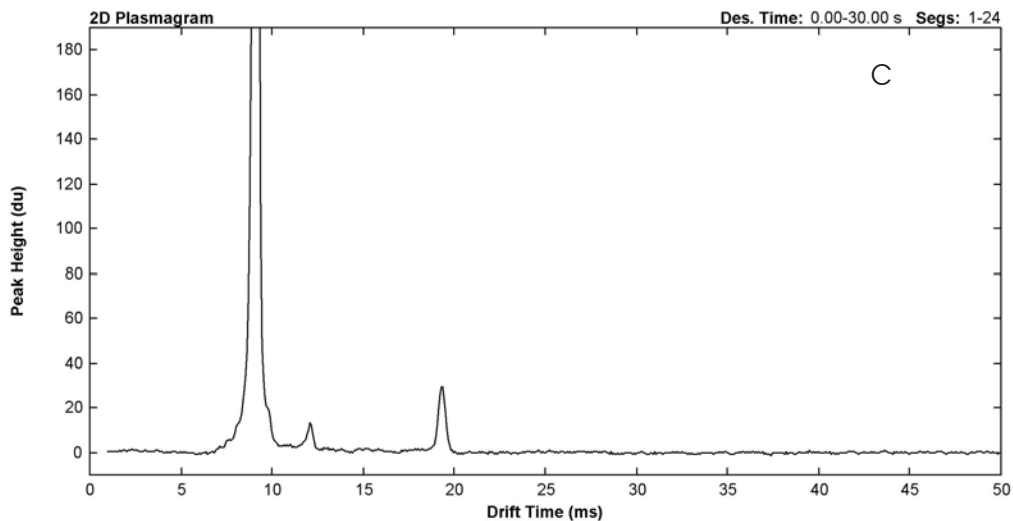


Figure 3.9: Ion mobility spectra of (A) verapamil, (B) $10 \times$ diluted blank urine, and (C) verapamil spiked urine sample.

3.4 Conclusion

A new SPME/SELDI-IMS system was constructed and evaluated. A laser was employed to introduce the SPME extracted analytes to an IMS device. $250 \mu J$ and 20 Hz were determined as the optimum laser parameters. The extraction parameters for verapamil were investigated. Direct extraction from urine sample was performed using PPY coated SPME/SELDI fiber without any further cleanup, and a $2 \mu g mL^{-1}$ detection limit in urine sample could be obtained. The analysis of the urine sample (including the sample preparation) could be done within minutes. The combination of the simplified sample preparation with SPME and fast analysis with IMS makes SPME/SELDI-IMS a potential tool for the fast screening of drugs.

Chapter 4

Evaluation of SPME/SELDI

Coatings

The preparation of three SPME/SELDI coatings, PPY, polythiophene (PTH), and polyaniline (PAN) were described here. The characterization of the coatings, including morphology, laser energy profile, and the capacity of the coatings are also discussed here.

4.1 Experimental

4.1.1 Chemicals

Pyrrrole, aniline, thiophene, anhydrous ferric chloride, TOAB, hydrochloric acid were purchased from Sigma-Aldrich (St. Louis, MO). Ammonium persulfate was

purchased from BDH Chemicals (Toronto, ON, Canada). HPLC grade ethanol, methanol, isopropanol, chloroform and nanopure water were used for all of the experiments.

4.1.2 Preparation of SPME Fibers

High OH silica optical fibers with core diameters of 600 μm were purchased from Polymicro Technologies Inc.(Phoenix, AZ) for the performance assessment of different optical configurations. The connector ferrule, F-112 epoxy glue, polishing disc and polishing films (5, 3, 1 and 0.3 μm) were purchased from Thorlabs Inc.(Newton, NJ). The silica optical fibers were cut into 1-meter sections with a capillary cutter from Restek (Bellefonte, PA). One end of the optical fibers was glued to a connector ferrule with F-112 epoxy glue from Thorlabs Inc.(Newton, NJ). After 24 hours curing time, this fiber connector end was polished with polishing films to ensure maximum light throughput. The other end of the optical fiber, hereafter called the sampling end, was coated with a polymer coating and used for the extraction. About 1 cm of the optical fiber was first cut from the sampling end, to ensure a fresh clean working surface. Then the fiber tip was etched with 400-grit silicon carbide polishing paper. The etching step ensured that the polymer adhered to the fiber tip. The tip was then sonicated in methanol to remove any impurities on the fiber tip. After the fiber tip was rinsed with water, it was ready for the coating process.

When the fibers were prepared for the capacity evaluation trial with a GC,

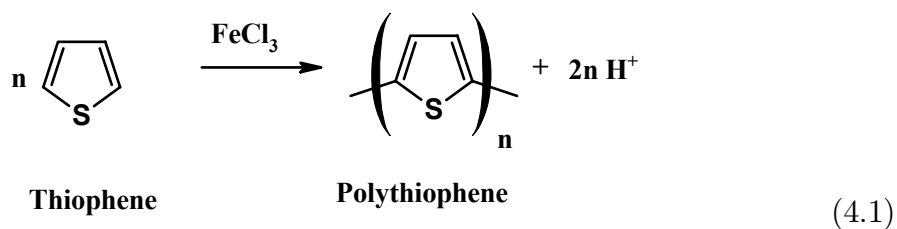
about 2 cm of fiber from the tips was carefully covered with silicone gel. This was done to ensure the coating was only deposited on the fiber tips. Therefore only the analyte extracted by the fiber tips could be desorbed and analyzed.

4.1.3 Preparation of PPY Coated Fibers

The preparation of PPY coated fibers is described in Chapter 2.

4.1.4 Preparation of PTH Coated Fibers

Polythiophene coated fibers were prepared using the chemical polymerization method shown in Equation 7.5.^[93] A total of 2.4 g of FeCl_3 was first thoroughly dried at about 100 °C in a reaction flask for one hour under reduced pressure with the presence of dry nitrogen gas. This drying step was followed by the addition of 50 mL of dry chloroform. Up to 10 optical fibers were prepared in the same flask by dipping the tips in the FeCl_3 and CHCl_3 mixture. Subsequently, 0.42 g of thiophene monomer was added dropwise into the mixture with stirring. The reaction mixture was then stirred for 48 hours at room temperature under a continuous flow of nitrogen. The fibers were then removed and rinsed with methanol. A dark-red color coating could be observed after ferric chloride was rinsed off from the fiber tips.



4.1.5 Preparation of PAN Coated Fibers

2 mL aniline was dissolved in 30 mL of pre-cooled (1 °C) 1 M HCl. 1.15 g APS was dissolved in 20 mL of 1 M HCl which had been pre-cooled in an ice bath to 1 °C. The aniline solution was placed in a 100 mL flask with a magnetic stirring bar. The flask was placed in an ice bath on a magnetic stirring plate. The SPME fibers were immersed in the solution at a depth of 2 mm. The APS solution was added to the aniline solution dropwise within one minute with constant stirring. Three to five minutes after all of the APS was added to the flask, the solution started to change from a blue-green hue to intense blue-green with a coppery glint. The solution was stirred for 1.5 hours, and the temperature was maintained below 5 °C. The fibers were then removed and rinsed with methanol. A blue-green color coating could be observed on the fiber tips.

4.1.6 Sampling Process

TOAB stock solution was prepared to a 10 mg mL⁻¹ with ethanol, and then diluted with ethanol to the desired concentration. The extraction process involved the immersion of the SPME fiber tip in the sample solutions at a depth of 2-3 mm.

Unless otherwise stated, the extraction times for TOAB was 1 minute. The side of the fiber was wiped with a Kimwipes[®] and MeOH. The tip was then air dried for 2 minutes.

4.1.7 Instrumentation

The Q-switched Nd: YAG laser, with an emitting wavelength of 355 nm, was purchased from New Wave Research Inc.(Fremont, CA). Laser energy emitted from the sampling end of the SPME/SELDI fiber was detected with a portable pyroelectric single-channel joule meter (Molelectron, Portland, OR). The SPME/SELDI-IMS experiments were performed on a modified IONSCAN model 400B (Smiths Detection, Mississauga, ON, Canada) ion mobility spectrometer. The details of the SPME/SELDI-IMS technique are described in Chapter 3.

IMS was programmed in the positive mode, using nicotinamide as the calibrant. The drift tube length was 7 cm and the drift field was 214 V cm^{-1} . The drift tube temperature was maintained at $234 \text{ }^\circ\text{C}$, and the heater for the desorber was disabled. The drift and exhaust flow rates were set to 300 mL min^{-1} . The sampling time was 30 s, and the scan range was 50 ms. The shutter width was set at $200 \text{ } \mu\text{s}$.

The coating capacity evaluation was performed with a SRI 9300B GC-FID system (SRI instruments, Torrance, CA). The column was a 1 m 0.53 mm MXT-5 silicosteel[®] GC column (Restek, Bellefonte, PA) with a $1.00 \text{ } \mu\text{m}$ coating thickness. The temperature of the GC oven was initially held at $70 \text{ }^\circ\text{C}$ for 0.5 min, then ramped to $300 \text{ }^\circ\text{C}$ at $20 \text{ }^\circ\text{C min}^{-1}$. The hydrogen carrier gas flow rate was set at 10

$mL\ min^{-1}$. Extracted analytes were then desorbed in methanol and injected into the GC for analysis.

The laser repetition rate was set at 20 Hz. Unless otherwise indicated, the laser energy was $250\ \mu J$ when coupled to IMS. The SEM images were taken with a LEO 1530 field emission scanning electron microscope (SEM). The accelerant voltage was set at 10 kV.

4.2 Results and Discussion

4.2.1 Characteristic of Coatings

The morphology of the coatings was examined with SEM. The magnification of these SEM images was 50K. As shown in Figure 4.1, the PPY coated fiber tip was covered with cauliflower shaped PPY coating, and the surface was porous. The PTH coated fiber tip was covered by a filament-shaped coating. The PAN coated fiber tip looked smoother than the other two coatings at the same magnification. The SEM image of the PAN coating at a 100K magnification (not shown here) exhibited a surface covered with very small ball-shaped polymers.

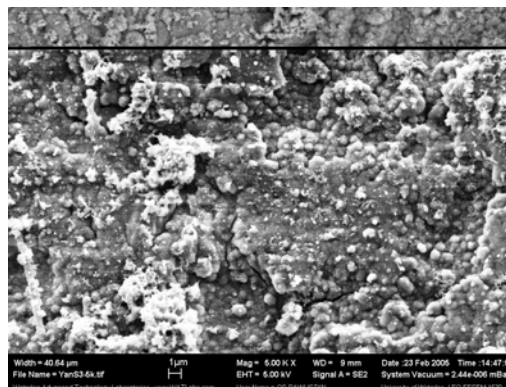
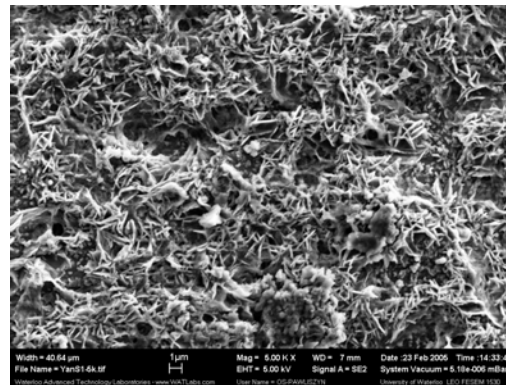
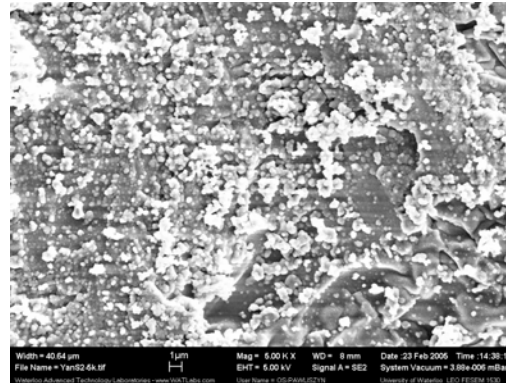


Figure 4.1: SEM images of PPY (upper pane), PTH (middle pane) and PAN (bottom pane) coated fiber tip.

4.2.2 Laser Energy Profiles

The laser energy profiles of the three coatings were examined with IMS. The laser energy profile of PPY coating was discussed in Chapter 3. The maximum signal intensity of the protonated molecular ion could be obtained at a laser energy of 250 μJ when desorbed from the PPY coating.

Similar laser energy profiles were also obtained with the PTH and PAN coatings. The intensity of protonated ion reached the maximum at 250 μJ . The relative intensities of protonated ion over cluster ion were different for the three coatings. The difference on the relative intensities might be explained with the difference between the structure of coatings effected the ionization process.

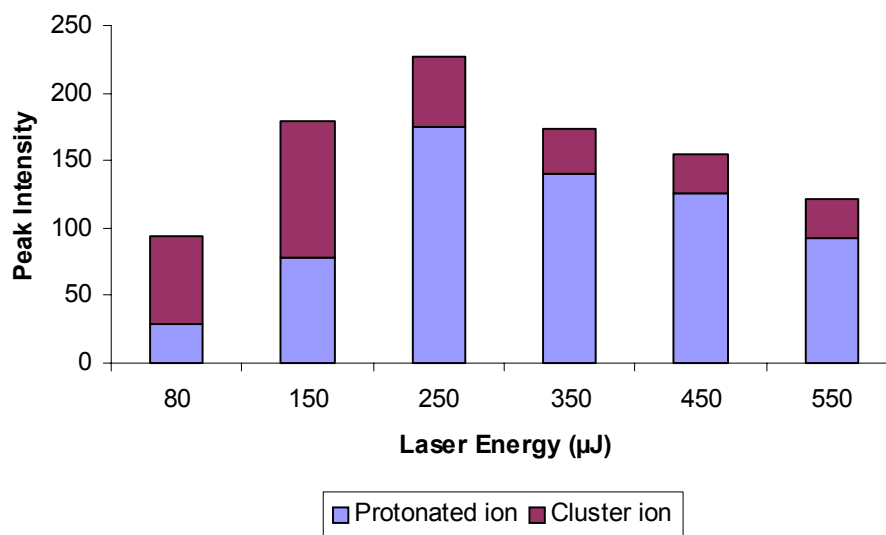


Figure 4.2: Laser energy profile obtained with PPY fibers.

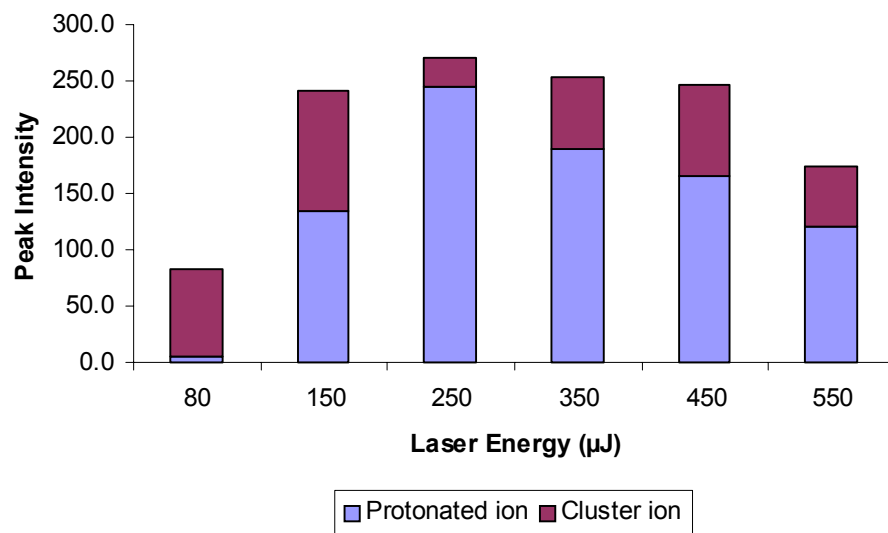


Figure 4.3: Laser energy profile obtained with PTH fibers.

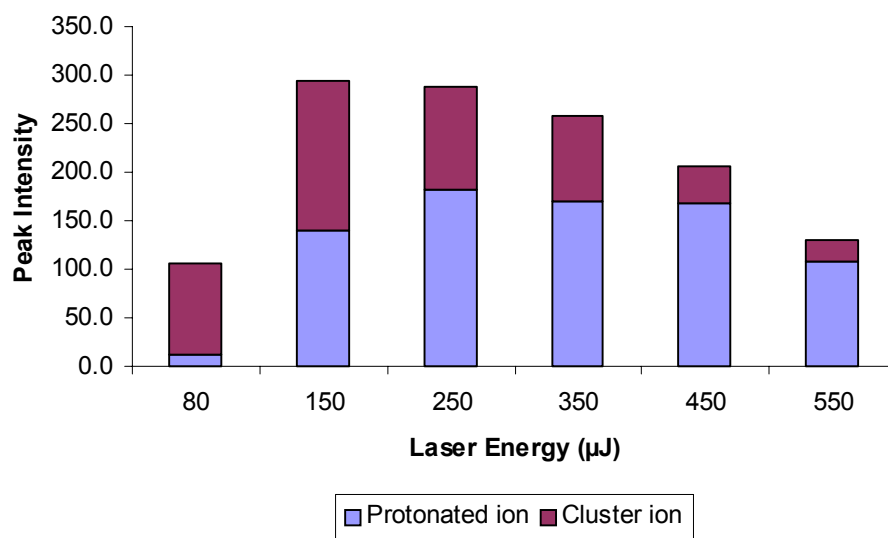


Figure 4.4: Laser energy profile obtained with PAN fibers.

4.2.3 Comparison of Coating Capacities with GC

The capacity of the coatings was estimated with a GC. TOAB was chosen as the test compound. The calibration curve (Figure 4.5) was first obtained by injecting 1 μL of TOAB solution at various concentrations.

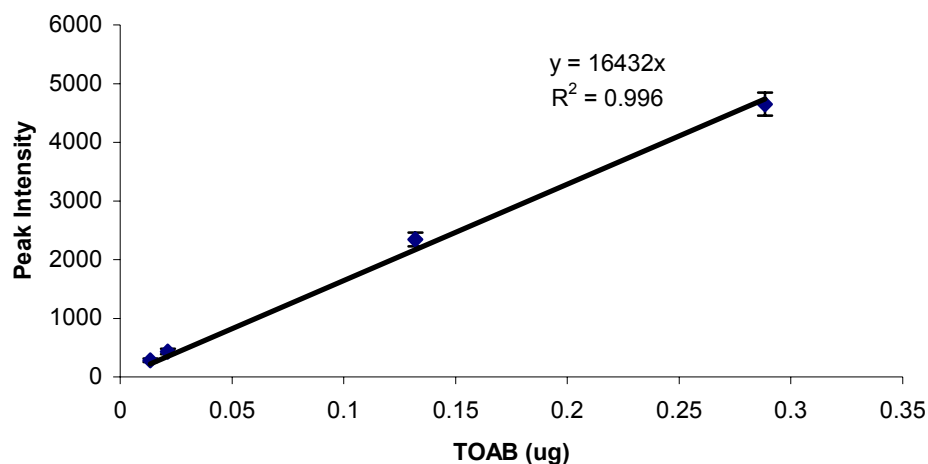


Figure 4.5: Calibration curve of TOAB obtained with GC.

The extraction was performed with 5 fibers for each coating. The 5 fibers extracted from 1 mL of 1.24 mg mL^{-1} TOAB in a EtOH: Water (2:3) solution for 10 minutes. The fibers were removed and wiped the side with a KimWipe[®] and MeOH. Then the fibers were left to air dry for 2 minutes. The fibers were desorbed in 50 μL MeOH for 2 minutes following the extraction. Then the volume of MeOH solution was reduced to 2-5 μL with nitrogen. This desorbed solution was injected into the GC for analysis. The amount extracted by each coating was calculated and shown in Figure 4.6. The PPY coated fiber exhibited the highest capacity.

The capacity of the PAN fiber was about 30% less than that of the PPY fiber, and the capacity of the PTH fiber was approximately 50% less than that of the PPY fiber. This result confirmed the observation achieved with IMS, which illustrated that the highest signal intensity could be obtained with PPY coated fibers.

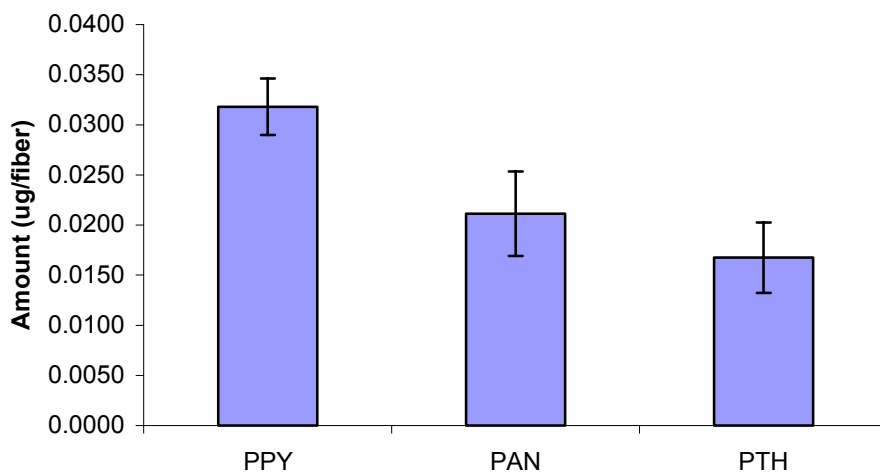


Figure 4.6: Comparison of coating capacities.

4.3 Conclusion

Three electroconductive polymers, PPY, PTH and PAN were prepared and tested with IMS and GC. It was observed that the PTH and the PAN coating could also be used as a surface to facilitate the ionization without a MALDI matrix, according to the results obtained with IMS. The laser energy profiles were also plotted, and the highest protonated ion intensities were also observed at 250 μJ laser energy for both the PTH and the PAN coating.

The capacity of the three coatings was evaluated with GC. The PPY coating exhibited the highest capacity among the three coatings. The performance of the PAN coating was superior to the PTH coating according to results obtained with GC. However, in the preliminary SPME/SELDI-MS experiment (result not shown in here), when the PAN coated fiber was evaluated, a series of background peaks from the coating were observed in the mass spectrum. Therefore, PPY and PTH coatings were used for further SPME-mass spectrometry experiments.

Chapter 5

Study of Ionization Mechanism for PEG

5.1 Introduction

After the introduction of MALDI and electrospray ionization to IMS, the application of ion mobility spectrometry has been extended to the analysis of biomolecules and synthetic polymers.^{[94]–[97]} The confirmation studies of complexes formed between alkali metal ions and synthetic polymers have been investigated extensively.^{[97]–[96]} Most of the reported studies employed MALDI-IMS/MS to obtain information about the cross section and the m/z value of the analytes. As the SPME/SELDI-IMS device used in this study was not combined with a mass spectrometry, the information that could be obtained was limited. However, the ionization mechanism for PEG could still be investigated with this device, and the exper-

imental results helped gain a better understanding of the ionization process on the PPY surface. The results obtained with IMS were confirmed with SPME/SELDI-QTOF MS. It was observed that when PEG was desorbed and ionized from the PPY surface, cationization occurred. Both potassium and sodium adducted ions were obtained. This observation is in agreement with the results obtained with other methods.

5.2 Experimental

5.2.1 Chemicals

Pyrrole, potassium sulfate, sodium sulfate, poly(propylene glycol) with average molecular weight of 400, poly(ethylene glycol) with average molecular weights of 200, 400, 600 and 1300-1600 were purchased from Sigma-Aldrich (St. Louis, MO). Ammonium persulfate was purchased from BDH Chemicals (Toronto, ON, Canada). The α -cyano-4-hydrocinnamic acid MALDI matrix was purchased from Agilent (Palo Alto, CA). HPLC grade ethanol, methanol, isopropanol and deionized water were used in all of the experiments.

5.2.2 Preparation of PPY Coated Fibers

High OH silica optical fibers with core diameters of 600 μm were purchased from Polymicro Technologies Inc.(Phoenix, AZ). The preparation procedure for these

fibers is described in Chapter 2.

5.2.3 Sampling Process

PPG 400, PEG 200, 400, 600 and 1300-1600 were dissolved in ethanol at a 10% (v:v) concentration. The potassium sulfate and sodium sulfate stock solutions were prepared in 1% (w:v) aqueous solution. This solution was then added to the PEG 400 solution to dilute it to 0.001%. The extraction process for IMS analysis involved immersion of the SPME fiber tip in the sample solutions at a depth of 2-3 mm shortly, then quickly removed and air-dried for 2 minutes. The volume of the sample solution was determined to be less than 0.1 μL .

5.2.4 Instrumentation

Experiments were performed on a modified IONSCAN model 400B (Smiths Detection, Mississauga, ON, Canada) ion mobility spectrometer, and Micromass Voyager QTOF mass spectrometer (Milford, MA). The Q-switched Nd: YAG laser, with an emitting wavelength of 355 nm, was purchased from New Wave Research Inc.(Fremont, CA, US). Laser energy emitted from the sample end of the SPME/MALDI fiber was detected with a portable pyroelectric single-channel joule meter Molelectron EM400 (Portland, OR, US).

Coupling SPME/SELDI to IMS Model 400B

The coupling of SPME/SELDI to IMS 400B has been described in Chapter 3. The experiments in this chapter were performed with two different ionization methods. One method involved the use of a ^{63}Ni source and the SPME/SELDI fiber was used to introduce analytes without firing laser pulses. The other method involved the use of laser pulses to desorb and ionize the analytes from the SPME/SELDI fiber without the use of ^{63}Ni source. IMS was programmed in the positive mode, using nicotinamide as the calibrant. The drift tube length was 7 cm and the drift field was 214 V cm^{-1} . The drift tube temperature was maintained at $234\text{ }^{\circ}\text{C}$, and the heater for the desorber was disabled. The drift and exhaust flow rates were set to 300 mL min^{-1} . The sampling time was 30 s, and the scan range was 50 ms. Unless otherwise indicated, the shutter width was set at $200\text{ }\mu\text{s}$.

Coupling of SPME/SELDI Fiber with Micromass QTOF MS

SPME/SELDI fiber was also coupled to a Micromass Ultima[®] QTOF mass spectrometer. The schematic diagram of this set up was shown in Figure 5.1. The nanospray source was removed. The original cone was replaced with a homemade sample cone with a larger hole (1 mm diameter) in the middle of the cone, for the insertion of the $600\text{ }\mu\text{m}$ SPME/SELDI fiber. The optimal depth of SPME/SELDI inserted in the sample cone was determined to be 2.5 cm. After sample extraction, the analytes were desorbed and ionized from the PPY coated fiber and analyzed by the QTOF MS.

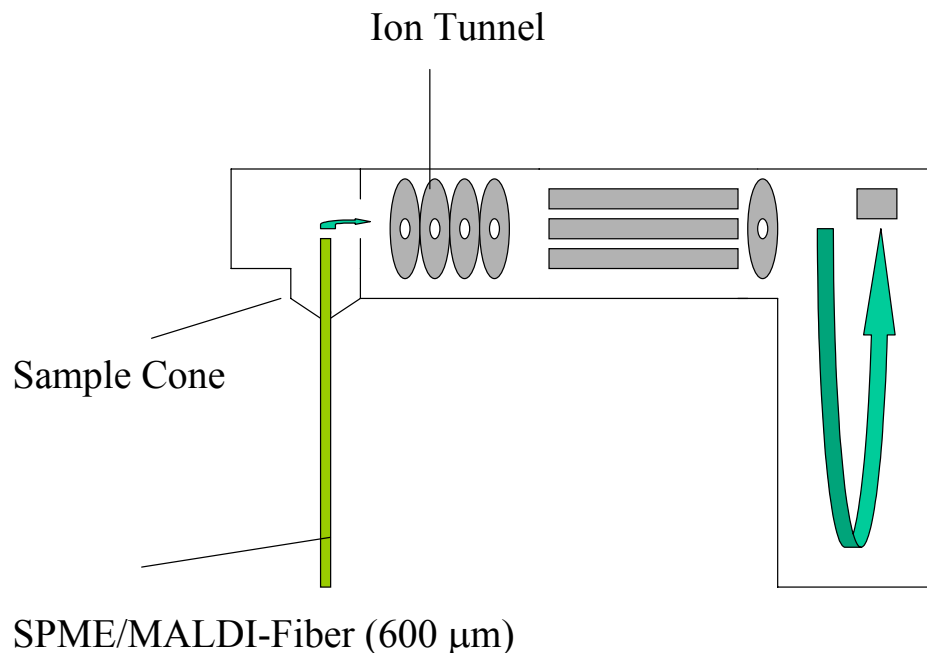


Figure 5.1: Schematic of SPME/SELDI-Micromass QTOF MS.

5.3 Results and Discussion

5.3.1 Comparison of Laser Desorption/Ionization and ^{63}Ni Ionization

Because samples could be ionized by ^{63}Ni ion source or by laser desorption/ionization with this SPME/SELDI-IMS device, the same analytes were examined with these two ionization methods and results are presented in this section. The drift times of the PEG peaks and the K_0 value calculated by Equation 5.1 are listed in Table 5.1.

$K_{0_{cal}}$ was the reduced mobility of nicotinamide, known as $1.88 \text{ cm}^2 \text{ V}^{-1} \text{ s}^{-1}$,

Peaks	Drift time (ms)	Cal. K_0 ($cm^2 V^{-1} s^{-1}$)	Cal. Mass (amu)
1	14.984	1.1382	326
2	16.009	1.0632	362
3	17.212	0.9889	402
4	18.443	0.9229	441
5	19.946	0.8533	487
6	20.826	0.8173	512

Table 5.1: PEG 400 peaks produced by Ni radioactive ionization.

and t_{cal} was the drift time of nicotinamide calibrant. The masses in Table 5.1 were calculated based on the mass-reduced mobility calibration curve shown in Chapter 3. In most cases, the method provides an approximate estimate of the ionic masses within 1-3% accuracy with the K_0 determination.

$$K_0 = \frac{K_{0cal} \cdot t_{cal}}{t_d} \quad (5.1)$$

The reduced mobility could also be calculated by Equation 5.2, when the nicotinamide calibrant peak was absent due to the removal of the ^{63}Ni ion source.

$$K_0 = \left(\frac{L^2}{t_d \cdot V} \right) \left(\frac{273}{T} \right) \left(\frac{P}{760} \right) \quad (5.2)$$

where L is drift length of the ion mobility drift tube in cm, V is the drift voltage, t_d is the drift time in second, T is drift tube temperature in K, and P is the pressure

Peaks	Drift time (ms)	Cal. K_0 ($cm^2 V^{-1} s^{-1}$)	Cal. Mass (amu)	Mass Difference (amu)
1	17.017	1.0002	396	70
2	18.134	0.9386	432	70
3	19.365	0.8790	470	68
4	20.663	0.8237	508	67
5	21.990	0.7740	544	57
6	23.293	0.7307	579	57

Table 5.2: PEG 400 peaks produced by laser desorption/ionization.

of drift gas in torr.

Laser desorption and ionization PEG was also performed with the PPY coated SPME/SELDI fiber. The drift times were listed in Table 5.2. The drift times of the laser ionized peaks were longer than those from the ^{63}Ni produced ion peaks. The calculated reduced mobility and mass values showed that larger ions were produced by laser ionization. The mass difference between the laser produced ions and the ^{63}Ni produced protonated ions were calculated to be around 70 amu. This difference could be attributed to the addition of hydrated sodium $Na(H_2O)_3$ or hydrated potassium ion $K(H_2O)_2$. However, the calculated masses were only approximate values, and more information was needed to confirm the identity of the laser produced peaks.

5.3.2 Addition of of Alkali Metal Ions

Because hydrated sodiated ions and hydrated potassiated ions might both be present in an ion mobility spectrum, potassium and sodium ions were added to the sample solution to help identify the laser produced peaks. It was expected that the alkali metal ions increasing the peak intensities should be those associated to analyte molecules. Thus, 0.001% potassium sulfate and sodium sulfate were added to the PEG solution, respectively. Higher alkali ion concentration, such as 0.01% are not suitable for this experiment, as this would precipitate the PEG during the preparation of the sample solution. CHCA matrix was also added to the PEG solution with a 1:1 ratio, to exam its effect on the ionization process. If the laser produced ions were protonated molecule ions, then the addition of CHCA matrix should have increased the intensity of all the peaks.

The results are shown in Figure 5.2. The addition of the potassium ions increased the peak intensities by over 60%, and the addition of the sodium ions decreased the peak intensities. This suggests that these ions might be potassium hydrated ions. The observation that the adding of the CHCA matrix did not increase the peak intensities also supports this conclusion. The reason why the addition of the sodium ions decreased the peak intensities is not clear.

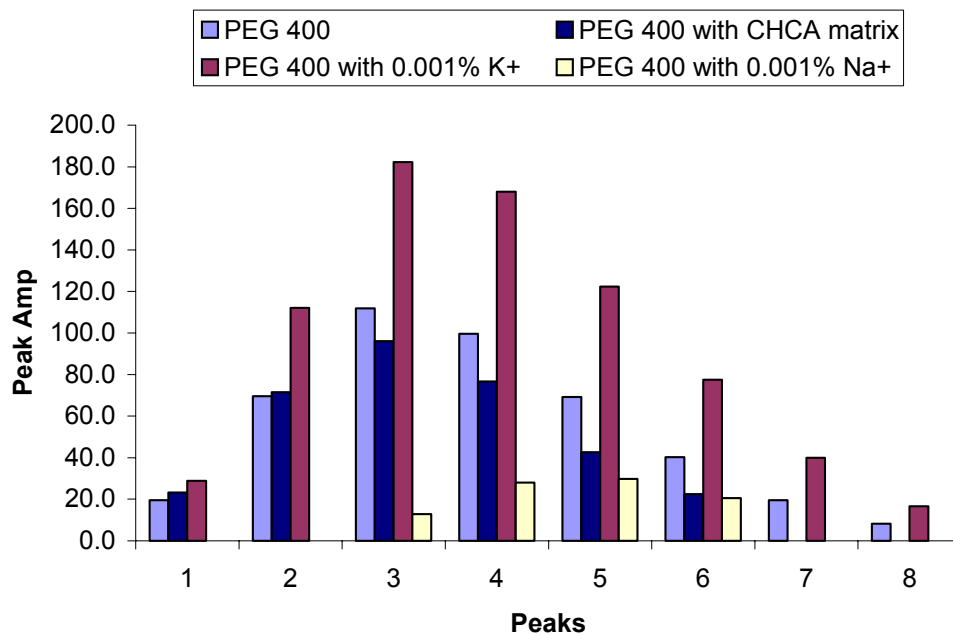


Figure 5.2: Comparison of the peak intensities with the addition of alkali metal ions.

5.3.3 Confirmation with SPME/SELDI Coupled to QTOF MS

As the information about the mass of the laser produced ions could not be obtained with IMS, the same experiment was conducted with a Micromass QTOF MS. The mass of the ions is shown in Table 5.3.

Both sodiated and potassiated ions were observed in all of the spectra. If the relative intensities of the potassiated and sodiated ions are compared, the intensities of the potassiated ions were higher than those of the sodiated ions in all of the spectra. The intensities of the sodiated ions were still lower than those of the

n	[PEG+Na]⁺	[PEG+K]⁺
(No. of monomer units)	(amu)	(amu)
9	437.19	453.19
10	481.24	497.21
11	525.25	541.24
12	569.26	585.26
13	613.31	629.27
14	657.34	673.29
15	701.37	717.33
16	-	761.31

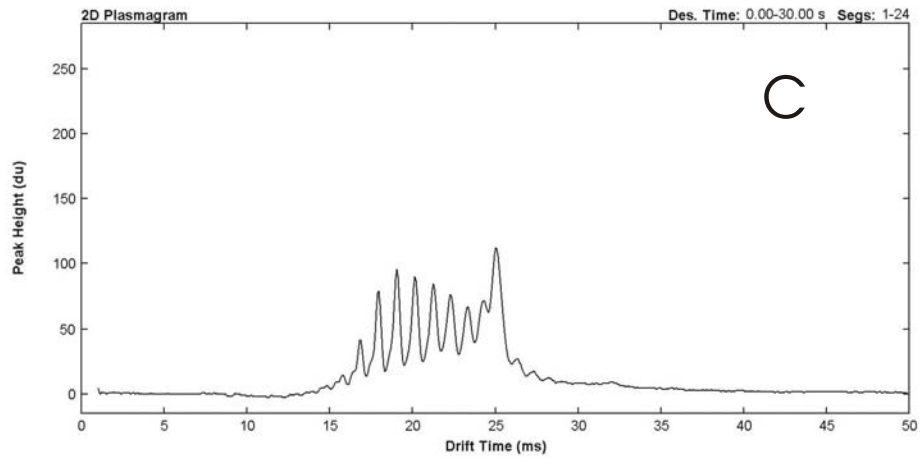
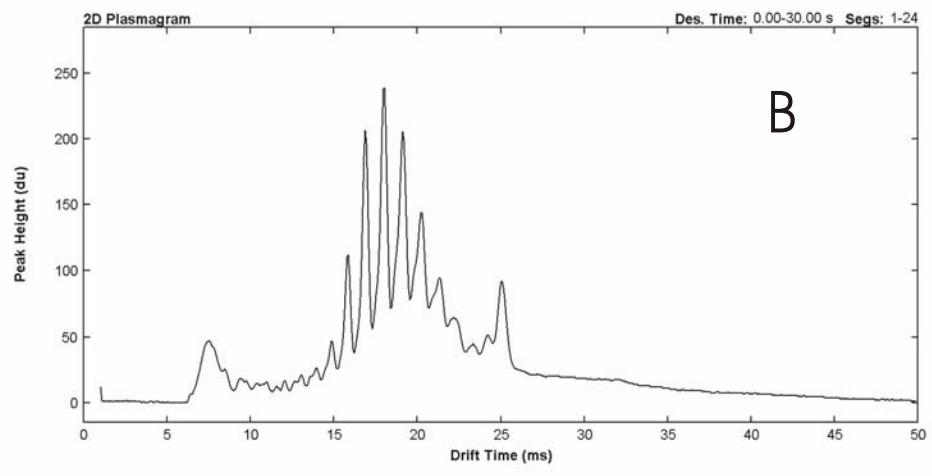
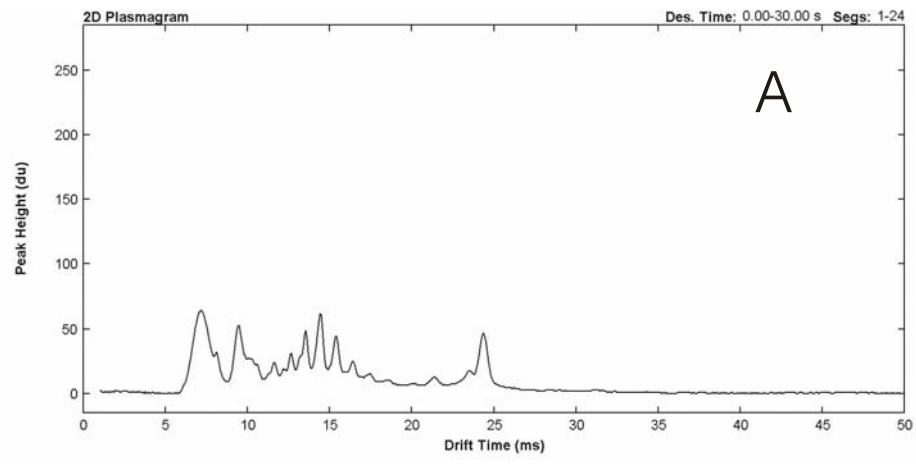
Table 5.3: Mass table of laser produced ions.

potassiated ions, even with the addition of the sodium ions. This phenomenon is different with the findings of Chen and co-workers.^[100] In their work, PEG 400 was directly ionized from the pencil line on a silica gel TLC plate with UV laser. The intensities of the sodiated ions were higher than those of the potassiated ions in the spectrum. The different substrates, PPY vs pencil line on silica gel, might account for the difference among the peak intensities. The lack of protonated ions indicates that the ionization that occurred on PPY surface was mainly cationization, not protonization.

5.3.4 Application

Five polymers, PEG 200, 400, 600, 1300-1600 and PPG 400 were examined with the SPME/SELDI-IMS device. The spectra are shown in Figure 5.3. The concentration of the sample solution was 1 mg mL^{-1} for all of the analytes. The extraction time was maintained at 1 minute. The drift times in the spectra ranged from 10 to 20 ms for PEG 200 (Figure 5.3A), 15 to 25 ms for PEG 400 (Figure 5.3B) and 17 to 30 ms for PEG 600 (Figure 5.3C). The drift times increased as the molecular weight increased. However, in the PEG 1300-1600 spectrum (Figure 5.3D), the overlapped peaks ranged from 10 to 30 ms, suggesting the presence of fragment peaks. This might be explained by the presence of molecule ions that were too large to be detected by IMS. These spectra exhibit improved resolution compared with those reported in the literature.^[80] The distribution of PPG 400 peaks (Figure 5.3E) was different than that of PEGs' peaks. In addition, the drift times for these peaks were approximately from 18 to 27 ms, which were longer than those for the PEG 400 peaks. The mass difference between the two monomers might account for this observation.

In summary, these ion mobility spectra demonstrate the potential of using SPME/SELDI-IMS for the fast identification of different synthetic polymers.



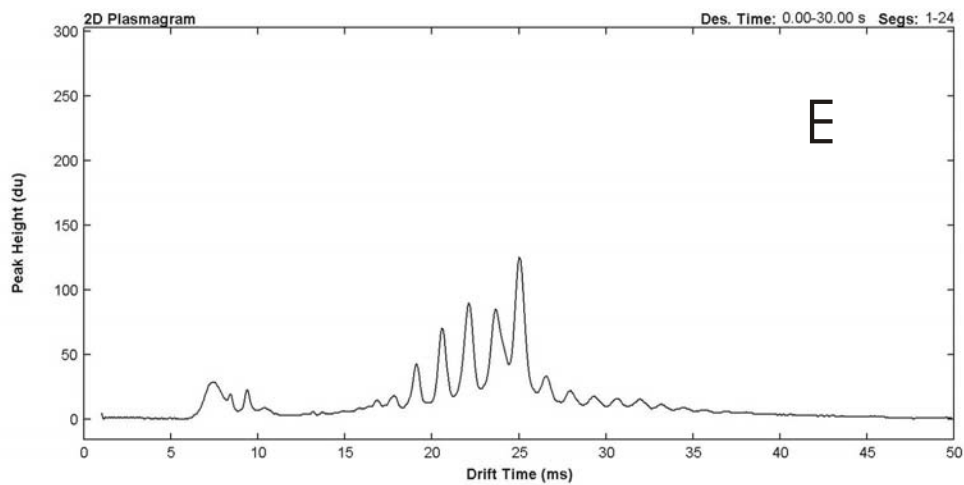
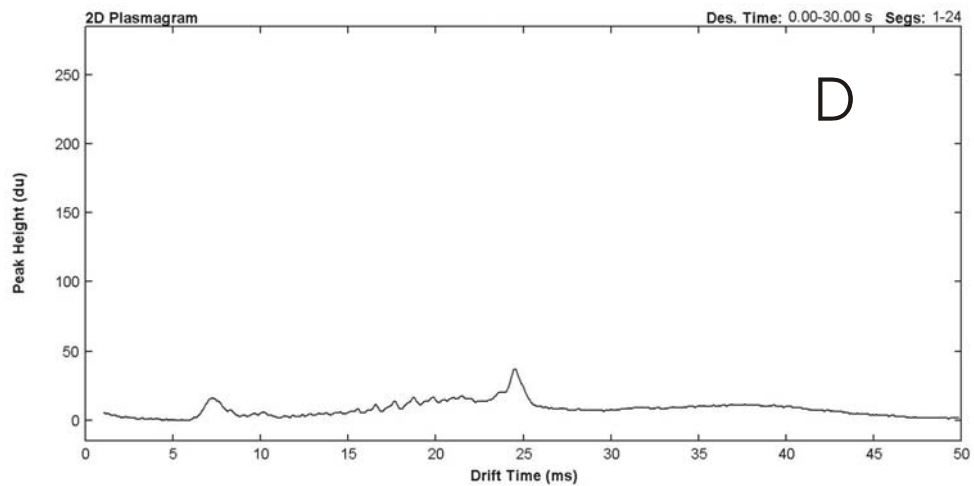


Figure 5.3: Ion mobility spectra of synthetic polymers. A. PEG 200; B: PEG 400; C. PEG 600; D: PEG 1300-1600; E: PPG 400.

5.4 Conclusion

In this chapter, laser desorption SPME/SELDI coupled to IMS was employed for the analysis of non-volatile synthetic polymers. The ionization mechanism of PEG 400 was studied with this device. It was found that the potassiated ions and sodiated ions were both present in the ion mobility spectra. Alkali metal ions were added to the PEG solution to facilitate the interpretation of the laser produced ions. The addition of the potassium ions increased the intensity of the potassiated ion, but the addition of the sodium ions caused a decrease in the peak intensities. The results obtained with QTOF MS confirmed the present of both potassiated and sodiated ions. This result confirmed that cationization might be the main ionization process when polymers are directly ionized from a PPY coated silica surface.

Four PEGs with different average molecular weights and PPG 400 were also tested with this SPME/SELDI device. The ion mobility spectra of these polymers could be used for the fast identification of synthetic polymers, as the difference between the spectra reflected the difference between the structures.

Chapter 6

The Coupling of SPME/SELDI with Mass Spectrometry

6.1 Introduction

Matrix-assisted laser desorption/ionization, developed in the middle of the 1980s, [29] has become one of the most powerful tools to analyze biomolecules. However, it has been a challenge to use MALDI for the analysis of low-mass analytes, because of the presence of matrix related ions in the low mass range of spectra. The choice of the matrix, the analyte to matrix ratio and the method used to apply the matrix can all influence the ionization efficiency dramatically. These factors are critical to obtaining a higher sensitivity. The optimization of these parameters is time consuming, thus limiting the utility of MALDI-TOF in several important applications, including automated, high-throughput analysis.

Efforts have been made, and several approaches have been developed to overcome these limitations. Inorganic compounds have been used as a matrix since the development of the MALDI technique. The use of ultrafine metal powder in protein analysis was first reported by Tanaka et al.^[28] and Karas^[29] in 1988. Since then, many other inorganic materials including graphite particles,^[101] fine metal powder or metal oxide powder,^[102] silver thin-film substrates or particles^[103] and silica gel^[104] have been used in MALDI-MS analysis of small molecules. A systematic investigation of the experimental parameters of these studies were reported by Schürenberg et al. for peptides and proteins.^[50] However, these methods still required the optimizing of many experimental parameter, including the use of different particle materials, particle sizes and suspended liquids. Due to this reason, these inorganic materials were not suitable to be an alternative for matrix. It is understood that derivatives of benzoic acid, cinnamic acid and related aromatic compounds are also good matrices for peptides and proteins, due to these compounds can absorb UV light, and then transfer the energy to ionize the analytes.

Several matrix-free approaches have employed other materials,^{[39]–[56]} including silicon.^[39] SELDI (surface enhanced laser desorption/ionization) is one of the matrix-free techniques. A SELDI surface can be employed to transfer the laser energy to ionize the analytes instead of using a matrix. As an example, Laser desorption/ionization on porous silicon (DIOS) reported by Wei et al.^[39] has been very successful and has already been commercialized. In this technique, porous silicon is employed as a desorption plate, to which the sample solution is applied,

and then laser pulses are used to desorb and ionize the sample from the plate. This method is very efficient for molecules smaller than 3kDa.^[105] However, The DIOS surface needs to be very clean, thus limiting the use of this technique to directly analyse biological samples.

Lin and Chen have reported yet another approach, desorbing and ionizing peptides and small proteins from a sol-gel-derived 2,5-dihydroxybenzoic acid (DHB) film.^[55] By entrapping the commonly used matrix DHB in the polymer frame, matrix was no longer needed when the sample solution was added on this film. However, the concentration of DHB needed to be carefully controlled to avoid the presence of matrix-related peaks in the mass spectrum. Teng and Chen also used the same polymer as a SPME coating to couple SPME with laser desorption mass spectrometry,^[56] but the optical fibers used in their experiments were just the support of the sol-gel-derived DHB polymer. It was therefore necessary to tape the coated fiber on a MALDI plate for MALDI analysis.

Solid phase microextraction has been used in various applications and has been combined with a number of different analytical methods as a fast and convenient sampling technique. As mentioned previously, the traditional sample preparation procedure for MALDI MS is time consuming and multiple parameters need to be optimized to obtain acceptable sensitivity. The use of SPME for both sample preparation and a means of introduction for MALDI is a possible solution for these issues. A SPME/MALDI fiber was first proposed by Tong et al.,^[5] but in the study, the matrix was still used to aid the ionization of analytes.

PPY is a conductive polymer which can be used as an energy storage material, a corrosion resistant coating and a chemical sensor.^[106] PPY co-polymer membrane has also been used for gas separations.^[107] Recently, PPY and related copolymers were used as SPME fiber coating, subsequently coupled with LC/MS for the analysis of PAHs.^[7] The results exhibit better selectivity and sensitivity toward polar compounds and nonpolar aromatic semi-volatile compounds, compared with commercially available SPME products.

In this study, the results of the application of a PPY coated SPME/SELDI fiber are presented. The PPY coating on fiber tip is employed as the extraction phase and the surface to enhance the ionization of an analyte. The optical fiber is employed as the support of PPY coating, as well as the media to transfer UV laser light to the tip of the fiber, where the PPY coating is deposited. This SPME/SELDI technique accomplishes sampling, sample preparation and sample introduction on a single fiber. Moreover, free of matrix background, this technique is a promising method for quantitative analysis of small peptides and drugs.

6.2 Experimental

6.2.1 Materials

Tetraoctylammonium bromide (TOAB), leucine enkephalin, hydroperoxide, sulfuric acid, bovine serum albumin (reduced and carboxymethylated BSA), HPLC grade ethanol, acetone and isopropanol were purchased from Sigma-Aldrich (St. Louis,

MO). Hydrofluoric acid and ammonium persulfate were purchased from BDH (BDH Chemicals, Toronto, Canada). The α -cyano-4-hydrocinnamic acid MALDI matrix was purchased from Agilent (Palo Alto, CA). Prior to digestion, protein samples were prepared at 5 mg mL^{-1} in 50 mM ammonium bicarbonate (BDH Chemicals, Toronto, ON, Canada) buffer adjusted to pH 8.5 with ammonium hydroxide (Fisher Scientific, Nepean, ON, Canada). Digestions were carried out with a ratio of 20:1 protein:trypsin. Proteins were digested for 4 hours at 37 °C, and the digests were stored at -20 °C prior to use. Digests were reconstituted in water with 0.1% formic acid. Nanopure deionized water was used exclusively in these experiments.

6.2.2 Preparation of PPY SPME/SELDI Fiber

High OH silica optical fibers with core diameters of 600 μm were purchased from Polymicro Technologies Inc.(Phoenix, AZ). The preparation procedure was described in chapter 2.

6.2.3 Instrumentation

Experiments were performed using a prototype Q-TOF MS (MDS Sciex, Concord, ON, Canada) mass spectrometer, and a modified 4000 QTRAP[®] mass spectrometer (MDS SCIEX, Concord, ON, Canada) with a modified AP MALDI ion source as reported previously.^[108] The Nd:YAG laser used had an emission wavelength of 355 nm and was purchased from New Wave Research Inc.(Fremont, CA). Laser energy was detected with a Moletron EM400 laser energy meter, purchased from

Molelectron Detector Inc.(Portland, OR). A square linear translation stage from Edmund Industrial Optics (Barrington, NJ) was used to set up the outer optical to focus the laser onto the fiber connector. A 15 cm convex lens, purchased from Newport (Fountain Valley, CA), was used to focus the laser light.

6.2.4 SPME/SELDI-QTOF MS

A prototype Q-TOF mass spectrometer (MDS Sciex, Concord, ON, Canada) was employed in these experiments. To couple this device with the SPME/SELDI fiber, the electrospray ion source was removed. The SPME/SELDI fiber was inserted into a brass tube (I.D. 1 mm, 5 cm in length) and placed 5 mm in front of the orifice hole (Figure 6.1). A voltage of 3000 V was applied between the bronze holder and the orifice plate to repel the ions produced at the fiber tip into the mass spectrometer.

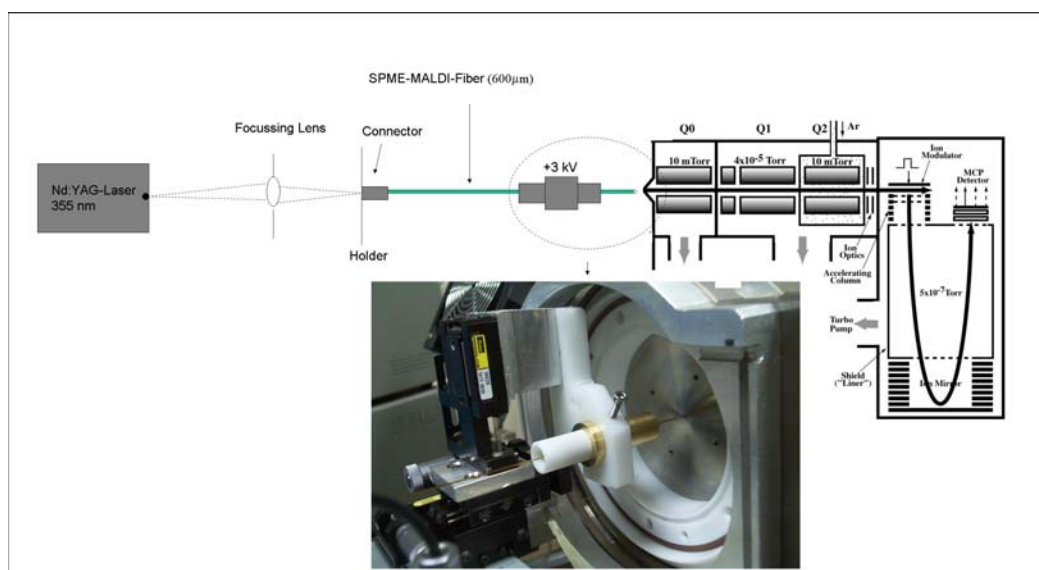


Figure 6.1: Schematic of SPME/SELDI-SCIEX prototype QTOF MS device.

Leucine enkephalin solution was prepared with water in concentrations range from 1 to 9 pmol μL^{-1} . The sample extraction process was same as mentioned above. Following the extraction step, the fiber was inserted into the brass holder, the laser pulse was fired manually and data was collected by the mass spectrometer.

6.2.5 SPME/SELDI-QqLIT MS

To further investigate the sensitivity of SPME/SELDI device, the SPME/SELDI fiber was also coupled to a high performance hybrid quadrupole-linear ion trap (QqLIT) mass spectrometer with a modified AP MALDI source (MDS Sciex, Concord, ON, Canada). This modified AP-MALDI source can improve the AP MALDI performance for peptides by a factor of approximately two over previous iterations, the details about the modified AP-MALDI source was described in Chapter 7.

The set-up was shown in Figure 6.2. The front flange of the AP-MALDI source was removed. An alligator clip was attached to the SPME fiber at about 1cm from the fiber tip. The other end of this clip was connected to the high voltage power supply to the MALDI plate. With the presence of the electroconductive polymer on the side, a high voltage could be applied on the SPME fiber tip to draw the ions into the MS. The voltage used in this experiment was 2000V.

Using the coated optical fibers, performance comparisons were made using two different laser illumination geometries. The first geometry involved attachment of the laser directly to the opposite end of the coated optical fiber in a similar fashion to experiments described above. With this configuration (hereafter referred to as

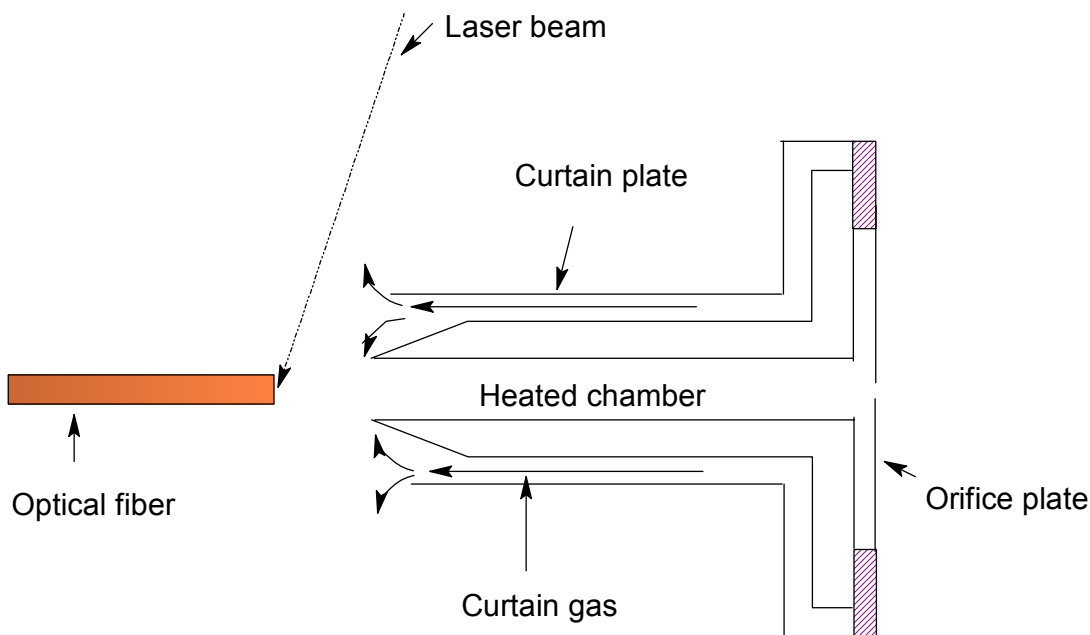


Figure 6.2: Schematic of the coupling of SPME fiber with Qtrap MS.

transmission geometry), the laser light was transmitted through the optical fiber ($600\ \mu\text{m}$), conductive polymer, and then sample extraction surface. This geometry essentially results in backside illumination of the polymer and sample. The second optical configuration (hereafter referred to as reflection geometry) involved attachment of the laser to the standard optics in the AP MALDI source ($200\ \mu\text{m}$ fiber) such that the light was directed at approximately a 28° angle to the front side of the fiber surface as described previously.^[108]

6.3 Results and Discussion

PPY coated SPME/SELDI fibers exhibited higher sensitivity than previous studies employing SPME/MALDI fibers. [5] Additionally, as well as transferring UV light to the sample end of the fiber, PPY coating can also act as the surface to help ionizing analytes. Additional experimental parameters were also investigated with the IMS, including the relationship between the extraction surface area and signal intensity, the relationship between concentration and signal intensity, as well as the laser desorption profile. The mass spectrum of a peptide leucine enkephalin, obtained using a PPY fiber, is presented and the detection limit was estimated for this analyte.

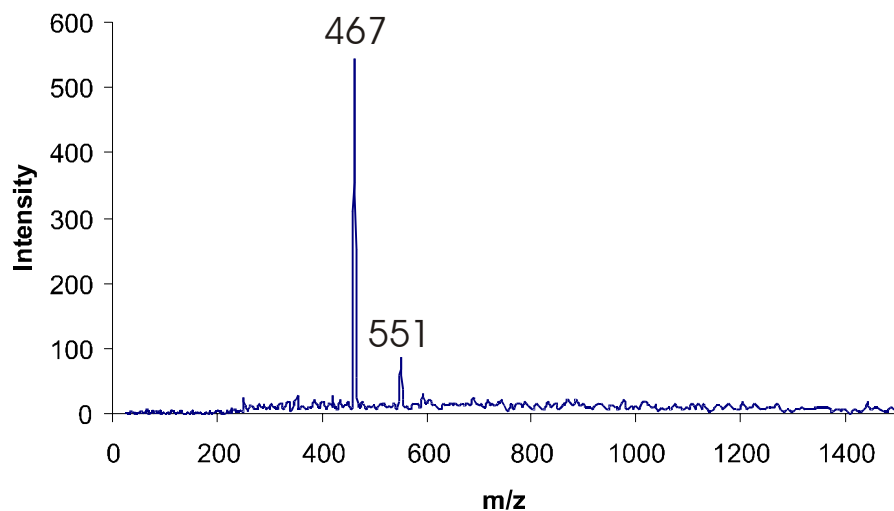


Figure 6.3: Mass spectrum of $1 \mu\text{g mL}^{-1}$ TOAB after extraction with the PPY SPME/SELDI fiber. Extractio time, 1min.

6.3.1 Results from Q-TOF MS

To verify that PPY can perform as an effective surface for ionization, the PPY coated fiber was coupled with the Q-TOF mass spectrometer as described above. First, the mass spectrum of a blank, freshly prepared PPY fiber was recorded, and no peaks were observed (Figure 6.4A). A $1 \mu\text{g mL}^{-1}$ TOAB solution was used as a model analyte. The mass spectrum of TOAB after 20 laser shots is illustrated in Figure 6.3. Only two peaks were observed, including m/z 467 from $[\text{N}(\text{C}_8\text{H}_{17})_4]^+$ and m/z at 551. The identity of the second peak is not known.

The performance of the PPY fiber was then evaluated with the peptide leucine enkephalin (M.W. 555). The PPY fiber was used to extract the analyte as previously described. Without using a matrix, three peaks were observed, at m/z 556, 578 and 594, which could be attributed to $[\text{M}+\text{H}]^+$, $[\text{M}+\text{Na}]^+$ and $[\text{M}+\text{K}]^+$ respectively (Figure 6.4B). Besides, further ions were detected as shown in Figure 6.4B. Additionally, the baseline is higher than in Figure 6.4A. The higher baseline may indicate that the interferences, such as PPY oligomers or other substances originating from the coating, were released when peptide leucine enkephalin was bounded to the coating.

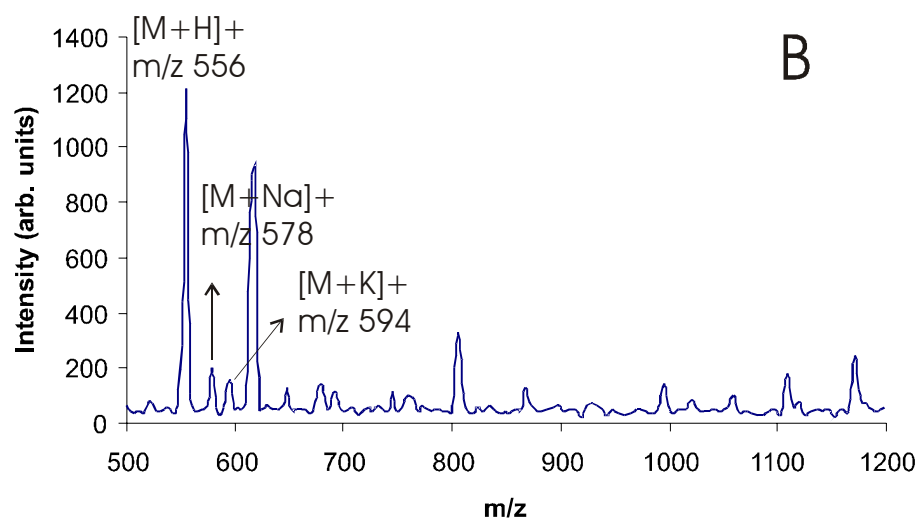
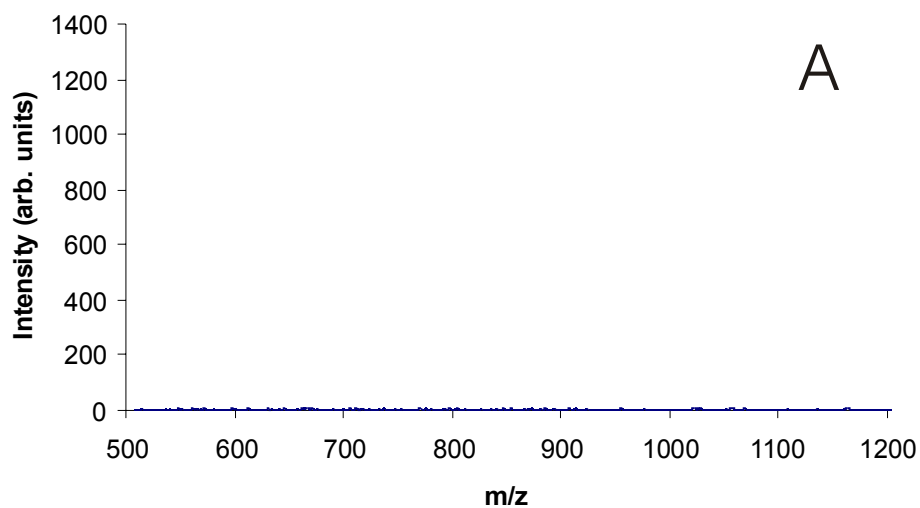


Figure 6.4: Mass spectra of (A) PPY fiber blank and (B) after extraction from $9 \text{ pmol } \mu\text{L}^{-1}$ leucine enkephalin from an aqueous solution without the addition of matrix. Extraction time, 1 min.

To estimate the sensitivity of the method, aqueous leucine enkephalin solutions in the concentration range 1-9 pmol μL^{-1} were tested. Under current experimental conditions, the detection limit was determined as 2.2 pmol μL^{-1} . Compared with other methods using reflection geometry for SELDI, these detection limits are high. For example, Schüürenberg et al. obtained a detection limit of 100 amol μL^{-1} for various peptides using prestructured 200 nm gold spots as the target surface with conventional MALDI.^[109] It is not clear why the detection limits of the present SPME/SELDI method are higher, because it was shown above that the analyte could be quantitatively desorbed from the tip by firing 30-50 laser shots with laser energy between 130 and 400 μJ . It is proposed that the higher detection limit of the SPME/SELDI method is due to two reasons. One is that the mass spectra shown here were obtained by a single laser shot, not the average or accumulation of signals obtained with a group of laser shots as used for conventional MALDI or SELDI. In addition, the ion transmission from the fiber into the mass spectrometer could be non-optimized and thus insufficient.

In order to investigate whether water molecules incorporated in the pores of PPY polymer contribute to the ionization process, storage conditions of the fibers were also evaluated in these studies. Two PPY fibers were prepared and coated at the same time; then one fiber was dried in nitrogen, while the other was soaked in water after being coated. A 9 pmol μL^{-1} leucine enkephalin was used as the analyte. No difference in intensity of the $[M+H]^+$ peak was observed, although the intensity of the $[M+K]^+$ peak obtained with the second fiber is higher than that of

the corresponding peak from the first fiber.

As for DIOS, the mechanism of how the surface helps to ionize the analyte is still not well understood. Possible reasons include that PPY polymer can both absorb and transfer UV light,^[110] which is also the main characteristic of commonly used MALDI matrices. PPY is a conductive polymer so it can transfer electrons, and electron transfer is one of the proposed mechanisms for MALDI.^[111] The results obtained for the PPY coating also demonstrated the possibility of using other conductive polymers as coatings of a SPME/SELDI fiber. However these results are preliminary in nature and more analytes need to be tested on this fiber to understand the full potential of using PPY fibers for other biomolecules, and the extent of the mass range that can be accessed.

6.3.2 Results from QqLIT MS

To further explore the sensitivity of the SPME/SELDI technique, the SPME/SELDI fibers were also coupled to a QqLIT mass spectrometer with a modified AP MALDI source. The investigation of coating ionization efficiency, the comparison of laser geometries, and the reproducibility were discussed in detail in chapter 7. It was observed that the sensitivity of SPME/SELDI fiber could be dramatically improved by using MS with better ion transmission. The use of reflection geometry, and incorporation of a MALDI matrix could improve the sensitivity by two orders of magnitude. If not specifically stated, all the following experiments were run with reflection geometry.

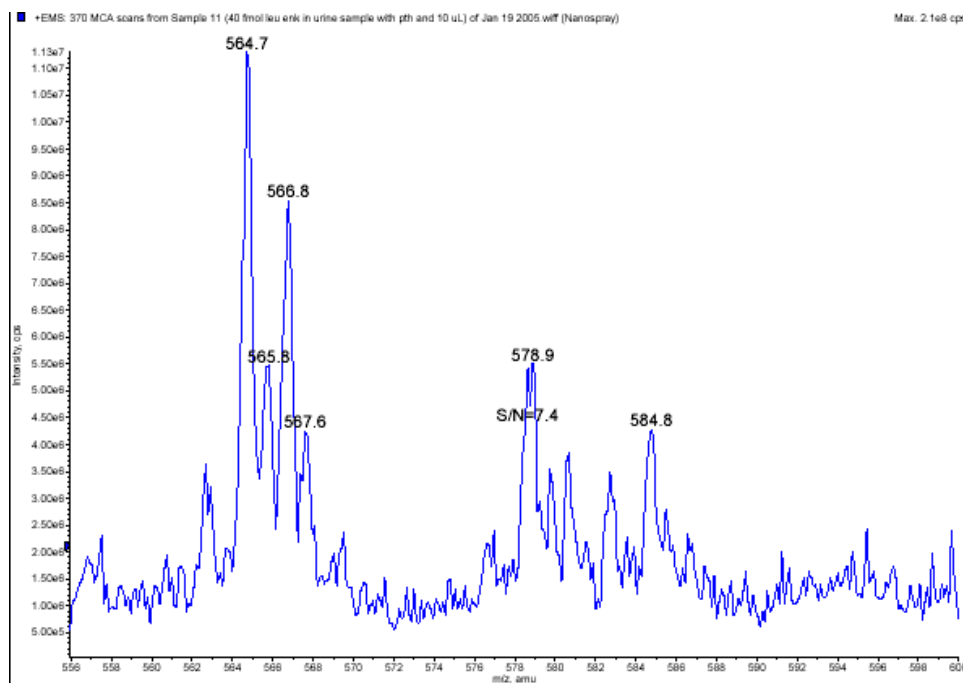


Figure 6.5: Detection limit of leucine enkephalin in urine ($40 \text{ fmol } \mu\text{L}^{-1}$).

Detection Limit of Spiked Urine Samples

Undiluted urine samples were spiked with leucine enkephalin and examined with modified QqLIT MS. Concentration of $2 \text{ pmol } \mu\text{L}^{-1}$, $200 \text{ fmol } \mu\text{L}^{-1}$ and $40 \text{ fmol } \mu\text{L}^{-1}$ were tested. PTH coated fiber was used to extract from spiked urine solution for 5 minutes. Then the SPME/SELDI fiber was rinsed shortly with water and air dried for 2 minutes. The detection limit for leucine enkephalin in urine was determined as $40 \text{ fmol } \mu\text{L}^{-1}$ at S/N 7 for the sodiated ion (m/z 578.9) (Figure 6.5). This LOD was about 100 times lower than that obtained with QTOF MS (approximately $4.5 \text{ pmol } \mu\text{L}^{-1}$). It showed that the sensitivity could be improved by improving the ion transmission. Only $[\text{M}+\text{K}]^+$ ions and $[\text{M}+\text{Na}]^+$ ions could be

seen in the spectra. The presence of these two ions is due to the high concentration of salt present in the urine samples.

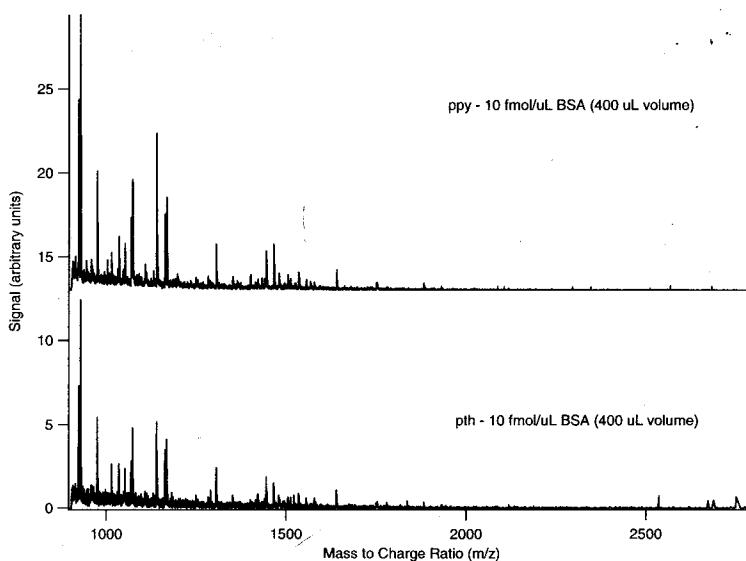


Figure 6.6: MS spectra of BSA digest obtained with PPY and PTH fibers.

Analysis of BSA Digest Sample

PPY and PTH coated optical fibers were both used for the detection of BSA digest sample. The experimental conditions were the same as mentioned above. The concentrations of BSA digest used in this part of experiment were 9, 5 and 2 fmol μL^{-1} .

Considering that the extraction equilibrium could be reached in one minute in previous experiments, 5 minutes was chosen as the extraction time. To make sure

5 minutes was sufficient to reach the extraction equilibrium, a comparison of 5-minute and 40-minute extraction time was performed by extracting from 10 fmol μL^{-1} BSA digest and matrix mixture (1:1 ratio). The intensities are about the same, suggests that 5 minutes extractions is sufficient for this sample.

1 μL of 5 fmol μL^{-1} BSA digest and matrix mixture (1:1 ratio) was also spotted on fiber tip for comparison. But the high noise level, caused by excess matrix on the tip, made it difficult to identify the analyte peaks.

When the equilibrium extraction was performed, the LOD of both PPY and PTH fiber was 2 fmol μL^{-1} . PPY and PTH coated fibers were compared by extracting from 10 fmol μL^{-1} BSA digest solution and the spectra were shown in Figure 6.6. Overall peptide peaks with higher intensities could be obtained with PPY fiber. This might be explained by the higher polarity of PPY coating than that of PTH coating, and the possibility of the formation of hydrogen bonds between PPY and the peptides.

6.4 Conclusion

SPME/SELDI combines sampling, sample preparation and sample introduction with ionization and desorption of the analytes. Because of these advantages, SPME/SELDI has the potential for the direct analysis of biomolecules and small organic molecules in living systems. It has been reported that PPY coated SPME devices could be used to accomplish in-vivo drug analysis in dogs.^[88] Current SELDI-

chip based analytical methods do not allowed the study of drugs and peptides in living systems. In this study, the feasibility of SPME/SELDI to extract and ionize peptides from a solution without adding matrix was demonstrated.

The SPME/SELDI fibers were coupled to QTOF and QqLIT MS, respectively. Better sensitivity could be obtained with QqLIT MS, as the modified AP MALDI source facilitated the ion transmission. Application of this technique to urine sample and BSA digest were demonstrated using both PPY and PTH fibers. The LOD for leucine enkephalin in urine was determined as 40 fmol μL^{-1} with PTH coated fiber; and the LOD for BSA digest was 2 fmol μL^{-1} for both PTH and PPY fibers. The good performance of PPY and PTH coating was obtained when analyzed small drug and protein digest. However, the throughput of this technique was low compared with other MALDI methods. In addition, the performance of SPME/SELDI coupled to MS, such as sensitivity, reproducibility, are still under investigation and require further improvement. As the solution to these issues, a high performance multiplexed SPME/MALDI plate was constructed and evaluated. The details will be described in chapter 7.

Chapter 7

Development of SPME/AP

MALDI Plate

7.1 Introduction

MALDI has become a powerful technique for the analysis of proteins and peptides by mass spectrometry (MS) since its introduction in 1988.^[29] Though MALDI has enabled the routine identification of biomolecules, the need to increase the throughput of the method has been recognized. Sample preparation for MALDI is still the time limiting step, because it dictates the quality of the MS spectra. Efforts have been made to produce more uniform co-crystals between the analytes and the matrix, to improve the performance and reproducibility.^{[112][113]} Others have attempted to combine the sample extraction onto the MALDI target.^[57] SELDI protein chip arrays are commonly used in proteomic research. These SELDI devices

still require substantial sample preparation and the automation is also expensive.

As a simple and efficient sample preparation technique, SPME has been widely used with GC [87] and more recently with liquid chromatography.[88] Recently several research groups have coupled SPME to other types of mass spectrometers. Meurer and coworkers demonstrated direct coupling of SPME with an electron ionization mass spectrometer.[3] Referred to as fiber introduction mass spectrometry, this method was used to analyze volatile and semi-volatile compounds by direct insertion of a poly (dimethylsiloxane) coated SPME fiber into the ion source after headspace extraction. Teng and Chen reported the combination of SPME with MALDI-MS.[56] A sol-gel-derived 2,5-dihydroxybenzoic acid film was employed as the SPME extraction coating and the substrate to help ionization without the addition of a matrix. After extraction, the SPME fiber was attached on a MALDI plate with double-sided carbon tape. This procedure was not amenable to automation and only the analytes on one side of the SPME fiber could be introduced to the MS. Direct coupling of an SPME fiber to a laser desorption mass spectrometer has also been described with ion mobility [5] and QTOF instruments.[8] The SPME/MALDI fiber was employed both as the SPME extraction phase and MALDI substrate, however, the sensitivity was poor ($\text{pmol } \mu\text{L}^{-1}$ detection limits).

This paper further investigates the coupling of SPME/MALDI to mass spectrometry. A multiplexed SPME plate was coupled to a high performance hybrid quadrupole - linear ion trap (QqLIT) with a modified AP MALDI source. Due to the extraction time (2-10 minutes) is typically the rate-limiting step for SPME/AP

MALDI analyses (MALDI MS times can be as low as a few seconds when complete sample depletion is not required, or high repetition rate lasers are used), the sample throughput can be improved by a factor approaching the number of fibers on the device. In this case, a 16-fiber embedded SPME/MALDI plate was constructed for demonstration. The multiplexed plate permits 16 simultaneous extractions from a 96-well plate, substantially improving throughput over previous configurations where successive sampling was achieved in a serial fashion. In addition, the use of a single plate with the fibers embedded, allows for highly reproducible extraction times between replicates as opposed to immersion of separate fibers. In addition to parallel sampling, this system also improves throughput by simplifying the sample preparation for MALDI. In addition, a number of operational parameters were optimized to improve the system performance. Optimization of the laser illumination geometry provided more than a 100-fold improvement in the S/N ratio for peptides. The addition of α -cyano-4-hydrocinnamic acid (CHCA) matrix to the extraction solvent gave improvements of approximately 100 \times and 32 \times for the absolute signal and S/N ratio for peptides, respectively. Analytical performance was also improved by using extraction fibers with increased surface areas (larger extraction capacity) and an improved atmosphere-vacuum interface. The combination of all these improvements gave detection limits of less than 500 amol μL^{-1} for protein digests with typical fiber-fiber reproducibilities on the order of 13-31%. For these studies 2 different SPME coatings were evaluated (PPY and PTH) and the extraction efficiency was determined. This system presents a low cost, easy to use high

throughput sample preparation tool for AP MALDI-MS analysis.

7.2 Experimental

7.2.1 Chemicals

Pyrrole, thiophene, anhydrous ferric chloride, tetraoctylammonium bromide, formic acid, angiotensin II, angiotensin I, bradykinin, glufibrinopeptide b and bovine serum albumin (reduced and carboxymethylated BSA) were purchased from Sigma-Aldrich (St. Louis, MO). Isopropanol and ammonium persulfate were purchased from VWR (Toronto, ON, Canada). The α -cyano-4-hydrocinnamic acid MALDI matrix was purchased from Agilent (Palo Alto, CA). Prior to digestion, protein samples were prepared at 5 mg mL^{-1} in 50 mM ammonium bicarbonate (BDH Chemicals, Toronto, ON, Canada) buffer adjusted to pH 8.5 with ammonium hydroxide (Fisher Scientific, Nepean, ON, Canada). Digestions were carried out with a ratio of 20:1 protein:trypsin. Proteins were digested for 4 hours at 37 °C, and the digests were stored at -20 °C prior to use. Digests were reconstituted in water with 0.1% formic acid. Nanopure deionized water was exclusively used in these experiments. A four-peptide mixture containing angiotensin II, angiotensin I, bradykinin and glufibrinopeptide b was prepared in water with 0.1% formic acid.

7.2.2 Preparation of PPY and PTH Coated Fibers

High OH silica optical fibers with core diameters of 600 μm were purchased from Polymicro Technologies Inc.(Phoenix, AZ). The PPY and PTH fiber preparation procedure have been described in chapter 4.

7.2.3 Preparation of Multiplexed SPME/MALDI Plate

Glass rods with 2 mm diameter obtained from the University of Waterloo glass shop were used to prepare the SPME fiber tips for the multiplexed SPME/AP MALDI plate. The glass rods were cut into 3 cm sections, and then one tip and the sides of the rods were etched with 400-grit silicon carbide polishing paper. The tip was then cleaned with the same procedure described above. The glass fiber tips were then coated with PPY and PTH using the same coating procedures described in chapter 4.

A standard ABI stainless steel MALDI plate (AB/MDS SCIEX, Concord, ON, Canada) was used to prepare the multiplexed plate. A total of 16 holes were drilled on the plate and sixteen coated SPME tips were glued into place. The tips were cut so that the sampling ends protruded from the flat surface of the plate by approximately 5 mm. The tips were positioned to provide alignment with the wells on a 96-well plate to permit simultaneous extraction from multiple wells.

7.2.4 Extraction Process

Samples were diluted to various concentrations in water containing 0.1% formic acid. Various concentrations of α -cyano-4-hydrocinnamic acid MALDI matrix were mixed with a 1:1 volume ratio with the sample solutions prior to extraction. For some experiments, no matrix was added to the extraction samples.

The extraction process involved immersion of the SPME fiber tips in the sample solutions at 2-3 mm in depth. Typically extraction times were 2-10 minutes. The tips were air dried for 2 minutes after extraction. Experiments showed that an aqueous rinse was insufficient to prevent carry-over, so after every run, the PPY fiber tips were cleaned by soaking in methanol for one minute followed by a rinse with water and methanol, respectively. The PTH tips were cleaned by soaking in acetonitrile/water (50:50) followed by rinsing with methanol/water (50:50) for 30 seconds each. Different rinse procedures were used for the two coatings to account for differences in stability with organic solvents.

The preliminary coating evaluation was carried out with a SRI 9300B GC system with a FID detector (SRI instruments, Torrance, CA). The column was a 1 m 0.53 mm MXT-5 silicosteel[®] GC column (Restek, Bellefonte, PA) with a 1.00 μm coating thickness. The temperature of the GC oven was initially held at 70 °C for 0.5 min, then ramped to 300 °C at 20 °C \cdot min⁻¹. The hydrogen carrier gas flow rate was set at 10 mL \cdot min⁻¹. Extracted analytes were then desorbed in methanol and injected into the GC for analysis. Both coatings were evaluated for comparison.

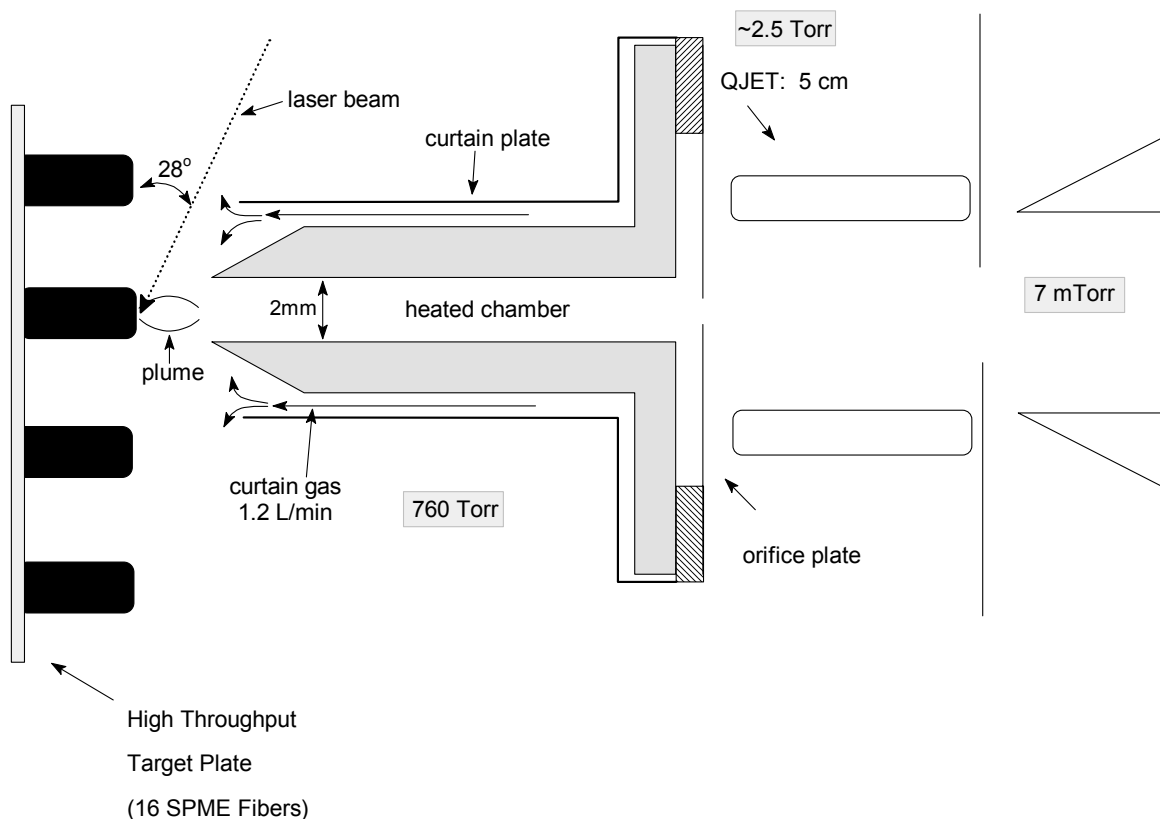


Figure 7.1: Schematic of the SPME/AP MALDI configuration. The target plate held an array of 16 SPME extraction fibers.

7.2.5 SPME/AP MALDI Coupled to a QqLIT MS

SPME devices were coupled to a modified 4000 QTRAP[®] mass spectrometer (MDS SCIEX, Concord, ON, Canada) with a modified AP MALDI ion source as reported previously.^[108]

The instrumental modifications involved increasing the gas throughput of the interface by a factor of four with a larger orifice plate aperture (0.6 mm). In addition, a QJETTM Ion Guide was incorporated to replace the standard skimmer

as shown in Figure 7.1 to reduce the gas load on subsequent vacuum stages.^[114] This configuration improved AP MALDI performance for peptides by a factor of approximately 2 over previous iterations (data not shown). The laminar flow chamber temperature was maintained at 200 °C for all experiments. A nitrogen laser from LSI (Franklin, MA) was used for all experiments with a 10 Hz repetition rate. The AP MALDI source stage was repositioned by removal of shims so that the tips of the SPME rods could be placed approximately 2 mm in front of the laminar flow chamber entrance. Approximately 2000 V was applied to the stainless steel sample plate. For experiments with the optical fibers, the standard source flange was removed and the fibers were placed approximately 2 mm from the inlet of the laminar flow chamber. An alligator clip was fastened to the SPME fiber about 1cm from the fiber tip to provide a potential onto the electroconductive polymer to improve the sampling efficiency for ions. The voltage used in these experiments was 2000 V.

Using the coated optical fibers, performance comparisons were made using two different laser illumination geometries. The first geometry involved attachment of the laser directly to the opposite end of the coated optical fiber in a similar fashion to experiments described in the literature.^[8] With this configuration (hereafter referred to as transmission geometry), the laser light was transmitted through the optical fiber (600 μm), conductive polymer, and then sample extraction surface. This geometry essentially results in backside illumination of the polymer and sample. The second optical configuration (hereafter referred to as reflection geometry)

involved attachment of the laser to the standard optics in the AP MALDI source (200 μm fiber) such that the light was directed at approximately a 28 ° angle to the front side of the fiber surface as described previously.^[108]

7.3 Results and Discussion

7.3.1 Optimization of Performance

Comparison of Transmission and Reflection Geometry

In previous direct couplings of SPME and AP MALDI ^{[5][8]} only transmission geometry was employed. Experiments were conducted with samples of BSA digest to compare the performance with the two illumination geometries. Similar laser fluence was used for both geometries. Figure 7.2 shows an example of the performance comparison for a 5 minute extraction from a sample of 10 fmol μL^{-1} BSA digest using a single PTH fiber. The Y axes were scaled identically for the two sets of data so that they could be compared directly. Although these data were generated using a PTH fiber, similar trends were observed using PPY fibers as well. There was a substantial background when using transmission geometry, however peptide peaks could not be observed at the 10 fmol level. In contrast, a large number of peptide peaks could be observed with S/N ratios ranging up to 17 when using reflection geometry even though the optical fiber was positioned in the same location within the source region for both experiments. In order to achieve similar S/N ratios for

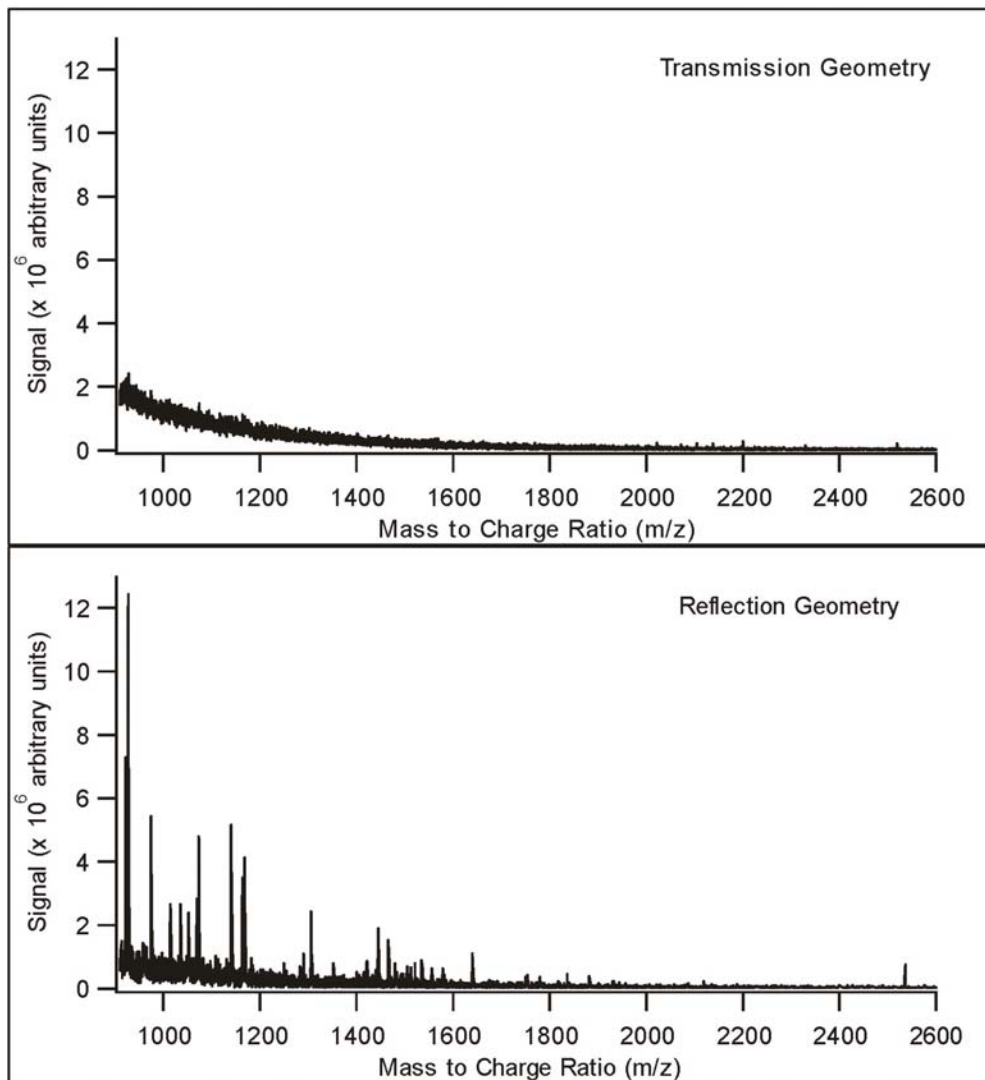


Figure 7.2: Comparison of performance for a 10 fmol μL^{-1} sample of BSA digest with transmission (upper pane) and reflection geometry (lower pane). The extraction time was 5 min and a PTH fiber was used for these experiments. Trap operational parameters: scan speed, 4000 Da/s; fill time, 150 ms.

this sample using transmission geometry, the BSA digest concentration had to be increased to greater than 1 pmol μL^{-1} . For these experiments, the sample surface was illuminated until no further ion current was generated with both optic configurations. As the entire surface was illuminated simultaneously with transmission geometry, sample depletion from the surface required approximately 10 s. However with reflection geometry, the laser was focused to a spot size of approximately 225 by 325 μm so that the ablation area was approximately four times smaller than the fiber surface area. Quantitative removal of analyte required rastering around the fiber surface. Under these conditions, analyte signals were observed for approximately 3 min. Even though no further ion current could be obtained from these fibers, some analytes were still present on the surface of the fibers. Additional analyte signal (much weaker) could be regenerated by respotting matrix onto the tips. Therefore, it was critical to use the aggressive wash procedures described in the experimental section between each sample to prevent carry-over. Reflection geometry was used for all other experiments described in this paper.

Ionization Efficiency for Conductive Polymers

Matrix addition to the extraction sample was also evaluated to try to improve the analytical performance of the SPME/AP MALDI system. Extractions were carried out using a sample of 100 fmol μL^{-1} angiotensin II. Data were collected directly from the acidified aqueous sample solvent, sampling from solvent prepared by mixing the sample solvent directly with undiluted a-cyano matrix (1:1 ratio),

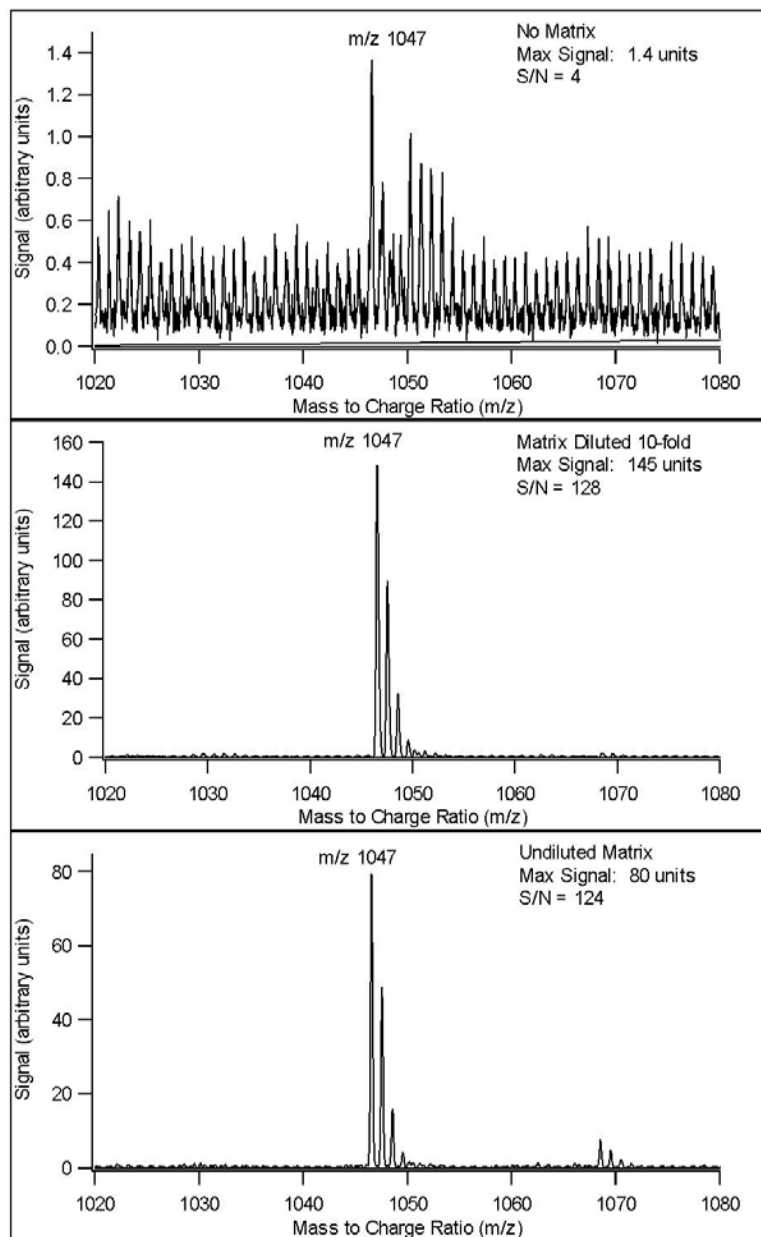


Figure 7.3: Comparison of performance for $100 \text{ fmol } \mu\text{L}^{-1}$ angiotensin II using direct ionization from the surface of the PPY fiber (no matrix addition) and incorporating various amounts of matrix to the extraction solvent. Top pane, no matrix addition; middle pane, 10-fold diluted matrix added; bottom pane, undiluted matrix added.

Trap operational parameters: scan speed, 250 Da/s; fill time, 150 ms.

and mixing the sample solvent directly with α -cyano matrix (1:1 ratio) that was diluted by a factor of 10 with water containing 0.1% formic acid. For each of the three extraction conditions, four separate runs were conducted with different tips.

Average data obtained using PPY fibers is presented in Figure 7.3 with the Y axes scaled identically for comparison purposes. The addition of matrix to the extraction solution provided a dramatic improvement in SPME/AP MALDI performance. The addition of undiluted matrix provided increases of $57\times$ and $31\times$ for the absolute signal and S/N for protonated angiotensin II. Dilution of the matrix provided an additional signal improvement (approximately a factor of 2), but the S/N ratio was essentially unchanged. The increased ion intensity with matrix dilution was likely due to the resulting increase in aqueous content of the extraction solution (50% aqueous \rightarrow 95% aqueous) since the matrix was diluted with acidified water. The higher aqueous content may increase the distribution constant for the analyte in the extraction phase. In addition, the decrease of the total amount of matrix in the extraction solution may decrease the competition for the surface, allowing more peptides to be adsorbed. Therefore, for all further experiments in this paper aqueous samples were mixed with a 1:1 ratio with α -cyano matrix diluted $10\times$. Similar behavior was observed with SPME devices coated with PTH.

Comparison of PPY and PTH Coatings

Conductive coatings of PPY and PTH were evaluated. GC experiments were initially conducted to compare the extraction ability and reproducibility for the two

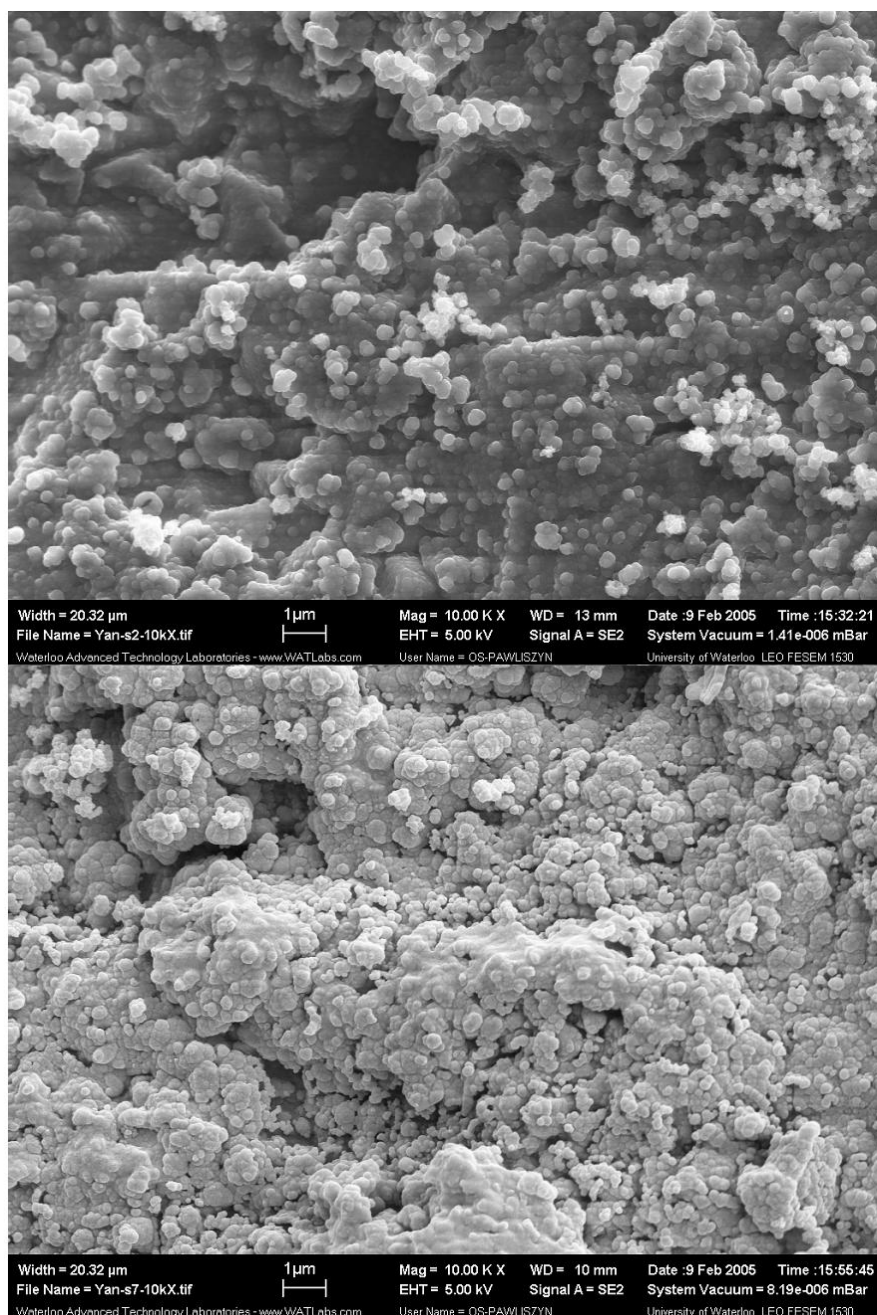


Figure 7.4: Scanning electron microscope images of the PPY coating (upper pane) and the PPY coating after extraction from a mixture containing $10 \text{ fmol } \mu\text{L}^{-1}$ BSA digest and matrix (lower pane). Operational parameters were 5000 V and $10000\times$ for the accelerate voltage and magnification.

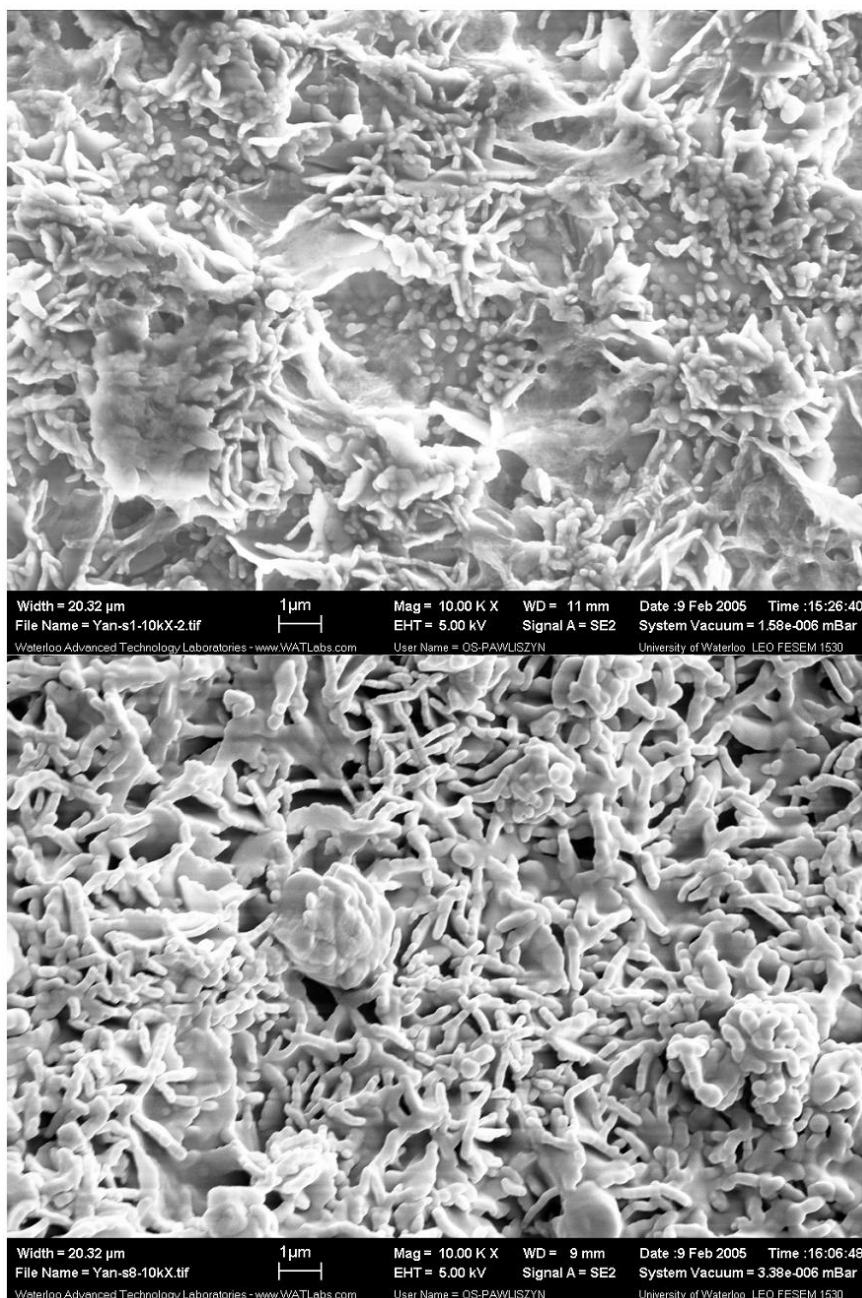


Figure 7.5: Scanning electron microscope images of the PTH coating (upper pane) and the PTH coating after extraction from a mixture containing $10 \text{ fmol } \mu\text{L}^{-1}$ BSA digest and matrix (lower pane). Operational parameters were 5000 V and $10000\times$ for the accelerate voltage and magnification.

polymer coatings. GC experiments showed signal improvements of $1.9\times$ for the PPY fibers as opposed to the PTH fibers. In addition, the run-run reproducibility (as measured by the relative standard deviation) was 9% for the PPY fibers and 21% for the PTH fibers. Experiments with the QqLIT also showed poorer performance and reproducibility with the PTH fibers (data not shown). Differences in performance and reproducibility may be related to differences in the fiber surface morphologies.

Scanning Electron Microscopy (SEM) was used to evaluate the homogeneity of the extraction surfaces with the PPY (Figure 7.4) and PTH coated devices (Figure 7.5). Similar conditions were used for the acquisition of the images with the two coatings, and the magnification was $10\,000\times$. The top image depicts the surface of the coated fiber prior to extraction and the bottom image depicts the surface of the coated fiber after extraction from a mixture containing $10\text{ fmol }\mu\text{L}^{-1}$ BSA digest. The surface of the PTH coated fiber (Figure 7.5) showed a lack of surface uniformity with areas of filament-shaped particles and areas with alternate morphologies. The picture taken after extraction showed the presence of a number of areas where there appeared to be gaps in the extracted material. The surface of the PPY coated fiber (Figure 7.4) shows a more homogeneous morphology (ball-shaped structures). In addition, there appeared to be a more uniform and continuous layer of material on the surface after the extraction procedure. This difference in surface structure may be the reason for the improved performance with the PPY coated fibers. PPY coated fibers were used for all of the rest of the experiments described in this paper.

A number of PPY coated tips were also examined with blank extraction from the 10X diluted matrix solution to look for the presence of extra peaks resulting from ionization of various subunits of the PPY polymer. It was not possible to observe any peaks that corresponded to polymer ions. These results suggest that the polymer coatings might not be able to be ionized with the current laser fluence ($380 \text{ J} \cdot \text{m}^{-2}$). Another possible explanation for the lack of PPY related ions in the mass spectra was that the proton affinity of the matrix may be substantially higher than the proton affinity of PPY related molecules.[115]

7.3.2 Evaluation of Analytical Performance

Extraction Efficiency

The capacity of the SPME coating limits the amount of analyte that can be extracted from a particular sample. Typically this means that the actual amount of sample adsorbed on the fiber surface is substantially lower than the amount of sample initially present in the extraction solution. Therefore, experiments were conducted with a four-peptide mixture to evaluate the extraction efficiency using the large diameter (2 mm) fibers mounted on the surface of the multiplexed SPME plate. Extraction efficiencies depend on a number of parameters including solvent composition, temperature, analyte affinity for the solid phase, extraction time, and analyte concentration. Prior to these experiments, the solvent composition was optimized to water with 0.1% formic acid as described above for Figure 7.3. The optimum temperature was approximately 25 °C with reduced ion count rates at

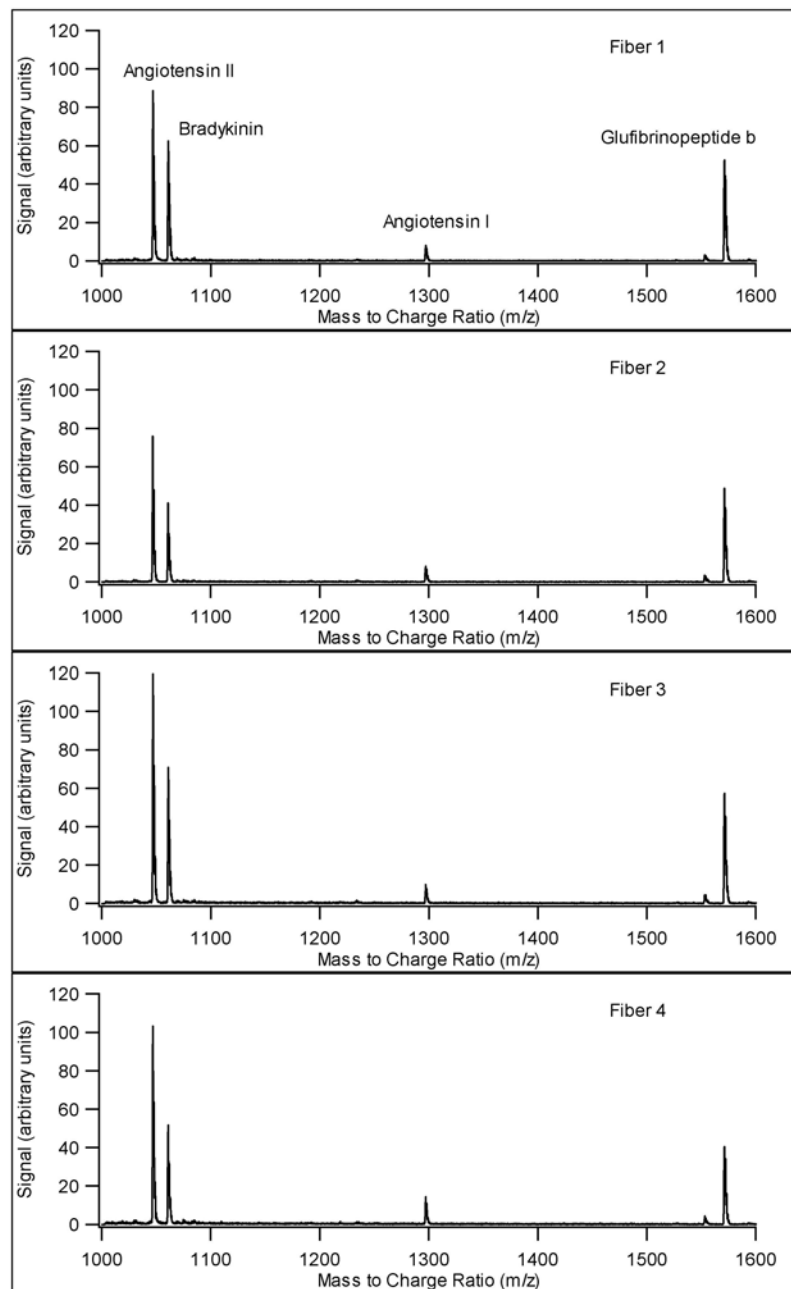


Figure 7.6: Mass spectra of four peptide mixture extracted by PPY fibers. Sample concentration, $20 \text{ fmol } \mu\text{L}^{-1}$ angiotensin II, bradykinin, angiotensin I and glufibrinopeptide b with 10-fold diluted matrix. Trap operational parameters: scan speed, 4000 Da/s; fill time 150 ms.

both higher and lower extraction temperatures (data not shown). In order to evaluate the extraction efficiencies, 1 μL of a sample containing 20 fmol μL^{-1} of four different peptides was spotted onto the tip of four separate SPME fibers. Data were accumulated from each fiber until the sample was depleted from the surface and the four runs were averaged. After cleaning, the same four fibers were used to extract from wells containing 40 μL of the same mixture (20 fmol μL^{-1}). Data were accumulated from each fiber until the samples were depleted from the surface and the 4 runs were averaged. The peak intensities were compared for the four peptides and the extraction efficiencies were calculated using Equation 7.1.

$$\text{Extraction efficiency} = \frac{\text{signal intensity}_{\text{extracted sample}}}{\text{signal intensity}_{\text{deposited sample}}} \times \frac{20 \text{ fmol} \cdot \mu L^{-1} \times 1 \mu L}{20 \text{ fmol} \cdot \mu L^{-1} \times 40 \mu L} \times 100\% \quad (7.1)$$

The extraction efficiencies were 0.3%, 0.2%, 0.1%, and 0.4% for angiotensin II, bradykinin, angiotensin I, and glufibrinopeptide b, respectively. As all the four peptides extracted by fiber coating is less than 1 %, it can be concluded that 40 μL is sufficient for future quantitative analysis by SPME. [116] It is important to note that the calculated extraction efficiencies only accounted for peptides adsorbed on the coated end of the fiber tips, as it was not possible to sample from the sides of the fiber tips with this configuration. The differences in peptide structure likely account for differences in the extraction efficiencies. In addition, as the extraction efficiencies depend on sampling time and concentration, it is important to note that the calculated efficiencies provide an efficiency estimate that is only valid for the

conditions described above.

Reproducibility and Sensitivity

Tip – tip reproducibility was evaluated with four PPY coated tips using samples of the four peptide mixture containing 20 fmol μL^{-1} of each peptide as shown in Figure 7.1. In each case, data were acquired until the sample was completely depleted from the tip of the fiber. Separate SPME tips (labeled fibers 1-4) were used for simultaneous extraction from four different sample wells. The four spectra were qualitatively similar showing the presence of the molecular ion for the four peptides as well as a small peak corresponding to the dehydration of glufibrinopeptide b. A quantitative comparison of the signal and S/N ratio for the four peptides is presented in Table 7.1. Typical RSDs (N = 4) for the signal intensity and S/N ratio ranged from 13-31% and 11-27%, respectively. This was a substantial improvement over previous iterations and was likely due to a number of factors such as the improved control with simultaneous sampling, improved SPME technique, improved laser optics, and the more stable atmosphere to vacuum interface.^[108] In addition, the multiplexed plate allowed all extractions to be conducted simultaneously, reducing the total analysis time. The S/N ratios from these experiments can be used to estimate detection limits of 362 amol μL^{-1} , 619 amol μL^{-1} , 2.2 fmol μL^{-1} , and 295 amol μL^{-1} for angiotensin II, bradykinin, angiotensin I, and glufibrinopeptide b, respectively. These detection limits represent improvements on the order of 1000-7500 \times over previously published data ^[8].

	angiotensin II		bradykinin		angiotensin I		glufibrinopeptide b	
fiber	signal	S/N	signal	S/N	signal	S/N	signal	S/N
No.	($\times 10^7 au$)	ratio	($\times 10^7 au$)	ratio	($\times 10^7 au$)	ratio	($\times 10^7 au$)	ratio
1	8.9	153	6.2	108	0.81	26	5.2	224
2	7.6	201	4.1	109	0.83	31	4.9	257
3	12.0	180	7.1	106	1.0	25	5.7	199
4	10.0	129	5.2	64	1.5	30	4.1	130
AVE.	9.6	166	5.7	97	1.0	28	5.0	203
RSD(%)	19	19	23	23	31	11	13	27

Table 7.1: Quantitative comparison of fiber-fiber reproducibility for extractions from four different sample wells.

Analytical performance was also evaluated for protein digests. Figure 7.7 shows an example of this for samples of BSA digest in which the Y axes have been scaled identically for comparison purposes (the m/z values of the peptide peaks are shown in Table 7.2 and 7.3).

Figure 7.7 shows data acquired (average of 8 runs each) for samples of 5 fmol μL^{-1} BSA digest, 500 amol μL^{-1} BSA digest, and a blank sample containing only matrix mixed with acidified water. The extraction times were 5 min, 10 min, and 10 min, respectively. Blank runs were taken before and after each of the measurements with the fibers to ensure that carry-over was not an issue. On average the peak heights and S/N ratios were approximately $6\times$ and $5\times$ lower for the 500 amol μL^{-1} extractions than the 5 fmol μL^{-1} extractions, respectively. These data suggest that the data generated with the lower concentration may have benefited from the extended extraction time. This is expected since the extraction process relies upon diffusion of analyte molecules to the fiber surface. Therefore, longer extraction times result in more analyte adsorbed on the fiber surface before the extraction equilibrium is reached. Future research will be focused on improving performance further with extended extraction times as well as improving the homogeneity of the extraction material on fiber surfaces with the goal of achieving quantitative analysis. New extraction materials such as antibody coating are also under investigation for this purpose.

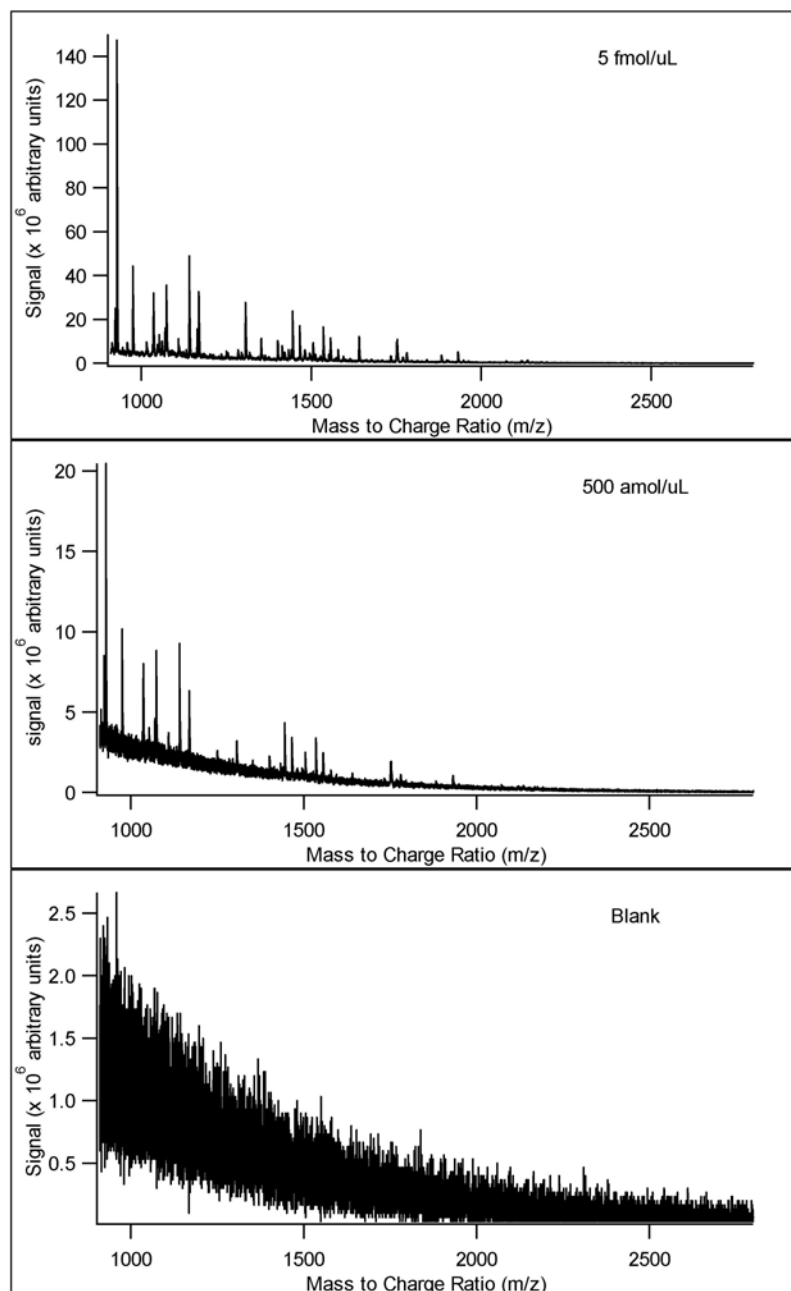


Figure 7.7: Analytical performance for samples of 5 fmol μL^{-1} BSA digest (top pane), 500 amol μL^{-1} BSA digest (middle pane), and a blank (bottom pane). Samples were extracted for 5, 10, and 10 min, respectively. Trap operational parameters: scan speed, 4000 Da/s; fill time, 20 ms; and Q0 trapping enabled.

Peptide Ion (m/z)	5 fmol μL^{-1} BSA digest	500 amol μL^{-1} BSA digest
2116.8	+	
1962.9	+	
1947.0	+	
1930.8	+	+
1881.9	+	
1749.7	+	+
1674.8	+	
1640.0	+	+
1577.8	+	+
1555.6	+	+
1534.7	+	+
1511.8	+	
1504.6	+	
1497.6	+	
1479.8	+	
1465.6	+	+
1444.6	+	+
1420.7	+	
1399.7	+	+

Table 7.2: List of the BSA digest peptide peaks.

Peptide Ion (m/z)	5 fmol μL^{-1} BSA digest	500 amol μL^{-1} BSA digest
1352.7	+	
1305.7	+	+
1293.6	+	
1283.7	+	
1255.6	+	
1249.6	+	+
1168.5	+	+
1163.6	+	
1140.5	+	+
1108.5	+	+
1073.5	+	+
1069.4	+	+
1052.4	+	
1035.5	+	+
1014.6	+	
1002.6	+	
974.5	+	+
927.5	+	+
922.5	+	+
Total numbers of peptides	38	20

Table 7.3: List of the BSA digest peptide peaks (continued).

7.4 Conclusion

A new multiplexed SPME/AP MALDI plate was designed and evaluated on a QqLIT with a modified AP MALDI source. The experimental parameters were optimized to obtain a significant improvement in performance. The incorporation of diluted matrix to the extraction solution improved the absolute signal and S/N by 104× and 32×, respectively. The incorporation of reflection geometry for the laser illumination improved the S/N ratio by more than two orders of magnitude. Reproducibility was also improved as a result of these changes and the improved atmosphere-vacuum interface used for these experiments. The fully optimized high throughput SPME/AP MALDI configuration described in this paper generated detection limit improvements on the order of 1000-7500× those achieved prior to these modifications. This system presents a possible alternative for qualitative proteomics and drug screening.

Chapter 8

Laser Desorption SPME as Fast Sample Introduction Method for Fast GC Analysis

8.1 Introduction

The principles and theory of fast GC were established in the 1960s.^{[117][118]} However, its application remained limited until recently. The need for analytical methods that are low cost, and provide high throughput has initiated widespread research in method development for high-speed GC analysis. New technologies include microbore (≤ 0.1 mm *i.d.*) columns, methods for very fast column heating such as at-column heating, inlet devices that inject very narrow sample plugs, dual-column methods for enhancing selectivity, and the use of time-of-flight mass spectrometry

for high-speed data acquisition have been developed for fast GC analysis.

Reviews of the fundamentals of fast GC and method development are found in a number of publications [119]–[124]. One of the main goals of method development is to obtain optimized resolution between the critical components in a preparation in the shortest practical time. Resolution is a function of theoretical plates N , retention factor k , and separation factor α .

$$R_S = \left(\frac{\sqrt{N}}{4} \right) \left(\frac{\alpha - 1}{\alpha} \right) \left(\frac{k_{ave}}{1 + k_2} \right) \quad (8.1)$$

When separation speed is fully optimized, then sample capacity and/or separation power often suffer. Maximization of the aforementioned factors occurs at the expense of both sample capacity and separation power. Therefore, any fully optimized fast GC method is a compromise between speed, capacity and resolution. Korytar and co-worker provide a more specific description of the factors involved in fast GC method development.^[125] The basic steps of method optimization that are critical for the development of fast separations include the need to:

- Minimize the required resolution;
- Maximize the available selectivity; and
- Reduce the analysis time at a constant resolution.

The definitions of fast GC have also been widely discussed. Van Deursen and co-worker proposed the following simple definitions, based on a peak width at half

height (2.354σ): fast GC refers to peak widths of 1-3 sec, with analysis times in minutes; very fast GC refers to peak widths of 30-200 msec, with analysis times in seconds; and ultra-fast GC refers to peak widths of 5-30 msec and separations in less than 1 sec.^[126]

Klee and Blumberg have provided detailed descriptions of method development, theory, and practice in fast GC.^{[127][128]} They describe that analysis speed can be increased in several ways, including:

- Faster carrier gas flow rate;
- Faster temperature program heating rate;
- Faster carrier gas;
- Shorter, smaller, thinner film column; and
- Low outlet pressure detector.

It is often difficult to attempt to optimize all of these variables at once. These factors could be achieved by implementing appropriate instrumentation. Namely, the use of hydrogen as a carrier gas, the use of a narrow-bore capillary column, and GC ovens with resistive heating system provide fast and reproducible heating rates up to $1200\text{ }^{\circ}\text{C min}^{-1}$. In addition, the injection system is also a critical component of fast GC. To minimize the input band-width, the injected sample plug has to be narrow compared to the total chromatographic band broadening. A split injector is a simple option for fast GC injection system. Milliseconds of injection band-width

can be obtained when operated at very high split ratios.^[129] However, a poor detection limit is the main drawback of this approach. Programmed temperature vaporization and on-column injection techniques can also be combined with fast GC. But precautions are necessary to successfully use these techniques.

Laser desorption has previously been used as an alternative sample introduction method for fast GC/MS analysis.^[130] A XeCl excimer pulsed laser with pulse energy of 3 mJ was used to desorb the analytes from the sample surface, and the laser desorbed analytes were then thermally vaporized and introduced into the GC inlet. A laser was also used in laser pyrolysis fast GC and GC/MS for the fast characterization of synthetic polymers.^[131] Polymers are inherently difficult to analyze due to their high molecular weight and lack of volatility. In laser pyrolysis, the interaction of laser energy with the sample generates a high temperature plume, rapid quenching and thermal shock, which produces a range of pyrolysis products. The laser energy used for pyrolysis has to be high enough to reach the high temperatures required for pyrolysis.

As mentioned in Chapter 1, the use of a laser to desorb analytes on the tip of an optical fiber for fast GC analysis was reported in 1987 by Pawliszyn and Liu, even before the SPME technique was developed.^[60] Subsequently, research has focused on the development of SPME devices, SPME coatings and the fundamental study of this novel technique. Because the volatile and semi-volatile analytes on SPME fiber can be thermally desorbed in a GC injector, the coupling of laser desorption SPME to GC has not been further investigated.

It was reported that the amount of desorbed neutral species can be much larger than the amount of desorbed ions if the optimal laser intensity is used.^[132] Therefore, laser desorption SPME/SELDI can also be used to introduce analytes in the neutral form for fast GC and GC/MS analysis. As the laser ablated area is exactly the same as the cross section of the optical fiber, the analytes can be quantitatively desorbed and analyzed if the experimental parameters are optimized and well controlled.

In this chapter, the use of laser desorption SPME as a sample introduction approach for fast GC analysis was demonstrated. A PPY coated SPME fiber was coupled to a portable GC equipped with a FID detector, and GC/MS. Synthetic polymer PEG 400 was used for demonstration. The results illustrate that laser desorption is an effective desorption method for the introduction of low-volatile compounds into a GC system. Good separation between the polymer peaks was obtained, even with a short capillary column.

8.2 Experimental

8.2.1 Chemicals

Pyrrole, poly(ethylene glycol) 400, and α -cyano-4-hydrocinnamic acid (CHCA) were purchased from Sigma-Aldrich (St. Louis, MO). Ammonium persulfate was purchased from BDH Chemicals (Toronto, ON, Canada). HPLC grade ethanol, methanol, isopropanol and deionized water were used for all of the experiments.

8.2.2 Preparation of PPY Coated SPME Fibers

High OH silica optical fibers with core diameter of 300 μm were purchased from Polymicro Technologies Inc.(Phoenix, AZ). The preparation procedure is described in Chapter 2.

8.2.3 Sampling Process

Polyethylene glycol 400 was dissolved in ethanol at a 10% (v:v) concentration. For the GC/FID analysis, the fiber tip was carefully dipped in a 10% PEG solution and then wiped carefully with a Kimwipes[®] to remove the solution on the sides of the fiber. The fiber was then air dried for 2 mins. The 10% solution was diluted to 10 ppm with water for subsequent GC/MS analysis. The extraction process involved the immersion of the SPME fiber tip in the sample solutions at a depth of 2-3 mm. The extraction times were 1 min. Following extraction, the SPME fiber was wiped carefully with a Kimwipes[®] to remove the solution on the sides of the fiber. The tip was then air dried for 2 minutes.

8.2.4 Instrumentation

Experiments were performed using a SRI 9300 series portable GC system with a FID detector (SRI Instruments, Torrance, CA), and a Saturn 4D GC/MS (Varian, Palo Alto, CA). The frequency tripled Q-switch Nd:YAG laser (355 nm emission wavelength) was purchased from New Wave Research Inc.(Fremont, CA). The laser

was operated at remote control mode, therefore a homemade laser control box was constructed to start the laser and control the parameters such as repetition rate, number of laser pulses etc. The schematic of the laser control box is shown in Appendix C. The laser repetition rate was set to be 20 Hz. Laser energy was detected with a Molectron EM400 laser energy meter, purchased from Molectron Detector Inc.(Portland, OR). A 15 cm convex lens, purchased from Newport (Fountain Valley, CA), was used to focus the laser light. The laser source, lens and the X, Y, Z stage with SPME fiber connector were set up on a square linear translation stage from Edmund Industrial Optics (Barrington, NJ).

8.2.5 Laser Desorption to GC/FID

A SRI 9300 series portable GC system with a FID detector (SRI Instruments, Torrance, CA) was employed first for the coupling of the laser desorption to the GC trial. The column used was a 1 m \times 0.53 mm MXT-5 silicosteel[®] GC column (Restek, Bellefonte, PA) with a 1.00- μ m film thickness. The on-column injector was located inside of the GC oven. Therefore the temperature of the injector was the same as the oven temperature. The schematic of the GC injector with laser desorbed SPME was shown in Figure 8.1. A SPME needle assembly was used to guard the optical SPME fiber when it pierced the GC septum. Since the outer diameter of the SPME fiber was approximately 0.4 mm, and the inner diameter of the megabore adapter was about 0.6 mm, it was very difficult to directly insert the SPME fibre into the GC column through the megabore adapter. Thus, a short

stainless steel tubing (1 cm length, 0.5 mm outer diameter) was placed between the septum and the column to guide the SPME fiber into the GC column. The hydrogen carrier gas flow rate was set at 10 mL min⁻¹. The temperature of the GC oven was initially set at 150 °C and ramped to 280 °C at 20 °C min⁻¹. Unless otherwise noted, the laser energy was set at 200-300 μJ , and 200 laser pulses were fired to desorb the analyte in 10 seconds.

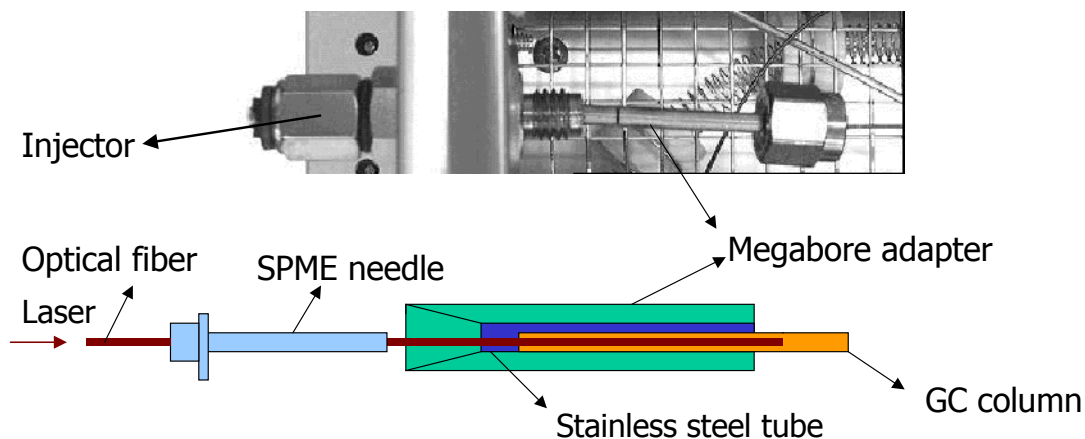


Figure 8.1: Schematic of laser desorption SPME to GC.

8.2.6 Laser Desorption to GC/MS

An optical SPME fiber was coupled to Saturn 4D GC/MS to examine the difference between laser desorption and thermal desorption. A 2 × 0.25 mm MXT-5MS GC column (Restek, Bellefonte, PA) with a 0.25- μm film thickness was used. The pre-column pressure was set at 10 psi. The scan mass range was set at 300-650. The GC oven temperature was initially set at 80 °C, held for 2 minutes, and then

ramped at $20\text{ }^{\circ}\text{C min}^{-1}$ to 280°C . The SPI injector temperature was set at $100\text{ }^{\circ}\text{C}$ and then ramped at $150\text{ }^{\circ}\text{C min}^{-1}$ to 280°C . The transfer line temperature was set at $290\text{ }^{\circ}\text{C}$. The laser energy was set at $200\text{--}300\text{ }\mu\text{J}$, and 200 laser pulses were fired to desorb the analyte in 10 seconds.

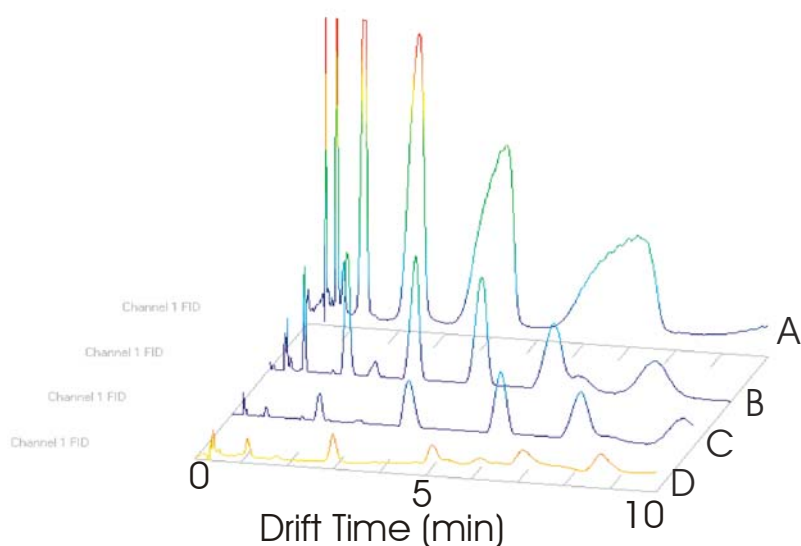


Figure 8.2: Laser desorption PEG 400 to GC using different temperature parameters. From top to bottom: A: $200\text{ }^{\circ}\text{C}$ ramped at $40\text{ }^{\circ}\text{C min}^{-1}$ to $280\text{ }^{\circ}\text{C}$, then hold for 10 mins; B: $200\text{ }^{\circ}\text{C}$ ramped at $30\text{ }^{\circ}\text{C min}^{-1}$ to $280\text{ }^{\circ}\text{C}$, then hold for 10 mins; C: $200\text{ }^{\circ}\text{C}$ ramped at $20\text{ }^{\circ}\text{C min}^{-1}$ to $280\text{ }^{\circ}\text{C}$, then hold for 10 mins; D: $150\text{ }^{\circ}\text{C}$ ramped at $20\text{ }^{\circ}\text{C min}^{-1}$ to $280\text{ }^{\circ}\text{C}$, then hold for 10 mins.

8.3 Results and Discussion

8.3.1 Laser Desorption PEG to GC/FID

Determining the Temperature Programming Parameters

Temperature parameters were optimized as illustrated in Figure 8.2. According to preliminary experiment results, the initial temperature was set at 150 °C. A high initial temperature was chosen because SPME is a solvent-free technique, and there is no need to start analyses at a low temperature to evaporate the solvent. Since the maximum operating temperature of this column is 280 °C, the final temperature was set at 280 °C and held for 10 min. It was observed that the peaks with longer retention time were broad and short due to the oven temperature. At least six peaks were observed in each chromatogram.

Involvement of CHCA Matrix

It is understood that the addition of a CHCA matrix could improve the signal intensities with the coupling of a SPME/SELDI fiber to MS, due to the improvement of ionization efficiency. It is not clear, however, if the MALDI matrix influences on the desorption process. Thus, PEG 400 was used as testing compound to examine the effect of the MALDI matrix on laser desorption to GC, and the chromatograms are presented in Figure 8.3. The figure shows no apparent difference between chromatogram B (without the matrix) and C (with the matrix), if the retention times and the intensities of the peaks are compared. There are two

more peaks in chromatogram C, which had the same retention times as the peaks in the CHCA chromatogram (D). Thus, it is thought, these peaks are a result of the CHCA matrix. According to these results, it is tentatively concluded that the addition of a MALDI matrix has no apparent effect on the signal intensity in a GC chromatogram. However, additional data is required to confirm this tentative conclusion, particularly related to the identity of the peaks in the chromatograms.

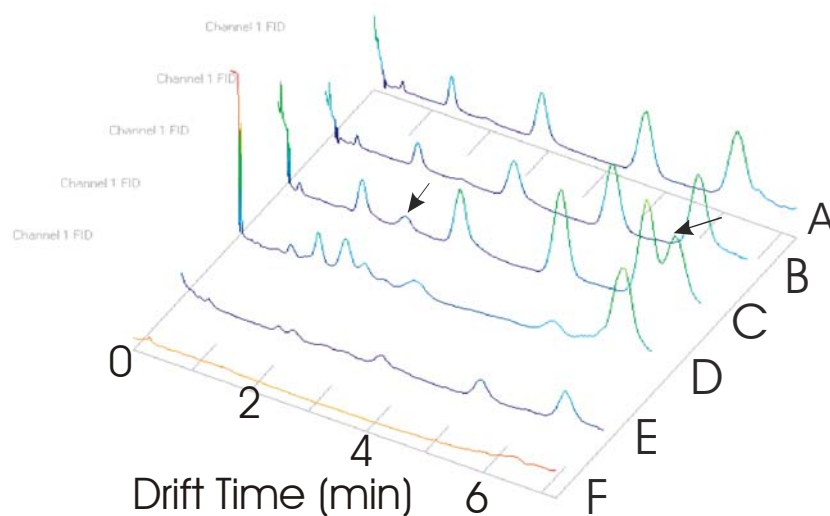


Figure 8.3: Laser desorption PEG to GC/FID. From top to bottom: A and B: laser desorption 10 % PEG 400; C: laser desorption 10% PEG 400 + 1 mg mL⁻¹ CHCA matrix; D: laser desorption 10 mg mL⁻¹ CHCA matrix; E: thermo desorption 10% PEG 400; F: blank. Temperature programming, 150 °C ramped at 20 °C/min to 280 °C, then hold for 4 mins.

Laser Desorption vs. Thermal Desorption

In Figure 8.4, the difference between laser desorption and thermal desorption was demonstrated. In chromatogram A, PEG was introduced to the GC via thermal desorption. The SPME fiber was left inside of the injector for 10 s, and then withdrawn from the injector. An overlapped multiple peak could be observed in this chromatogram. Chromatogram B and C were obtained with 5 seconds and 2 seconds of laser desorption, respectively. The SPME fiber was retrieved from the injector after the laser pulses were fired. Well separated peaks were observed in both chromatograms. The peak intensities in the 5 s laser desorption chromatogram were higher than those in the 2 s laser desorption chromatogram. This observation is attributed to a larger amount of analyte that is desorbed with a longer desorption time. Because all of the fibers were prepared by coating PPY on freshly cut fiber tips, and every SPME fiber was only used once in these experiments, the issue of carry-over from the fiber could be ignored. Blanks were run before and after each runs, no carryover was observed.

Effort was made to investigate the optimum laser energy and desorption time, but these experiments was not successful. Laser energies that ranged from 50 μJ to 600 μJ , desorption time that ranged from 1 s to 30 s were examined. However, the reproducibility of the peak areas was poor, and no further conclusion could be drawn based on these results. Possible reasons for the poor reproducibility might be:

- Inter-fiber difference between the fiber coatings (it was difficult to obtain uniform coating on the smaller surface), and/or
- The laser energy decreased during the desorption process. (It was observed that the laser energy decreased if the laser pulses were continually fired for tens of seconds. And the energy decreased even faster if laser output energy is higher. This decreasing on laser energy effected the reproducibility dramatically, as the GC signal intensity was directly related with the laser energy)

The information that could be obtained with this laser desorption SPME-portable GC system was limited, due to the configuration limitation, which did not provide a separate temperature controller for the injector, and information about the identity of the compounds could not be obtained directly. Despite these limitations, sharp and well separated peaks could be obtained with a 1 m megabore capillary column. These results demonstrated the applicability of using laser desorption SPME for fast GC analysis. Following the findings from these trials, laser desorption SPME was also coupled to GC/MS to further investigate this technique.

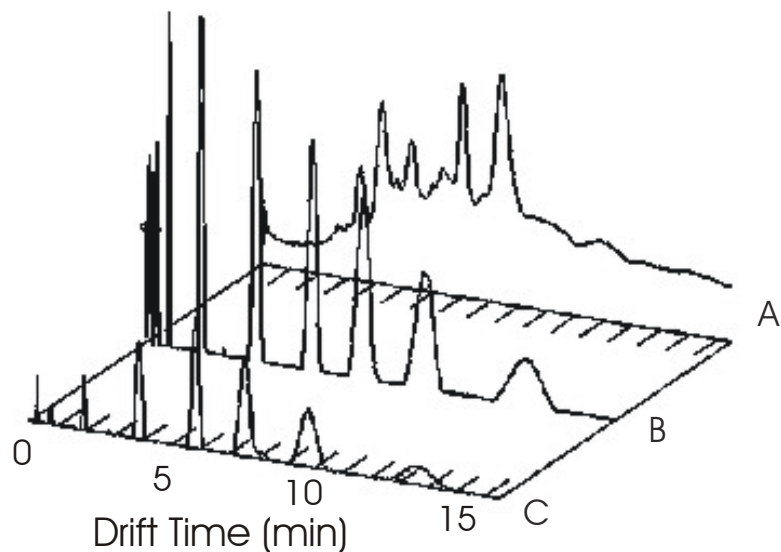


Figure 8.4: Thermal desorption and laser desorption PEG to GC/FID. Temperature programming, 150 °C ramped at 20 °C min⁻¹ to 280 °C, then hold for 10 mins. (A): 10 s thermal desorption from fiber tip; (B): laser desorption at 20 Hz for 5 s; (C): laser desorption at 30 Hz for 2 s.

8.3.2 Laser Desorption PEG to GC/MS

Laser desorption SPME was coupled to a Varian Saturn 4D GC/MS. After GC and ion trap detector operation parameters were optimized, laser desorption and thermal desorption SPME were performed with a 10 ppm PEG sample. The comparison between the laser desorption and thermal desorption obtained with GC/MS is presented in Figure 8.5. Figure 8.5A is the blank and Figure 8.5B is the chromatogram

produced from the thermally desorbed PEG. The SPME fiber was thermally desorbed inside of the injector for 10 s and then withdrawn from the injector. The high intensity peak at a retention time of approximately 7 min in this chromatogram was from the fiber coating. The mass spectrum of this peak had the same fragment ions as the mass spectrum of the blank PPY fiber. To eliminate the background peaks from the PPY coating, the PPY fibers were then conditioned at 150 °C for about one hour prior to use. Following this conditioning step, it is noted that the background in Figure 8.5C was much lower when the conditioned blank fiber was used. The background peak at 7 min was not shown. Well separated PEG peaks could be observed, in comparison with the chromatogram presented in Figure 8.5B. Blanks were checked before and after every run.

1 μL of 10 ppm PEG solution was injected into GC/MS for comparison. The retention times of the peaks in this chromatogram were the same as those obtained with laser desorption, but the peaks were broader (not shown here). The mass spectra of the peaks also exhibited the same fragment peaks at m/z 355, 429, 504. Hence, it was confirmed that the laser desorbed peaks were PEG peaks.

Following the injection of 1 μL of the 10 ppm PEG solution, carryover was observed. This might be due to the desorption of PEG on the inner surface of the injector. After three blank runs, there were still some carryover peaks in the chromatogram, suggesting the presence of trace PEG residue in the injector. One blank was run with a blank fiber inserted in the injector for 10 s and the results are shown in Figure 8.6A. Then the same fiber was used for another blank run with laser

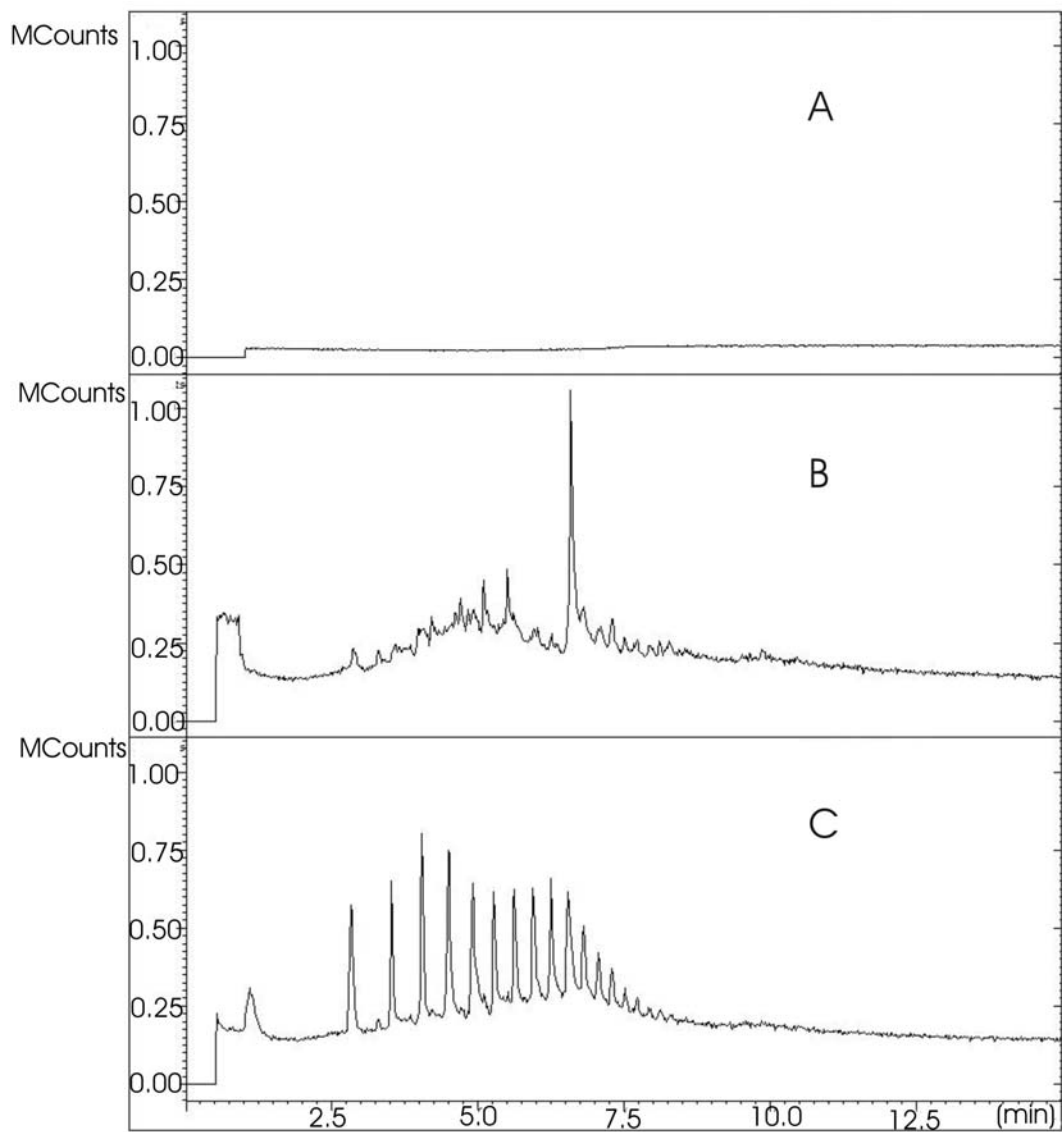


Figure 8.5: Comparison of laser desorption and thermal desorption with GC/MS. (A) blank; (B): thermal desorption PEG 400; (C): laser desorption PEG 400. Extraction time, 1 min; Concentration, 10 ppm. GC/MS operation parameters as described in the text.

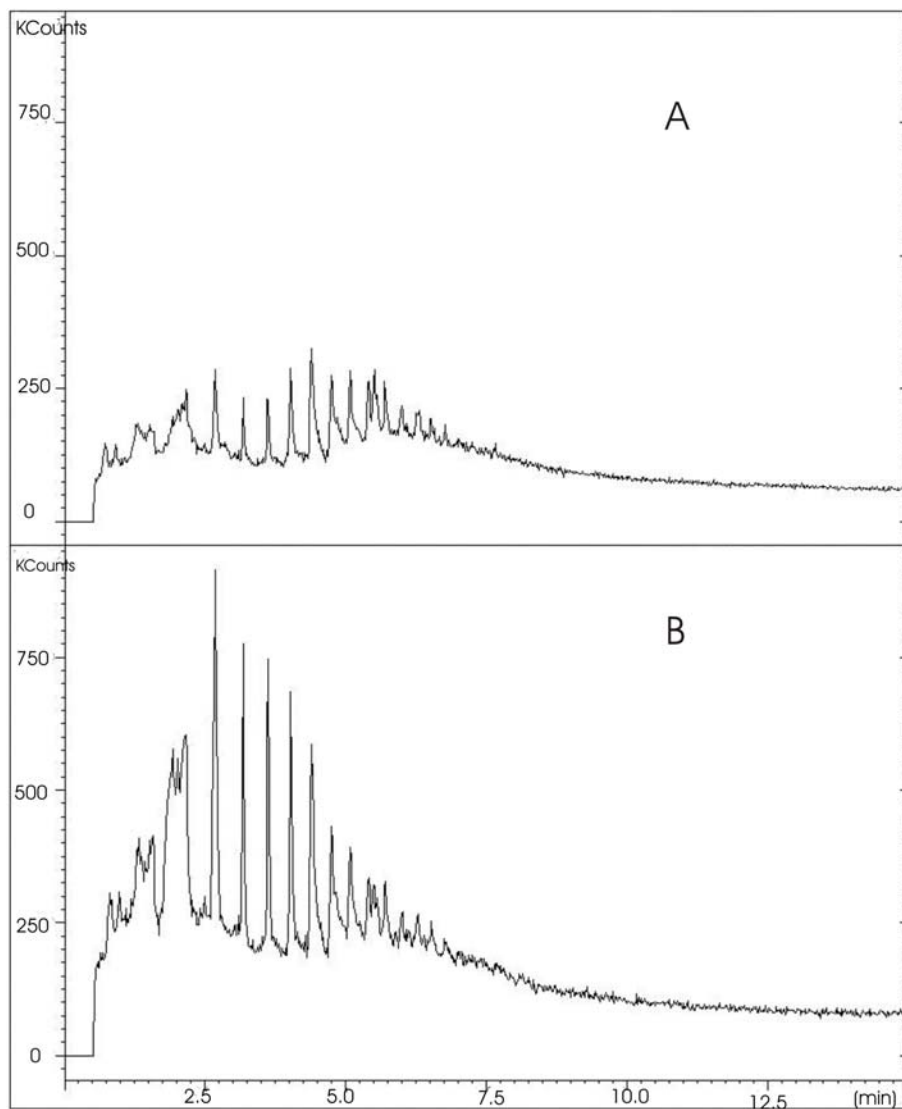


Figure 8.6: GC/MS chromatograms of laser desorption and thermal desorption. (A): thermal desorption the residue inside of SPI liner after injection; (B): laser desorption the residue after thermal desorption.

pulses fired (chromatogram shown in Figure 8.6B). The thermal desorption blank was run with the fiber inside of the injector to include all the possible sources of PEG residue, i.e., fiber, needle and injector. Some weak PEG peaks were still observed in the thermal desorbed blank chromatogram (Figure 8.6A). The subsequent laser desorbed blank chromatogram (Figure 8.6B) exhibited the same peaks, with three times higher intensity. This experiment was repeated two more times, and the peak intensities in the laser desorbed blanks were always higher than those in the thermally desorbed blanks. This findings suggest that the laser desorption was more effective for the desorption of non-volatile compounds for GC analysis.

8.4 Conclusion

Laser desorption SPME was employed as a sample introduction method for fast GC analysis of non-volatile synthetic polymers. The coupling of laser desorption SPME to GC/FID and GC/MS was pursued and the results were demonstrated in this chapter. It was observed that laser desorption was more efficient than thermal desorption when a non-volatile analyte PEG was used. Good separation was obtained even with a 1-m or 2-m column. Because the GC and GC/MS used in this work were not designed for fast GC analysis, some limitations were inherent in the analyses. For example, there was no fast heating system, the carrier gas flow rate was limited. The analysis time could not be shortened.

The pulse laser could be fired with a frequency of 20 Hz or higher, and it

was therefore possible to introduce analytes in a few seconds or less (tens of laser pulses or less) if the proper laser parameters were used. Therefore, laser desorption SPME could be used as a fast sample introduction method for fast GC analysis. These results demonstrate the potentials of laser desorption SPME as a sample introduction method for the fast GC analysis of non-volatile compounds such as synthetic polymers.

Chapter 9

Conclusions and Recommendations

The use of laser desorption as a sample introduction method for SPME has been investigated in this research. SPME fiber was coupled to three different types of analytical instruments using laser desorption: MS, IMS and GC (GC/MS). The construction of SPME/SELDI-IMS, SPME/SELDI-MS devices and the coupling of laser desorption to GC/GC-MS were introduced and evaluated here. Three new SPME coatings were developed and evaluated for laser desorption of SPME fibers. The applications of laser desorption SPME to these three analytical instruments were conducted to demonstrate the potential of this new technique.

9.1 SPME/SELDI-IMS

PPY coated SPME/SELDI fibers were developed, and were coupled to two IMS devices for the first time. SPME/ SELDI fibers combined sampling, sample preparation and sample introduction with ionization and desorption of the analytes. The setup of SPME/SELDI-IMS 350 device was described first. The data collection and analysis for signals produced by single laser pulses were used in the early stage of this work. The optimization of the PPY coating was investigated with this device, and the optimum coating procedure was determined. The characteristics of the PPY SPME/SELDI fiber was then evaluated. It was observed that the PPY coated fiber could reach an extraction equilibrium in one minute, and the analyte could be desorbed from the coating surface without the addition of a MALDI matrix. This suggested the possibility of fast analysis with this PPY SPME/SELDI fiber. A good linearity could be observed between the fiber surface area and the signal intensity, and between the concentration and the signal intensities. These results illustrated the possibility of using SPME/SELDI-IMS for quantitative analysis.

It was found that the S/N ratio, the intra-sample reproducibility and the throughput of this device required further improvement. Therefore, a new SPME/SELDI-IMS system with a faster data acquisition and a more powerful data analysis program was constructed and evaluated. The data acquisition throughput could be enhanced from less than 1 spectrum/min to 20 spectra/s. Hence hundreds of spectra could be accumulated to obtain improved sensitivity, reproducibility, and S/N ratio within tens of seconds. The laser operation parameters were also optimized;

250 μ J laser energy and 20 Hz laser repetition rate. Direct extraction of verapamil from urine sample was performed with a PPY coated SPME/SELDI fiber without any further cleanup. The analysis of the urine sample (including sample preparation) could be done within minutes. This SPME/SELDI-IMS device can be used for fast analysis of large and/or thermal labile molecules, such as drugs, polymers and biomolecules.

The ionization mechanism of PEG 400 was studied with SPME/SELDI-IMS 400B device. It was found that the potassium and sodium associated ions were produced by laser ionization. Alkali metal ions were added to the PEG solution to facilitate the interpretation of the laser produced ions. The addition of the potassium ions increased the intensity of the potassiated ion, but the adding of sodium ions caused a decrease in the peak intensities. The reason for this decrease is still not clear and warrants further research. The results obtained with QTOF MS confirmed the presence of both potassiated and sodiated ions. This result confirmed that the cationization is the main ionization process when polymers are directly ionized from a PPY coated silica surface.

Four PEGs with different average molecular weights and PPG 400 were also tested with this SPME/SELDI device. The difference between the ion mobility spectra of these polymers could be used for the fast identification of synthetic polymers.

Two other electroconductive polymers, PTH and PAN were prepared for SPME coatings and evaluated with IMS and GC. It was observed that PTH and PAN

coating could be used as surfaces to facilitate ionization without a MALDI matrix, according to the results obtained with IMS. The laser energy profiles were also plotted, and the highest protonated ion intensities were also observed at 250 μJ laser energy for both the PTH and the PAN coatings.

The capacity of the three coatings was evaluated with GC. The PPY coating exhibited the highest capacity among the three coatings. The preliminary SPME/SELDI-MS result illustrated relatively high background peaks from PAN coating in the mass spectrum. Therefore, the PAN coating was not used for further SPME-mass spectrometry experiments.

9.2 SPME/SELDI-MS

The SPME/SELDI fibers were coupled to a QTOF MS in the early stage of this research. The results confirmed the applicability of the coupling of SPME/SELDI with MS. It was demonstrated that the PPY coating functioned both as an extraction phase and as a surface to facilitate ionization. The LOD for leucine enkephalin was determined to be 2 pmol μL^{-1} .

This work was the first reported coupling of SPME/SELDI and MS. However, it should be noted that, the sensitivity was poor compared with other MALDI MS methods, and the technique requires further improvement.

The SPME/SELDI fibers were coupled to a QqLIT MS. Better sensitivity was expected as the modified AP MALDI source on the QqLIT MS exhibited a better

ion transmission efficiency than the QTOF MS. The analysis of the urine sample and the BSA digest were demonstrated with both PPY and PTH fibers. The LOD for leucine enkephalin in urine was determined to be $40 \text{ fmol } \mu\text{L}^{-1}$ with the PTH coated fiber. The LOD for the BSA digest was $2 \text{ fmol } \mu\text{L}^{-1}$ obtained with both the PTH and the PPY fibers. However, the throughput of this technique was low in comparison with other MALDI methods. In addition, the performance of the SPME/SELDI-MS, such as sensitivity, reproducibility, are still under investigation and require further improvement.

To address these issues, a new multiplexed SPME/AP MALDI plate was constructed and evaluated with a QqLIT MS with a modified AP MALDI source. The experimental parameters were optimized to achieve a significant improvement in performance. The incorporation of a diluted matrix to the extraction solution improved the absolute signal and S/N ratio by $104\times$ and $32\times$, respectively. The incorporation of reflection geometry for the laser illumination improved the S/N ratio by more than two orders of magnitude. Reproducibility was also improved as a result of these changes and the improved atmosphere-vacuum interface used for these experiments. The fully optimized high throughput SPME/AP MALDI configuration generated detection limit improvements on the order of $1000\text{-}7500\times$ those achieved prior to these modifications. Therefore, this system presents a possible alternative for qualitative proteomics and drug screening.

9.3 Laser Desorption SPME to GC

Laser desorbed SPME was employed as a sample introduction method for the fast GC analysis of low-volatile synthetic polymers. The coupling of laser desorption SPME to GC/FID and GC/MS was carried out and the results demonstrated improved performance of laser desorption over traditional thermal desorption for the analysis of synthetic polymer samples. Well separated peaks was obtained even with a 1-m or 2-m column. These results demonstrate the potentials of laser desorption SPME as a sample introduction method for the fast GC analysis of low-volatile compounds such as synthetic polymers.

9.4 Recommendations

To explore the application of laser desorption SPME to IMS, there are several approaches that could be used to improve the sensitivity. First, new SPME coatings with higher capacity, such as C18, and XDS particles could be used. Another option would be antibody immobilized surfaces, which offers higher affinity towards certain compounds. Second, reflection geometry can also be used for the coupling of SPME with IMS. Improved sensitivity is expected as this geometry exhibits higher sensitivity than transmission geometry in MS experiments.

The SPME/AP MALDI plate evaluated in these studies appeared to be a high-throughput, high sensitivity, good reproducibility, low cost sampling tool for MALDI-MS analysis of small peptides. Since the SPME technique is a very pow-

erful tool for quantitative analysis in spite of the sample size, with the involvement of high-repetition laser (for example, 1 kHz), high-throughput quantitative analysis with MALDI MS can be achieved. In addition, with the use of appropriate coatings such as C8 or C18 particles, cation and anion exchange particles, or functionalized surface with affinity towards different proteins, large molecules such as proteins could be analyzed with SPME/AP MALDI plate. Therefore, this approach might be an alternative for SELDI chips in the future.

As mentioned in several chapters, laser energy is a parameter that is directly related with signal intensity. The laser source used in this project did not have a feedback circuit or an attenuator to maintain the laser energy output at a constant value. As a result, the laser energy output value dropped when multiple laser pulses were fired. The reproducibility of the signal intensity was affected by this factor. Therefore this issue has to be addressed if quantitative analysis is desired.

With respect to laser desorption SPME for GC analysis, it was demonstrated to be an efficient desorption method for the introduction of non-volatile analytes into a GC for fast analysis. To further investigate this technique, an appropriately equipped GC with a fast heating system, and a MS detector with higher tolerance towards high carrier gas flow rate is desired. Caution should be taken during the sampling process. Only the tip of SPME fiber should be immersed in the sample solution. Otherwise the residue on the side of the fiber might be thermally desorbed, resulting in poor reproducibility. Carryover needs to be considered for the analysis of sticky polymer samples. Deactivated GC liner and disposable needle guide, or

on-column laser desorption are two options to resolve this issue.

Bibliography

- [1] R. G. Belardi and J. Pawliszyn. *Water Pollut. Res. J. Can.*, 24:179, 1989.
- [2] C. L. Arthur and J. Pawliszyn. *Anal. Chem.*, 62:2145, 1990.
- [3] E. C. Meurer; D. M. Tomazela; R. C. Silva; F. Augusto and M. N. Eberlin. *Anal. Chem.*, 74:5688–5692, 2002.
- [4] M. Walles; Y. Gu; C. Dartiguenave; F.M. Musteata; K. Waldron; D. Lubda and J. Pawliszyn. *J. Chrom. A*, 1067:197–205, 2005.
- [5] H. Tong; N. Sze; B. Thomson; S. Nascon and J. Pawliszyn. *Analyst*, 127:1207–1210, 2002.
- [6] P. Cheo. *Fiber Optics*. Prentice-Hall, Englewood, NJ, 1985.
- [7] J. Wu and J. Pawliszyn. *J. Chromato. A*, 909:37–52, 2001.
- [8] Y. Wang; M. Walles; B. Thomson; S. Nascon and J. Pawliszyn. *Rapid Commun. Mass Spectrom.*, 18:157–162, 2004.
- [9] T. Gorecki and J. Pawliszyn. *J. High Res. Chromatogr.*, 19:294, 1995.

- [10] J. Chen and J. Pawliszyn. *Anal. Chem.*, 67:2530, 1995.
- [11] Z. Liu and J. Pawliszyn. *Anal. Chem.*, 77:165–171, 2005.
- [12] Z. W. Hwang; Y. Y. Teng; K. P. Li and J. Sneddon. *J. Appl. Spectrosc.*, 45:435, 1991.
- [13] L. Moenke-Blankenburg. *Laser Micro-Analysis*. Wiley, New York, 1989.
- [14] L. J. Radziemski and D. A. Cremers. *Laser-Induced Plasmas and Applications*. Marcel Dekker, New York, 1989.
- [15] R. J. Saunders. *Met. Prog.*, 126:45, 1984.
- [16] R. J. Saunders. *Manuf. Eng.*, 198:50, 1987.
- [17] M. Moretti. *Laser Focus World*, April:95, 1990.
- [18] S. A. May. *Photon. Spectra.*, November:96, 1991.
- [19] S. Lerman. *IEEE J. Quantum Electron.*, QE-20:1465, 1984.
- [20] J. M. Isner; P. G. Steg and R. H. Clark. *IEEE J. Quantum Electron.*, QE-23:1756, 1987.
- [21] G. C. Riggle; R. C. Hoye and A. S. Ketcham. *Laser Applications in Medicine and Biology*. Plenum Press, New York, 1974.
- [22] S. Georgiou and F. Hillenkamp. *Chem. Reviews*, 103:317–319, 2003.
- [23] D. M. Hercules. *Pure Appl. Chem.*, 55:1869, 1983.

- [24] D. M. Hercules. *Analysis of Microelectronic Materials and Devices*. Wiley Press, New York, 1991.
- [25] R. N. Zare; J. H. Hahn and R. Zenobi. *Bull. Chem. Soc. Jpn.*, 61:87, 1988.
- [26] A. N. Shibano. *Laser Analytical Spectrochemistry*. Adam Hilger, Bristol, 1985.
- [27] R. Zenobi and R. N. Zare. *Advances in Multiphoton Spectroscopy and Processes*, volume 7. 1991.
- [28] K. Tanaka; H. Waki; Y. Ido; S. Akita; Y. Yoshida and T. Yoshida. *Rapid Commun. Mass Spectrom.*, 2:151–153, 1988.
- [29] M. Karas and F. Hillenkamp. *Anal. Chem.*, 60:2299–2301, 1988.
- [30] F. J. Vastola and A. J. Pirone. *Adv. Mass Spectrom.*, 4:107, 1968.
- [31] M. A. Posthumus; P. G. Kistemaker; H. L. C. meuzelaar and M. C. Ten Noever de Brauw. *Anal. Chem.*, 50:985, 1978.
- [32] C. D. Mowry and M. V. Johnston. *J. Phys. Chem.*, 98:1904, 1994.
- [33] M. Karas and U. Bahr. *Trends Anal. Chem.*, 5:90, 1986.
- [34] R. W. Dreyfus. *Microbeam Analysis-1989*. San Francisco Press, San Francisco, 1989.
- [35] P. Voumard; Q. Zhan and R. Zenobi. *Rev. Sci. Instrum.*, 25:2215, 1993.

- [36] K. Dreisewerd. *Chem. Rev.*, 103:395–425, 2003.
- [37] M. Karas and R. Krüg. *Chem. Rev.*, 103:427–439, 2003.
- [38] R. Knochenmuss and R. Zenobi. *Chem. Rev.*, 103:441–452, 2003.
- [39] J. Wei; J. M. Buriak and G. Siuzdak. *Nature*, 399:243–246, 1999.
- [40] J. J. Thomas; Z. Shen; J. E. Crowell; M. G. Finn and G. Siuzdak. *Proc. Nat. Acad. Sci.*, 98:4932–4937, 2001.
- [41] Z. Shen; J. J. Thomas; C. Averbuj; K. M. Broo; M. Engelhard; J. E. Crowell; M. G. Finn and G. Siuzdak. *Anal. Chem.*, 73:612–619, 2001.
- [42] E. P. Go; J. E. Prenni; J. Wei; A. Jones; S. C. Hall; E. Witkowska; Z. Shen and G. Siuzdak. *Anal. Chem.*, 75:2504–2506, 2003.
- [43] S. Trauger; E. P. Go; Z. Shen; J. V. Apon; B. Compton; E. S. P. Bouvier; M. G. Finn and G. Siuzdak. *Anal. Chem.*, 76:4484–4489, 2004.
- [44] A. Nordström; J. V. Apon; W. Uritboonthai; E. P. Go and G. Siuzdak. *Anal. Chem.*, 78:272–278, 2006.
- [45] S. Okuno; R. Arakawa; K. Okamoto; Y. Matsui; S. Seki; T. Kozawa; S. Tagawa and Y. Wada. *Anal. Chem.*, 77:5364–5369, 2005.
- [46] J. Sunner; E. Dratz and Y. Chen. *Anal. Chem.*, 67:4335–4342, 1995.
- [47] M. J. Dale; R. Knochenmuss and R. Zenobi. *Anal. Chem.*, 68:3321–3329, 1996.

- [48] J. A. McLean; K. A. Stumpo and D. H. Russell. *J. Am. Soc.*, 68:5304–5305, 2005.
- [49] C. Teng; K. Ho; Y. Lin and Y. Chen. *Anal. Chem.*, 76:4337–4342, 2004.
- [50] M. Schürenberg; K. Dreisewerd and F. Hillenkamp. *Anal. Chem.*, 71:221–229, 1999.
- [51] C. Chen and Y. Chen. *Anal. Chem.*, 76:1453–1457, 2004.
- [52] Chen W. Chen; L. Wang; H. Chiu; Y and C. Lee. *J. Am. Soc. Mass Spectrom.*, 15:1629–1635, 2004.
- [53] C. Pan; S. Xu; H. Zou; Z. Guo; Y. Zhang and B. Guo. *J. Am. Soc. Mass Spectrom.*, 16:263–270, 2005.
- [54] C. Pan; S. Xu; L. Hu; X. Su; J. Ou; H. Zou; Z. Guo; Y. Zhang. *J. Am. Soc. Mass Spectrom.*, 16:883–892, 2005.
- [55] Y. Lin and Y. Chen. *Anal. Chem.*, 74:5793–5798, 2002.
- [56] C. Teng and Y. Chen. *Rapid Commun. Mass Spectrom.*, 17:1092–1094, 2003.
- [57] T. W. Hutchens and T. T. Yip. *Rapid Commun. Mass Spectrom.*, 7:576–580, 1993.
- [58] G. Eiceman and Z. Karpas. *Ion Mobility Spectrometry*. CRC Press, 1990.
- [59] Y. Wang; B. B. Scheider; T. R. Covey and J. Pawliszyn. *Anal. Chem.*, 77:8095–8101, 2005.

- [60] J. Pawliszyn and S. Liu. *Anal. Chem.*, 59:1475–1478, 1987.
- [61] H. H. Hill Jr.; W. F. Siems; R. H. St. Louis and D. G. McMinn. *Anal. Chem.*, 62:1201A, 1990.
- [62] Y. H. Chen; H. H. Hill Jr. and D. P. Wittmer. *Int. J. Mass Spectrom. Ion Processes*, 154:1, 1996.
- [63] F. Karasek. *Anal. Chem.*, 46:710A, 1974.
- [64] E. W. McDaniel and E. A. Mason. *The Mobility and Diffusion of Ions in Gases*. John Wiley & Sons, New York, 1973.
- [65] Z. Karpas. *Anal. Chem.*, 61:684, 1989.
- [66] M. M. Metro and R. A. Keller. *J. Chromatogr. Sci.*, 11:520, 1973.
- [67] A. E. O’Keefe and G. C. Ortman. *Anal. Chem.*, 38:760, 1966.
- [68] R. L. Grob. *Modern Practice of Gas Chromatography*. John Wiley & Sons, New York, 1977.
- [69] S. D. Huang; L. Kolaitis and D. M. Lubman. *Appl. Spectrosc.*, 41:1371, 1987.
- [70] M. A. Baim and H. H. Hill Jr. *Anal. Chem.*, 54:38, 1982.
- [71] F. Karasek; H. H. Hill Jr.; S. H. Kim and S. Rokushika. *J. Chromatogr.*, 135:329, 1977.
- [72] C. Wu; W. F. Siems; J. Klasmeier and H. H. Hill Jr. *Anal. Chem.*, 72:391, 2000.

- [73] S. Rokushika; H. Hatano and H. H. Hill Jr. *Anal. Chem.*, 59:8, 1987.
- [74] R. L. Eatherton; M. A. Morrissey; W. F. Siems and H. H. Hill Jr. *J. High Resolut. Chromatogr. Chromatogr. Commun.*, 9:154, 1986.
- [75] C. Wu; H. H. Hill Jr.; U. K. Rasulev and E. G. Nazarov. *Anal. Chem.*, 71:273, 1999.
- [76] C. Wu; J. Klasmeier and H. H. Hill Jr. *Rapid Commun. Mass Spectrom.*, 13:1138, 1999.
- [77] C. J. Bramwell; M. Colgrave; C. S. Creaser and R. Dennis. *Analyst*, 127:1467, 2002.
- [78] K. J. Purves and R. Guevremont. *Anal. Chem.*, 71:2346, 1999.
- [79] K. J. Gillig; B. Ruotolo; E. G. Stone; D. H. Russell; K. Fuhrer; M. Gonin and A. J. Schultz. *Anal. Chem.*, 72:3965–3971, 2000.
- [80] C. J. Bramwell; C. S. Creaser; J. C. Reynolds and R. Dennis. *Inter. J. Ion Mobility Spectrom.*, 5:87, 2002.
- [81] T. Wyttenbach; J. E. Bushnell and M. T. Bowers. *J. Am. Chem. Soc.*, 120:5098, 1998.
- [82] B. T. Ruotolo; K. J. Gillig; E. G. Stone; D. H. Russell; K. Fuhrer; M. Gonin and A. J. Schultz. *Int. J. Mass Spectrom.*, 219:253, 2002.

- [83] W. E. Steiner; B. H. Clowers; W. A. English and H. H. Hill Jr. *Rapid Commun. Mass Spectrom.*, 18:882–888, 2004.
- [84] D. Young; K. M. Douglas; G. A. Eiceman; D. A. Lake and M. V. Johnston. *Analytica Chimica Acta*, 453:231, 2002.
- [85] G. A. Eiceman; D. Young and G. B. Smith. *Microchemical J.*, 81:108–116, 2005.
- [86] S. Motlagh C. I. Arthur and J. Pawliszyn. *Anal. Chem.*, 64:1187, 1992.
- [87] X. Yu; H. Yuan; T. Gorecki and J. Pawliszyn. *Anal. Chem.*, 71:2998–3002, 1999.
- [88] H. Lord; R. Grant; M. Walles; B. Incledon; B. Fahie and J. Pawliszyn. *Anal. Chem.*, 75:5103–5115, 2003.
- [89] E. J. Poziomek G. E. Orzechowska and V. Tersol. *Anal. Lett.*, 30:1437, 1997.
- [90] J. K. Lokhnauth and N. H. Snow. *Anal. Chem.*, 77:5938–5946, 2005.
- [91] P. Rearden and P. B. Harrington. *Anal. Chim. Acta*, 545:13–20, 2005.
- [92] K. G. Furton J. M. Perr and J. R. Almirall. *J. Sep. Sci.*, 28:177–183, 2005.
- [93] E. T. Kang; K. L. Tan; D. J. Liaw and H. H. Chiang. *J. Mat. Sci.*, 31:1295–1301, 1996.
- [94] T. Wyttenbach; G. von Helden and M. T. Bowers. *Inter. J. Mass Spectrom. Ion Proc.*, 165/166:377–390, 1997.

- [95] C. Illenseer and H. G. Löhmannsröben. *Phys. Chem. Chem. Phys.*, 3:2388–2393, 2001.
- [96] J. Gidden; T. Wyttenbach; A. T. Jackson; J. H. Scrivens and M. T. Bowers. *J. Am. Chem. Soc.*, 122:4692–4699, 2000.
- [97] G. von Helden; T. Wyttenbach and M. T. Bowers. *Science*, 267:1483–1485, 1995.
- [98] S. Lee; T. Wyttenbach; G. von Helden and M. T. Bowers. *J. Am. Chem. Soc.*, 117:10159–10160, 1995.
- [99] J. Gidden; T. Wyttenbach; J. J. Batka; P. Weis; A. T. Jackson; J. H. Scrivens and M. T. Bowers. *J. Am. Chem. Soc.*, 121:1421–1422, 1999.
- [100] Y-C. Chen and J-Y. Wu. *Rapid Commun. Mass Spectrom.*, 15:1899–1903, 2001.
- [101] Y. Chen; J. Shiea and J. Sunner. *Rapid Commun. Mass Spectrom.*, 14:86–90, 2000.
- [102] T. Kinumi; T. Saisu; M. Takayama and H. Niwa. *J. Mass Spectrom.*, 35:417–422, 2000.
- [103] E. P. C. Lai; S. Owega and R. Kulczycki. *J. Mass Spectrom.*, 33:554–564, 1998.
- [104] Q. Zhang; H. Zou; Z. Gou; Q. Zhang; X. Chen and J. Ni. *Rapid Commun. Mass Spectrom.*, 15:217–223, 2001.

- [105] W. Lewis; Z. Shen; M. Finn and G. Siuzdak. *Int. J. Mass Spectrom.*, 226:107–116, 2003.
- [106] T. Shothheim. *Handbook of Conducting Polymers*. Marcel Dekker, New York, 1998.
- [107] X. Li L. Wang and Y. Yang. *Reactive and Functional Polymers*, 47:125–129, 2001.
- [108] B. B. Schneider; C. Lock and T. R. Covey. *J. Am. Soc. Mass Spectrom.*, 16:176–182, 2005.
- [109] M. Schürenberg; C. Luebbert; H. Kalkum; H. Lehrach and E. Nordhoff. *Ana. Chem.*, 72:3436–3442, 2000.
- [110] H. Shiigi; M. Kishimoto; H. Yakabe; B. Deore and T. Nagaoka. *Analytical Sciences*, 18:41–44, 2002.
- [111] P. Juhasz; C. E. Costello and K. Biemann. *J. Am. Soc. Mass Spectrom.*, 4:399–409, 1993.
- [112] Y. Dai; R. M. Whittal and L. Li. *Anal. Chem.*, 71:1087–1091, 1999.
- [113] P. K. Chan and T. W. D. Chan. *Rapid Commun. Mass Spectrom.*, 19:1841–1847, 2000.
- [114] H. Javaheri; B. A. Thomson; C. P. T. Groth and M. Jugroot. *ASMS*, 320:448–456, 2000.

- [115] H. Pasch and W. Schrepp. *MALDI-TOF Mass Spectrometry of Synthetic Polymers*. Springer, Berlin, New York, 2003.
- [116] T. Gorecki and J. Pawliszyn. *Analyst*, 122:1079–1086, 1997.
- [117] D. H. Desty; A. Goldup and W. T. Swanton. *Gas Chromatography*. Academic Press, New York, 1962.
- [118] J. C. Giddings. *Anal. Chem.*, 34:314, 1962.
- [119] A. van Es. *High Speed Narrow Bore Capillary Gas Chromatography*. Heidelberg, 1992.
- [120] E. Overton and K. Carney. *Trends Anal. Chem.*, 13:252, 1994.
- [121] R. Sacks; H. Smith and H. Nowak. *Anal. Chem.*, 77:29A, 1998.
- [122] C. Cramers and P. Leclercq. *J. Chromatogr. A*, 842:3, 1999.
- [123] K. Matovska and S. Lehotay. *J. Chromatogr. A*, 1000:153–180, 2003.
- [124] N. H. Snow. *J. Liquid Chromatogr. Related Technol.*, 27:1317–1330, 2004.
- [125] P. Korytar; H. G. Janssen; E. Matisova and U. A. Th. Brinkman. *Trends Anal. Chem.*, 21:558–572, 2002.
- [126] M. van Deursen; J. Beens; H. G. Janssen; P. Leclercq and C. Cramers. *J. Chromatogr. A*, 878:205, 2000.
- [127] M. S. Klee and L. M. Blumberg. *J. Chromatogr. Sci.*, 40:234–247, 2002.

- [128] L. M. Blumberg and M. S. Klee. *Anal. Chem.*, 70:3828–3839, 1998.
- [129] A. J. van Es; H. G. Janssen; R. Bally; C. A. Cramers and J. A. Rijks. *J. High Resolu. Chromatogr. Chromatogr. Commun.*, 10:273, 1987.
- [130] T. Sharhar; S. Dagan and A. Amirav. *J. Am. Soc. Mass. Spectro.*, 9:28–637, 1998.
- [131] N. K. Meruva; L. A. Metz; S. R. Goode and S. L. Morgan. *J. Anal. Appl. Pyrolysis*, 71:313–325, 2004.
- [132] K. Dittrich and R. Wennrich. *Progress in Anal. Atom. Spectrosc.*, 7:139–198, 1984.

Appendix A

MATHCAD Program for IMS 350

Data Analysis

ORGIN : = 1

M : = *READPRN*("filename.CSV")

n : = *rows*(*M*)

n : = 1×10^4

T : = $M^{(1)}$

Y : = $M^{(2)}$

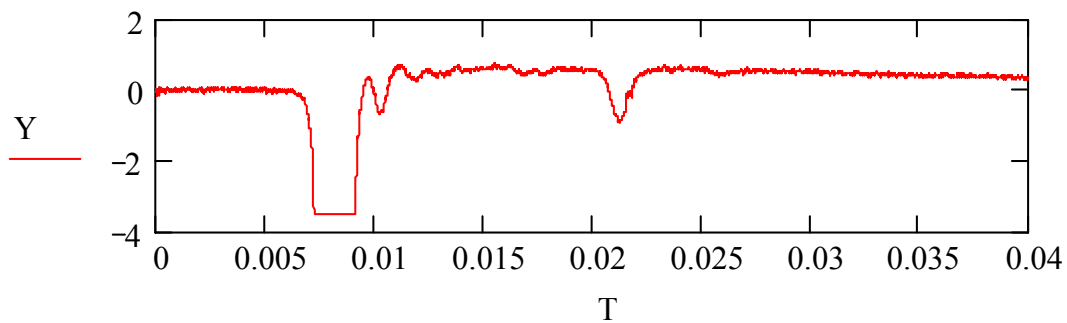


Figure A.1: Plotting IMS spectrum with Mathcad.

$$y(t) \quad : \quad = \text{linterp}(T, Y, t)$$

$$T_{5000} = 0.019916$$

$$Tin \quad : \quad = \frac{T_{5000} + T_{5001}}{2}$$

$$T_{5001} = 0.019920$$

$$Y_{5000} = 0.560000$$

$$Y_{5001} = 0.590000$$

$$(y(T)_{5000}) = 0.560000$$

$$y(Tin) = 0.575000$$

$$y(T_{5001}) = 0.590000$$

$$b \quad : \quad = a + \frac{b}{100}(d - a)$$

$$c \quad : \quad = a + \frac{c}{100}(d - a)$$

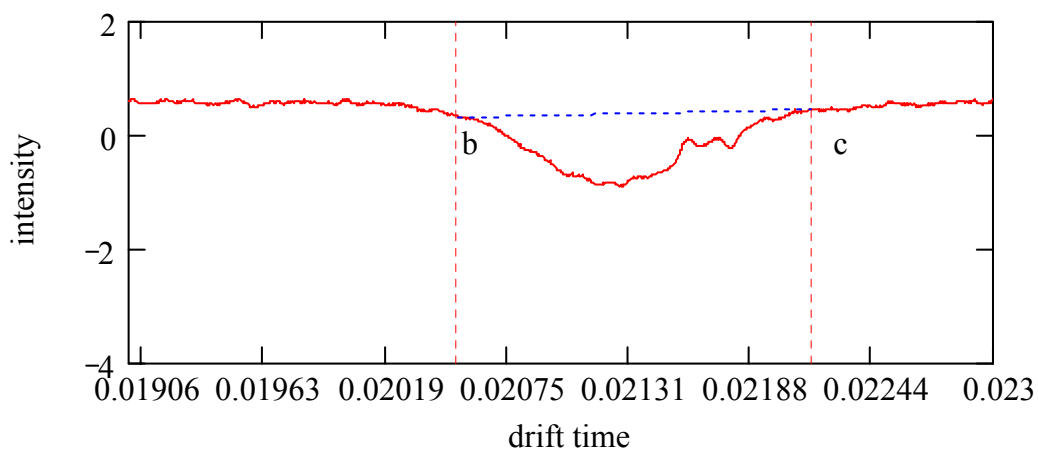


Figure A.2: Integrating peak area with Mathcad.

$$a \equiv 0.019$$

$$b = 0.020520$$

$$c = 0.022160$$

$$d \equiv 0.023$$

$$z(t) : = \text{linterp} \left[\begin{pmatrix} b \\ c \end{pmatrix}, \begin{pmatrix} y(b) \\ y(c) \end{pmatrix}, t \right]$$

$$z(b) = 0.31$$

$$z(c) = 0.45$$

$$A : = \int_b^c z(t) - y(t) dt$$

$$A = 1.017989 \times 10^{-3}$$

Appendix B

MATLAB Program for Data

Analysis

```
function yan( call, k )  
if nargin < 1, call = 'setup'; end;  
switch call  
    case 'setup'  
        yan_setup  
    case 'prefix'  
        yan_prefix  
    case 'files'  
        yan_files  
    case 'meansum'  
        yan_meansum
```



```

    case 'thr'

        yan_thr( k )

    case 'base'

        yan_base( k )

    case 'compute'

        if strcmp(k, 'thr'),    yan_compute_thr,    end
        if strcmp(k, 'base'),  yan_compute_base,    end

    case 'threed'

        yan_threed

end

return

%-----
% Setup Graphical User Interface
%-----

function yan_setup

global fig xy_axes

%-----

fig = openfig('yan_gui.fig', 'reuse');

figure(fig)

set(fig, 'DoubleBuffer',    'on')

set(fig, 'HandleVisibility', 'on')

```

```

set(gcf, 'MenuBar',          'figure')

%-----

prefix_edit    = findobj( fig, 'Tag', 'prefix_edit' );
files_edit     = findobj( fig, 'Tag', 'files_edit' );
meansum_popup  = findobj( fig, 'Tag', 'meansum_popup' );

thr1_button    = findobj( fig, 'Tag', 'thr1_button' );
thr2_button    = findobj( fig, 'Tag', 'thr2_button' );

base1_button   = findobj( fig, 'Tag', 'base1_button' );
base2_button   = findobj( fig, 'Tag', 'base2_button' );
base3_button   = findobj( fig, 'Tag', 'base3_button' );
base4_button   = findobj( fig, 'Tag', 'base4_button' );

Area_text      = findobj( fig, 'Tag', 'Area_text' );

threed_button  = findobj( fig, 'Tag', 'threed_button' );

xy_axes        = findobj( fig, 'Tag', 'xy_axes' );

%-----

set( prefix_edit, 'String', 'PTH1-5032104_' )
set( files_edit,  'String', '1' )

```

```

set( meansum_popup, 'String', {'mean', 'sum'} )
set( meansum_popup, 'Value',      1      )

%-----

set( prefix_edit,   'Callback', 'yan prefix' )
set( files_edit,   'Callback', 'yan files' )
set( meansum_popup, 'Callback', 'yan meansum' )

set( thr1_button,  'Callback', 'yan thr 1;   yan compute thr' )
set( thr2_button,  'Callback', 'yan thr 2;   yan compute thr' )

set( base1_button, 'Callback', 'yan base 1;  yan compute base' )
set( base2_button, 'Callback', 'yan base 2;  yan compute base' )
set( base3_button, 'Callback', 'yan base 3;  yan compute base' )
set( base4_button, 'Callback', 'yan base 4;  yan compute base' )

set( Area_text, 'String', '' )

% Also done in yan_readdata

set( threed_button, 'Callback', 'yan threed' )

%-----

```

```

%% yan_readdata  <- Don't run because initial prefix
may not be right

%-----
%-----

function yan_prefix

global fig

prefix_edit      = findobj( fig, 'Tag', 'prefix_edit' );
files_edit       = findobj( fig, 'Tag', 'files_edit' );

set( files_edit, 'String', '1' )

yan_readdata

return

%-----
%-----

function yan_files

yan_readdata

return

%-----
%-----

```

```

function yan_meansum

yan_readdata

return

%-----
%-----

function yan_readdata      % clear axes and plot

global fig xy_axes

global T Y Yall

prefix_edit    = findobj( fig, 'Tag', 'prefix_edit' );
files_edit     = findobj( fig, 'Tag', 'files_edit' );
meansum_popup  = findobj( fig, 'Tag', 'meansum_popup' );

%-----

prefix    = get( prefix_edit, 'string' );
files     = get( files_edit, 'string' );

files     = [ '[' files ']' ];
files     = strrep( files, '-', ':' );
files     = eval( files );

nfiles    = length( files );

```

```

%-----
meansum_s = get( meansum_popup, 'String' ); % {'mean', 'sum'}
i          = get( meansum_popup, 'Value' ); %      1 or  2

meansum    = meansum_s{i};                    %      mean or sum
%-----

axes( xy_axes )

cla( xy_axes )

n        = 10000;

T        = zeros(n, 1);

Yall = zeros(n, nfiles);
%-----

for i=1:nfiles

    file = [ prefix num2str( files(i) ) '.txt' ];

    A = load(file);

    T(:) = A(:,1);

    Yall(:,i) = A(:,2);

end

%-----

if strcmp( meansum, 'mean' )    Y = mean(Yall, 2);    end
if strcmp( meansum, 'sum' )    Y = sum(Yall, 2);    end

%-----

```

```

hold on

        plot(T, Y, 'b-')

        xlim = get(gca, 'XLim');

        zero_line = plot(xlim, [0 0], 'k-');

hold off

set( zero_line, 'Color', [0.5 0.5 0.5])

%-----

global Tthr Ythr Hthr

global Tbase Ybase Hbase

Hthr = zeros(1, 2+1);

Hbase = zeros(1, 4+2+1);

Tthr = Hthr;   Ythr = Hthr;

Tbase = Hbase;   Ybase = Hbase;

%-----

Area_text = findobj( fig, 'Tag', 'Area_text' );

set( Area_text, 'String', '' )

return

%-----

%-----

function yan_thr( k )    % k=1..2

```

```

global Tthr Ythr Hthr

global xy_axes

k = str2num(k);

if Hthr(k) ~= 0, delete( Hthr(k) ), end
if Hthr(3) ~= 0, delete( Hthr(3) ), end

[Tthr(k), Ythr(k)] = ginput(1);

ylim = get(xy_axes, 'YLim');

hold on
Hthr(k) = plot( [Tthr(k) Tthr(k)], ylim, 'k-' );
hold off

return

%-----
%-----

function yan_base( k )    % k=1..4

global Tbase Ybase Hbase

```



```

global xy_axes

k = str2num(k);

if Hbase(k) ~= 0, delete( Hbase(k) ), end
if Hbase(5) ~= 0, delete( Hbase(5) ), end
if Hbase(6) ~= 0, delete( Hbase(6) ), end
if Hbase(7) ~= 0, delete( Hbase(7) ), end

[Tbase(k), Ybase(k)] = ginput(1);

ylim = get(xy_axes, 'YLim');

hold on
style = {'r-', 'r-', 'm-', 'm-'};
Hbase(k) = plot( [Tbase(k) Tbase(k)], ylim, style{k} );
hold off

return

%-----
%-----

function yan_compute_thr

```

```

global xy_axes

global T Y

global Tthr Ythr Hthr

global thr

%-----
%
%*-----*----- ... ---/---*---*--- ... --*---*---\--- time
% #1      #2          a   ia          ib   b
%
%-----

if ((Hthr(1) ~= 0) & ...
    (Hthr(2) ~= 0)      )

    a = Tthr(1);
    b = Tthr(2);

    ia = min( find( T >= a ) );
    ib = max( find( T <= b ) );

    Ymin = min( Y(ia:ib) );
    Ymax = max( Y(ia:ib) );
    Ymean = mean( Y(ia:ib) );

```

```

    thr = -3*( Ymean-Ymin );

    xlim = get( xy_axes, 'Xlim' );

    hold on

    Hthr(3) = plot( xlim, [thr thr], 'k-' );

    hold off

end

return

%-----
%-----

function yan_compute_base

global base

global fig xy_axes

global T Y

global Tbase Ybase Hbase

%-----

if ((Hbase(1) ~= 0) & ...
    (Hbase(2) ~= 0) & ...
    (Hbase(3) ~= 0) & ...

```

```

(Hbase(4) ~= 0) )

ibase1 = find(                                     ...
            (Tbase(1) <= T) & (T <= Tbase(2))     ...
            );

ibase2 = find(                                     ...
            (Tbase(3) <= T) & (T <= Tbase(4))     ...
            );

base1 = mean( Y(ibase1) );
base2 = mean( Y(ibase2) );

%-----
xlim = get( xy_axes, 'XLim' );

hold on

Hbase(5) = plot( [Tbase(1) Tbase(2)], [base1 base1], 'r-' );
Hbase(6) = plot( [Tbase(3) Tbase(4)], [base2 base2], 'm-' );
Hbase(7) = plot( [Tbase(2) Tbase(3)], [base1 base2], 'k-' );

hold off

set( Hbase(7), 'Color', [0.5 0 1] )      % <- Purple

```

```

%-----
iarea = find(                                     ...
            (Tbase(2) <= T) & (T <= Tbase(3))    ...
        );

%-----
%
%          base2  -  base1
%  y(t) = ----- * (t-Tbase(2)) + base1
%          Tbase(3) - Tbase(2)
%
%-----

dt = T(2)-T(1);

Area = 0;

for i = iarea(1) : iarea(end)

    t    = T(i);

    slope = ( base2  -  base1  ) / ...
            ( Tbase(3) - Tbase(2) );

    y    = slope * (t-Tbase(2)) + base1;

    dA   = (y - Y(i))*dt;

    if (dA < 0),    dA = 0;    end

```

```

        Area = Area + dA;

    end

    Area_text = findobj( fig, 'Tag', 'Area_text' );

    set( Area_text, 'String', num2str(Area) );

end

return

%-----
%-----

function yan_threed

global T Yall

global fig

%-----

files_edit = findobj( fig, 'Tag', 'files_edit' );

files = get( files_edit, 'string' );

files = [ '[' files ']' ];

files = strrep( files, '-', ':' );

files = eval( files );

nfiles = length( files );

```

```
%-----  
figure(2)  
for i=1:nfiles  
  
    I = T*0 + files(i);  
  
    h(i) = plot3( T, I, Yall(:,i), 'k-' );  
  
    hold on  
  
end  
  
hold off  
  
view([ -2 6 ])  
  
return
```

Appendix C

Schematic of Control Box and Divider for IMS 400B

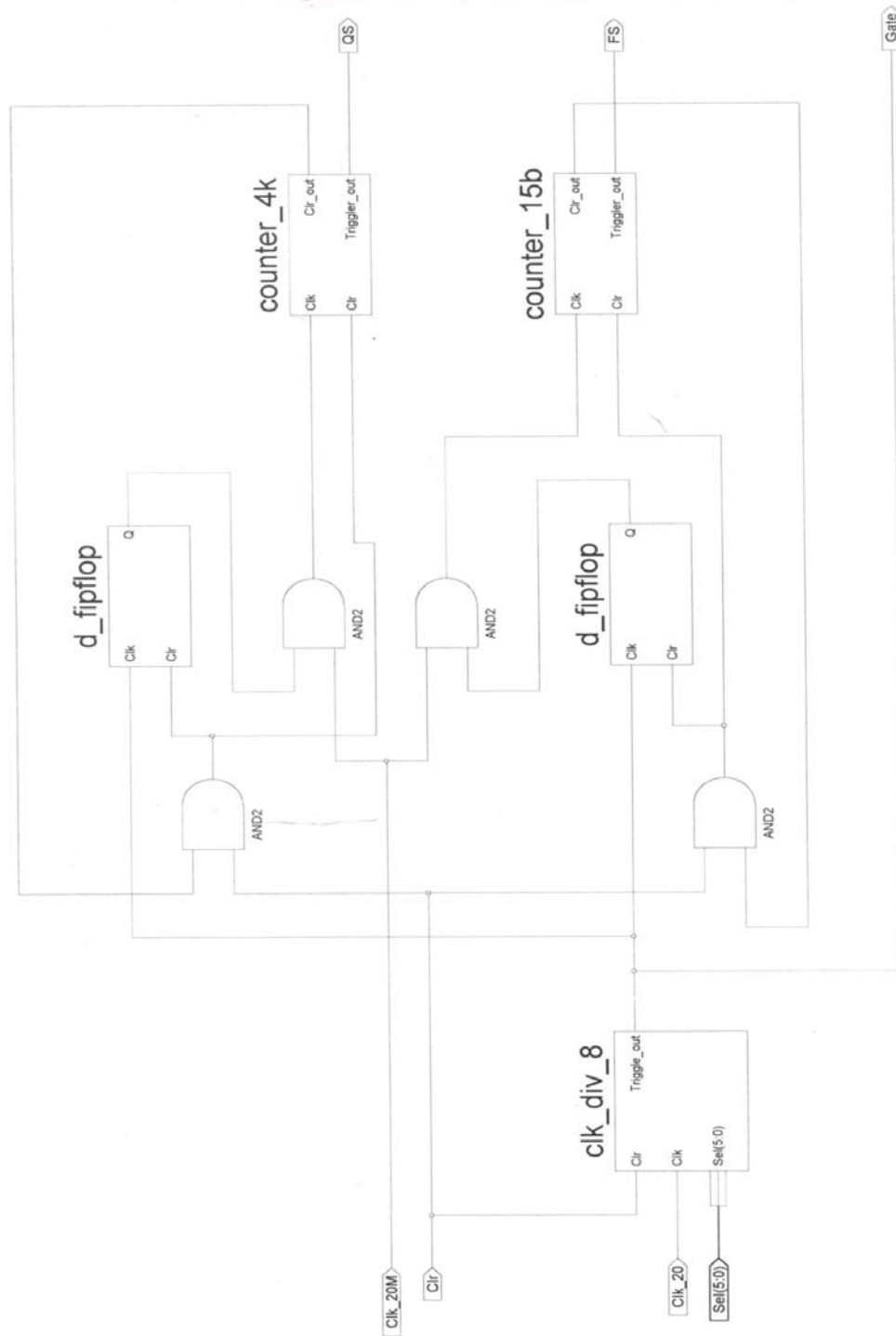


Figure C.1: Schematic of laser control box for coupling with IMS.

Appendix D

List of Abbreviations

AP	atmospheric pressure
APS	ammonium persulfate
BSA	bovine serum albumin
CE	capillary electrophoresis
CIEF	capillary isoelectric focusing
CHCA	α -cyano-4-hydroxycinnamic acid
DAQ	data acquisition
DHB	2,5-dihydroxybenzoic acid
DIOS	desorption/ionization on silicon
ESI	electrospray

FID flame ionization detector

GC gas chromatography

GC/MS gas chromatography/mass spectrometry

HPLC high-performance liquid chromatography

HPLC/MS high-performance liquid chromatography/mass spectrometry

IMS ion mobility spectrometry

L2MS two-step laser mass spectrometry

LC liquid chromatography

LD laser desorption

LDMS laser desorption mass spectrometry

LIF laser induced fluorescence detector

LOD limit of detection

MALDI matrix assisted laser desorption/ionization

MS mass spectrometry

NaDBS sodium dodecylbenzenesulfonate

PAHs polycyclic aromatic hydrocarbons

PAN polyaniline

PEG	poly(ethylene glycol)
PET	poly(ethylene terephthalate)
PMMA	poly(methyl methacrylate)
PPG	poly(propylene glycol)
PPY	polypyrrole
PTH	polythiophene
PTMEG	poly(tetramethyl)glycol
QqLIT MS	hybrid quadrupole-linear ion trap mass spectrometry
QTOF MS	quadrupole time-of-flight mass spectrometer
RSD	relative standard deviation
SELDI	surface enhanced laser desorption/ionization
SEM	scanning electron microscope
S/N	signal-to-noise ratio
SPME	solid-phase microextraction
TOAB	tetraoctylammonium bromide
WCID	whole column image detector
UV	ultra-violet